NASA CR-66857

A PROGRAM OF PROOF TESTS OF THE DUAL ABLATION MEASUREMENT TECHNIQUE

Final Report of Contract NAS1-8221 by

TSI THERMAL SYSTEMS, INC.

St. Louis, Missouri

for

NATIONAL AERONAUTICS AND SPACE ADMINISTRATION

NASA CR-66857

A PROGRAM OF PROOF TESTS OF THE DUAL ABLATION MEASUREMENT TECHNIQUE

January, 1970

Final Report of Contract NAS1-8221 by

TSI THERMAL SYSTEMS, INC.

St. Louis, Missouri

for

NATIONAL AERONAUTICS AND SPACE ADMINISTRATION

ABSTRACT

Under Contract NAS1-8221, TSI Thermal Systems, Inc, with the direction and assistance of NASA, Langley Research Center, performed a series of proof tests of the dual ablation measurement technique. The measurement of ablation by nucleonic techniques was proved not only feasible but realizable with state-of-the-art, commercially available hardware.

The eighteen-month contract effort was comprised of an integrated program of theoretical analysis, test model design and fabrication, instrumentation evaluation, nuclear calibration tests, plasma jet testing, and data reduction and correlation. The theoretical portion of the program determined those parameters significantly affecting measurement technique and its associated accuracy: signal attenuation, isotope activity ratio, and isotope activity levels.

In a series of plasma jet tests simulating vehicle entry environments, sensors fabricated of two parent heat shield materials (phenolic nylon and phenolic graphite) and impregnated with two radioactive tracers (In^{114m} amd $ZrNb^{95}$) were effectively utilized to trace char and char-virgin material interface recessions. With system measurement errors of less than 3.25 per cent, the dual ablation measurement systems demonstrated their potential

to characterize the performance of re-entry heat shield materials under actual flight environments.

Three nucleonic systems were employed in the test program: the breadboard and manufacturing prototype dual ablation sensor systems fabricated under Contract NAS1-5342, and a laboratory standard nucleonic sensor purchased and fabricated by TSI. The laboratory nucleonics system was more accurate than the other electronic processors, primarily because of improved circuitry and greater optimization propensity.

It is recommended that the successful proof testing of the dual ablation measurement technique be followed with the manufacture and test of a flight prototype dual ablation measurement system. The theoretical and empirical results of Contract NAS1-8221 should be utilized in incorporating design modifications prerequisite to maximum system accuracy.

This report contains a description of the program, data reduction techniques, discussion of results, conclusions and recommendations. Included in the appendices are supporting theoretical and test data, as well as detailed descriptions of instrumentation, the test model and test model holder, test facilities, and procedures for quality assurance, impregnation, and radioactive material safety and handling.

TABLE OF CONTENTS

LIST OF TABLES

LIST OF FIGURES

LIST OF SYMBOLS

E	-	System Measurement Error
N	-	Counting Rate Per Unit Time
τ	-	System Time Constant (Sample Time)
σ	-	One Sigma Statistical Uncertainty
Q	-	Activity Ratio
α	-	Isotope Activity Ratio
$\dot{q}$	-	Cold Wall Heat Flux
H	-	Stagnation Enthalpy
P	-	Stagnation Pressure
x	-	Thickness
Z	-	Transmission Efficiency
ρ	-	Density
B	-	Dose Buildup Factor
e	-	Recession Rate Measurement Error
cps	-	Counting Rate
V	-	Volts
mc	-	Millicuries
mev	-	Million Electron Volts
μ	-	Mass Absorption Coefficient

SECTION 1

INTRODUCTION

1.0 GENERAL

The provision of an ablative heat shield is the most frequently used technique to dissipate the energy and provide thermal protection to planetary entry vehicle payloads. Continuous measurement of the in-flight ablative characteristics of advanced heat shield materials is of vital importance in characterizing the materials in the entry environment. From the standpoint of thermal protection of the entry vehicle from severe heating environments, the most promising ablative heat shield materials decompose in two or more steps and provide a char surface capable of reradiating significant amounts of entry heating to the atmosphere. The locations of the char-virgin material interface as well as the char surface at any time during vehicle entry (when combined with thermal environment conditions) are important parameters in ablative heat shield material characterization.

The dual ablation measurement technique was conceived as a means of effectively monitoring the locations of the char-virgin material interface and char surface during flight re-entry. Its utilization would represent a significant advancement in the engineering characterization of ablative materials. Under Contract NAS1-8221, with the direction and assistance of NASA, Langley Research Center, TSI Thermal Systems, Inc., has conducted a program of proof tests of the dual ablation measurement technique. The feasibility of the dual ablation measurement concept was investigated by the Thermal Systems Department (forerunner of TSI Thermal Systems, Inc.) of Emerson Electric under NASA-Langley Contract NAS1-5342. One breadboard and two manufacturing prototype dual ablation measurement systems were designed and fabricated. Each system consisted of a ruggedized radiation detector and a signal processor.

1.1 Description of Dual Ablation Measurement Technique

TSI's dual ablation measurement technique provides a means of continuously monitoring the attrition of material without the addition of wires, tubes or other foreign matter which can alter the real performance of the heat shield material. The technique is illustrated in Figure 1, a system schematic. Two nuclear tracers impregnated into the ablative material and integrated into the heat shield provide continuous measurements of both surface locations without altering the material performance. Suitable instrumentation, calibration and data reductions are tailored to provide a precise continuous measurement of both the char surface and char-virgin material interface during exposure of the entry vehicle to severe heating environments.

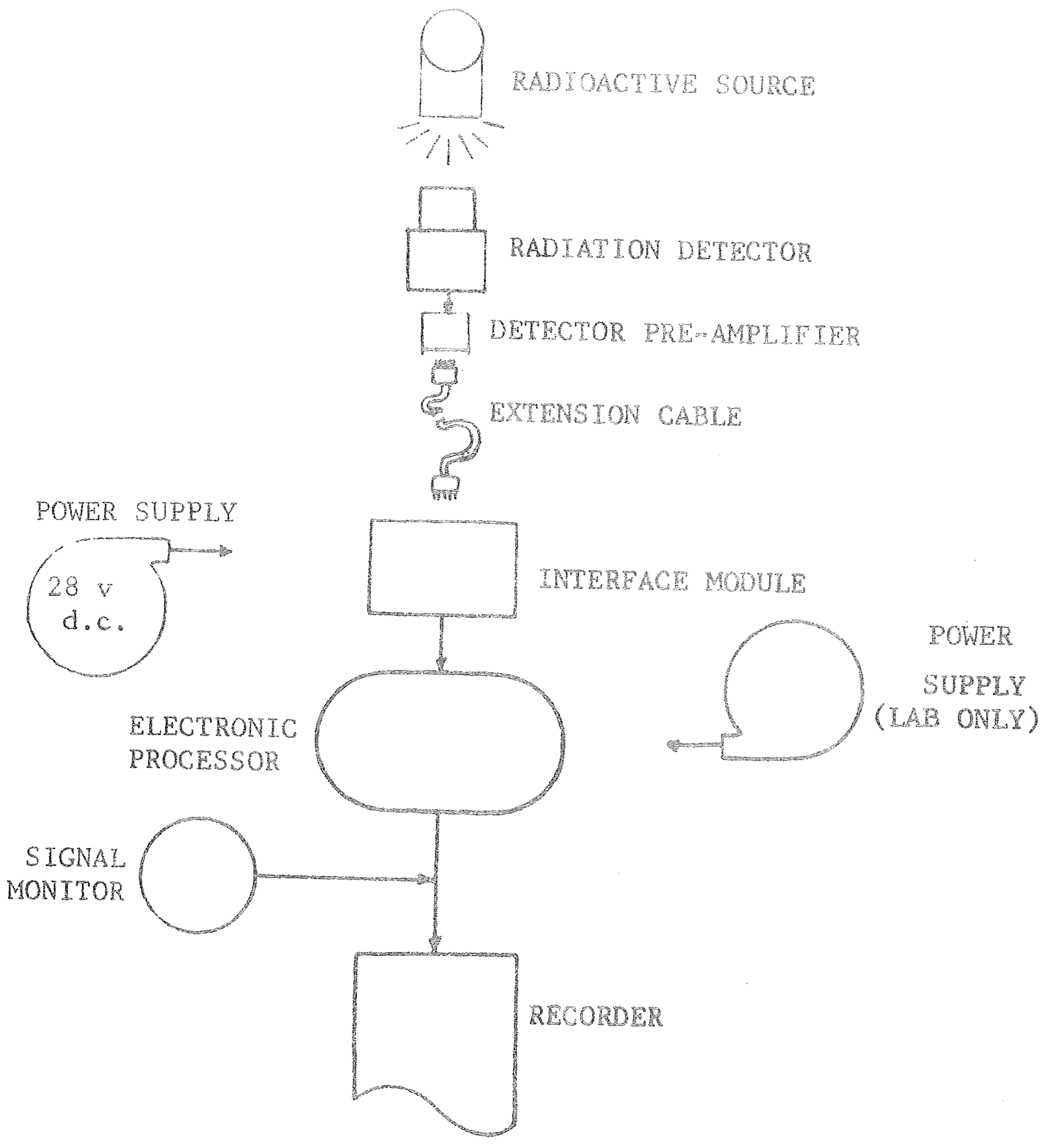

Figure 1. Dual Ablation Measurement System Schematic

The dual ablation nucleonic system functions through the sensing and discrimination of unique thermochemical and nucleonic properties of radioactive compounds incorporated into an ablation sensor basically composed of the parent heat shield material. With precisely controlled and uniform distribution of the radioactive materials, relationships may be developed between the intensity of radiation of specific energy levels and the thickness of material modes.

To accomplish this dual measurement, two radioactive tracers with significantly different emission energy levels are impregnated into a sensor of the parent heat shield material. The two radioactive tracers were selected during the performance of Contract NAS1-5342 on the basis of their characteristic likenesses to the chemical elements present in the virgin and char materials. That is, when exposed to entry heating, the radioactive tracer of one energy level is consumed in the same manner as that of the virgin material while the radioactive tracer of the second energy level is consumed in the same manner as that of the char material.

Other major considerations in the selection of the two isotopes were temperatures of sublimation; gamma emitters; availability; cost; specific activity, lack of chemical reactions with ablator; and half life. It was essential that one radioactive compound sublime at the decomposition temperature of the ablative material, with the second compound remaining in the char. This requirement is met by In^{114m} and $ZrNb^{95}$, which decompose at 820°F and 6400-7000°F respectively. The 820°F decomposition temperature of In^{114m} is in concert with the pyrolysis temperature of phenolic nylon and most commonly used organic binders. $ZrNb^{95}$ is employed in measuring the attrition rate of the char. Most compounds have no stability above 6000°F and are consumed either by sublimation of the carbon particles or by oxidation, diffusion, or physical erosion. The attrition of $ZrNb^{95}$, however, is simultaneous to that of the char and thus indicates on a real time basis the rate of depletion of the char layer. Its decomposition temperature is sufficiently different from the pyrolysis of the virgin phase of the material for it to remain when the char is formed.

The requirement of gamma emission and readily discriminated energy levels is also satisfied by the selection of In^{114m} and $ZrNb^{95}$. In^{114m} has a principle gamma emission of 0.19 Mev, while $ZrNb^{95}$ has a principle gamma emission of 0.72-0.77 Mev and can thus be easily discriminated. The two isotopes are readily available at costs feasible for wide application. The specific activities of both isotopes can be maintained at levels prerequisite to minimum hazards during handling. Neither In^{114m} or $ZrNb^{95}$ will react with the ablators tested (phenolic nylon and phenolic graphite). In^{114m}, with a half life of 50 days, and $ZrNb^{95}$, with a half life of 65 days, also meet the requirement of sufficient half life to allow ample time at the launch site as well as for calibration and transport.

1.2 Contract Objectives

In June of 1968, TSI Thermal Systems, Inc., began the performance of Contract NAS1-8221, awarded by NASA, Langley Research Center, for the purpose of proof testing the dual ablation measurement technique. The objectives of this contract included the following:

1) Precise determination of the accuracy with which the dual ablation measurement system could measure material ablation

2) Determination of the feasibility and practicability of developing flight measurement instrumentation employing this principle

3) Evaluation of the dual ablation measurement systems developed under Contract NAS1-5342 when exposed to severe heating environments similar to those expected during actual flight re-entry.

1.3 Scope of Report

Included in this report are the following:

1) A description of the theoretical and experimental work performed, the test facilities used, and the test models, sensors and holders employed

2) An explanation of data reduction techniques

3) A discussion of program results

4) Conclusions and recommendations.

The appendices represent phases of the overall program which were vital to the attainment of yet not directly related to the primary objectives of the program. Some of these peripheral areas include the theoretical determination of the isotope activity ratio; the theoretical and experimental determination of the required activity levels for each of the electronic processor systems; and the development and implementation of quality assurance and impregnation procedures. A complete listing of the appendices is included in the Table of Contents.

SECTION II

DESCRIPTION OF PROGRAM

1.0 PROGRAM OBJECTIVES

The two major objectives of Contract NAS1-8221 were to determine the accuracy with which the dual ablation measurement system could measure material ablation and to evaluate the measurement accuracy of the systems fabricated under Contract NAS1-5342. The first objective was met through a theoretical analysis and experimental verification using standard laboratory instrumentation hardware. The theoretical analysis included the effects of material attenuation, nuclear spectral overlap, flight activity levels, and instrumentation performance efficiency. The experimental verification was comprised of a series of plasma jet tests at heating environments similar to those anticipated during actual vehicle re-entry. The second objective was fulfilled through a series of plasma jet tests at conditions identical to those employed to determine the system's potential accuracy.

The contract effort was comprised of an integrated program of theoretical analysis, test model design and fabrication, instrumentation evaluation, nuclear calibration tests, plasma jet testing, and data reduction and correlation. The eighteen-month program was divided into the following phases:

Phase I	Program Definition
Phase II	Fabrication
Phase III	Nuclear Spectral Overlap Analysis and Development of Sensor Plug Impregnation Procedures
Phase IV	Electronic System Development
Phase V	Arc Tunnel Calibration Tests
Phase VI	Concept Accuracy Tests
Phase VII	Breadboard Measuring System Tests
Phase VIII	Reporting

Completion of these phases resulted in the fulfillment of the contract objectives: the efficacy of the dual ablation measurement technique was confirmed, and the measurement accuracy of the electronic processors fabricated under Contract NAS1-5342 was evaluated.

2.0 NUCLEONIC SYSTEM EVALUATION

The nucleonic technique of measuring char and virgin material attrition rates was theoretically and empirically analyzed during the pre-plasma jet testing efforts of Phase III. The theoretical portion of the overall program was designed to determine those parameters having a significant effect upon the measurement technique and its associated accuracy.

To determine the optimum sensor system for measuring material ablation, the effects of signal attenuation due to material, geometrical and electronic system effects were studied; the isotope activity ratio was optimized; and the overall activity levels were determined. The theoretical development of their relationship to system measurement accuracy was experimentally verified in the radiochemical laboratory. These theoretical and empirical results constituted the building blocks for the radioactive plasma jet tests. Theoretical system accuracy was further employed in determining the sources of error in the nucleonic measurement of material ablation. The effects of signal attenuation, isotope activity levels and isotope activity ratios, including their correlation with system measurement error, are discussed in detail in Appendix A.

To produce the highest possible system measurement accuracies commensurate with the performance parameters of the three nucleonic measurement devices, an optimum method of discriminating between the two radioactive tracers, In^{114m} and $ZrNb^{95}$, was determined. In developing the optimum means of isotope discrimination, the discrimination area, isotope activity levels, isotope activity ratio (nuclear spectral overlap), signal attenuation, and window location were considered. The operational values of each of the main parameters governing the optimum method of isotope discrimination were selected for each of the three nucleonic systems.

2.1 Optimum Isotope Discrimination

Optimum isotope discrimination is comprised of those parameters which enhance or degrade the discrimination properties of the isotope. Each of these effects was included in the Appendix A study, with a detailed treatment of their interrelationships explored.

The results of this investigation were to determine the major parameters affecting the discrimination optimization and the effects of their functional variation on the system measurement. In general those parameters which affect the isotope discrimination are

1) Discrimination area
2) Isotope activity ratio
3) Window locations
4) Isotope activity levels
5) Signal attenuation.

2.1.1 Discrimination Area

The discrimination area is defined as that spectral area in Channel 1 or 2 due to the primary isotope's activity which lies above the spectral area of the secondary isotope's spectral curve. This area represents the amount of total count rate (integrated count rate over the Channel 1 or 2 energy bands) which is everywhere greater than that of the secondary isotope's. The maximization of the discrimination area was found to be the single most important criteria in developing an optimum method of discrimination between the two isotopes. How each of the following parameters affected the discrimination area was the criterion for selection of the system performance parameters.

2.1.2 Isotope Activity Ratio (Nuclear Spectral Overlap)

In Phase III, several theoretical and experimental studies concerning the effect of isotope activity ratio on the optimization of isotope discrimination were performed. These studies necessarily involved the analysis of the effects of signal attenuation and electronic system performance.

The isotope activity ratio is defined as the ratio of the millicurie activity of the In^{114m} isotope to that of the millicurie activity of the $ZrNb^{95}$ isotope. Thus, assuming a fixed $ZrNb^{95}$ activity, an increase in the isotope activity ratio represents an increase in the amount of In^{114m} activity.

In Phase III, the isotope activity ratios for each of the three nucleonic systems were analyzed. It was found that an increase in isotope activity ratio generally increased the discrimination area in Channel 1 and decreased it in Channel 2. Material attenuation and electronic component inefficiencies tended to reduce the discrimination area in both channels, with a significantly greater effect on the lower energy channel than on the higher. The isotope activity ratio was parametrically examined as a function of signal attenuation (combination of material attenuation and electronic component inefficiency effects) and isotope activity levels.

The results were utilized to determine where the optimum choice of the two discrimination areas would exist in each electronic system to provide the best system performance (lowest system measurement error). An isotope activity ratio of ten was found to be an optimum choice for all three electronic processor systems.

2.1.3 Window Locations

The location of the electronic processor system's electronic windows is extremely critical to the maximization of the discrimination areas. The location of the windows and their effect upon system performance are discussed in both Appendix A and Appendix B.

The three nucleonic systems' window locations for each of the test series are shown in Table 7. The breadboard and manufacturing prototype window locations, which were fixed, could not be experimentally verified. The laboratory standard electronic processor system had adjustable windows and pulse amplification for effectively locating the windows at precisely the desired energy levels.

The discrimination areas are critical functions of window location. If the two points of intersection of the superimposed isotope spectra in Channel 1 are selected for the low energy window, then the Channel 1 discrimination area is maximized for that isotope activity level and ratio. In Channel 2, if the point of rise to the high energy peak is chosen for the lower window location, then the discrimination area is maximized. The upper window location in Channel 2 is of minor importance, but must be located above 0.85 Mev, the point where both isotopes' spectra are very near zero.

Since the choice of window location is critical to the effective discrimination of the two isotopes, a means for adjusting these windows is critical to the effective measurement of char and virgin material attrition. The electronic processor windows, however, were fixed and could not be optimized. The laboratory system was optimized in Phase VIA, with outstanding accuracy resulting. The laboratory system's windows were broadened to approximate those of the breadboard electronic processor in Phase VIB, with an accompanying increase in system measurement error by a factor of three.

2.1.4 Isotope Activity Levels

The levels of activity for each isotope were selected to provide the lowest system measurement error commensurate with the optimum discrimination of the two isotopes. Ideally, an increase in the isotope's activity at a fixed time constant represents a decrease in the measurement uncertainty of the isotope's counting rate according to the following relationship:

$$E = (N\tau)^{\frac{1}{2}}$$

In a real system, however, the increase of isotope activity creates undesirable side effects which tend to negate the effectiveness of activity increase in lowering measurement uncertainties.

The choice of isotope activity levels and system time constant was based upon the ablation rate tracking errors and measurement uncertainty of the system. The effects of pulse pile up and d.c. baseline shift brought about by the electronic systems' inefficiencies were incorporated into the empirical analysis. Both theoretical and empirical analyses are discussed in Appendix A.

At a time constant of one second, a millicurie level of 1.0 for the In^{114m} isotope and of 0.1 for the $ZrNb^{95}$ isotope were found to maintain system measurement error at less than 4 per cent for the phenolic nylon tests and no greater than 5 per cent for the phenolic graphite tests for all nucleonic systems. The laboratory standard nucleonics system performed within the 5 per cent system measurement error at isotope activity levels as low as 0.8 mc of In^{114m} and 0.08 mc of $ZrNb^{95}$. The breadboard and prototype electronic processors were found to perform well at 1.0 mc of In^{114m} and 0.1 mc of $ZrNb^{95}$. However, since the manufacturing prototype unit's matched detector was less efficient than the breadboard system's, the isotope activities were increased by 10 per cent for this unit.

2.1.5 Signal Attenuation

The effects of signal attenuation were considerable on the three nucleonic systems. In Phase III it was found that these effects were twofold. Not only did the attenuation of the signal decrease the measurable activity in each channel, but it also tended to shift the measured isotope spectra to lower energy levels. A gain adjustment in the laboratory system was required to bring their spectral curves in line with their theoretical emission peaks.

The loss in measurable activity was compensated for by an increase in the two isotopes' millicurie levels; however, the spectra shift were not so easily accommodated. When the isotope spectra were shifted by signal attenuation, they tended to move to electronically measured lower energy levels which displaced them in relation to a pre set choice of windows and pulse amplification. When the pulse amplification could be adjusted to properly locate the emission peaks, the window locations could be fixed. The isotope discrimination in each channel was then only minimally affected, provided that the optimization of the discrimination areas was originally considered in the setting of the windows. If the windows were also adjustable and not fixed, the discrimination areas could again be optimized by adjusting the windows, and the isotope discrimination was further enhanced.

The change in pulse amplification caused two effects in the nucleonics system--the random signal error was amplified and the high energy emmission peak was displaced upward slightly when the low energy emmission peak was properly located. In general, these are minor effects, but they do affect the system measurement accuracy. It is imperative to employ every effort to reduce the signal attenuation in the nucleonics system so that maximum system accuracy can be achieved.

3.0 DEVELOPMENT OF SENSOR IMPREGNATION AND QUALITY CONTROL PROCEDURES

The development of rigid material selection criteria and strict adherence to sensor plug impregnation techniques were prerequisite to the successful proof testing of the dual ablation measurement technique. Quality assurance tests and impregnation procedures were established for the sensor plug materials--phenolic nylon and phenolic graphite--during the early phases of the contract and modified during the test phases. Consistent discrimination of the phenolic nylon material was particularly important because of density variations, while controlled temperature storage (below 32°F) was essential to maintain the quality of the unmolded phenolic graphite.

Models and plugs fabricated from phenolic graphite were exceptionally uniform. On the other hand, there were variations in the phenolic nylon. Because the phenolic nylon material was uneven in quality, even careful material selection could not entirely eliminate all density variation, which caused the lack of uniformity.

To minimize variations in sensor plug activity, density and uniformity, a precise step-by-step cookbook approach to quality control was adopted. Where applicable, quality assurance tests and test fixtures were incorporated.

Quality assurance and impregnation procedures and tests developed by TSI during the performance of Contract NAS1-8221 are included in detail in Appendix C. Uniformity curves for each model are also included in this appendix.

4.0 ELECTRONIC SYSTEM DEVELOPMENT AND EVALUATION

Three nucleonic systems were employed during the program performance. Two, the breadboard and manufacturing prototype dual ablation sensors, were fabricated under Contract NAS1-5342. The third, the laboratory standard nucleonic sensor, was partly purchased and partly fabricated by TSI in Phase IV of Contract NAS1-8221. The laboratory standard system was utilized to prove that the measurement of the material attrition by nucleonic techniques was not only feasible but attainable with readily available state-of-the-art hardware. It further served as a basis for comparison in evaluating the measurement accuracy of the breadboard and prototype dual ablation measurement systems.

The design of the laboratory system was similar to the design of the breadboard and prototype systems. The laboratory system is depicted in Figure 2. An interface module was incorporated into the laboratory standard nucleonic system to provide a simple means of operating the nucleonic equipment. This module included both external and internal power supplies. These and other system components are fully described in Appendix B.

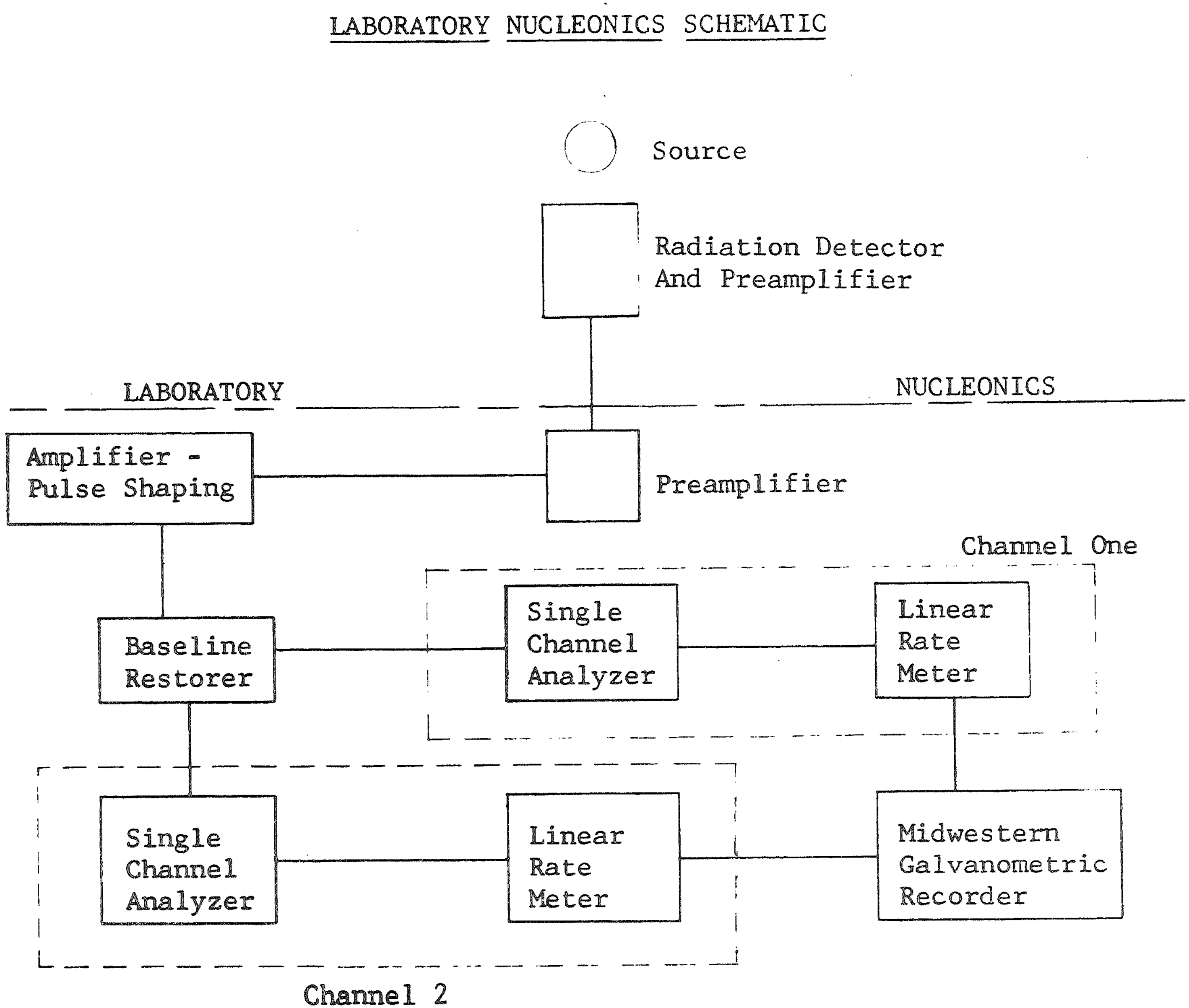

Figure 2, Laboratory Standard Nucleonics System Block Diagram

The evaluation of the measurement accuracy of the dual ablation measurement systems involved not only the three nucleonic sensing systems but also the supporting instrumentation of the two primary test facilities (the radiochemical laboratory at St. Louis University and Plasmadyne's plasma jet facility). Appendix B includes a description of the allied instrumentation at each of the test facilities and of equipment operation during plasma jet testing and calibration, as well as a discussion and comparison of the three nucleonic systems.

5.0 DESCRIPTION OF TEST MODELS AND TEST MODEL HOLDER

5.1 Test Models

To determine the performance of the ablation sensor system under simulated flight re-entry conditions, two representative re-entry materials were specified by the Government for the fabrication of the test models--phenolic nylon and phenolic graphite. Model designs were based on an analysis of the ablative performance of these materials, a review of the test objectives, and a study of the plasma jet facility capabilities. The test models were designed for the sensor plugs to fit without the use of adhesives or other foreign matter. A 0.010 inch step kept the sensor plug from being blown back and "press tight" fit and the plasma jet pressure prevented its moving forward during testing.

5.1.1 Phenolic Nylon Test Models

The phenolic nylon test models were 2.0 inch diameter cylindrical models with an "iso q" front surface. They were designed to provide an ablation rate which would thoroughly test the performance and accuracy of the dual ablation measurement system. A schematic of the phenolic nylon test model is depicted in Figure 3.

5.1.2 Phenolic Graphite Test Models

The phenolic graphite models were designed to simulate re-entry environments more severe than those of the phenolic nylon. Consideration of the general plasma jet nozzle flow field and the relative bulk of the test model holder led to the modification of the originally-planned 1.0 inch diameter cylindrical model. The final design, depicted in Figure 4, incorporated a 1.0 inch diamater "iso q" front surface with a conical body flaring to approximately 1.5 inches at the base.

5.2 Test Model Holder

The test model holder was developed to provide a THERMO-LAG coated, water-cooled housing to contain the radiation detector and provide a stable geometrical platform to which the test models could be attached. A schematic of the test model holder is depicted in Figure 5. The rear sting of the test models fit snugly into a one-inch diameter cavity in the front nose cap of the model

PHENOLIC NYLON

TEST MODEL

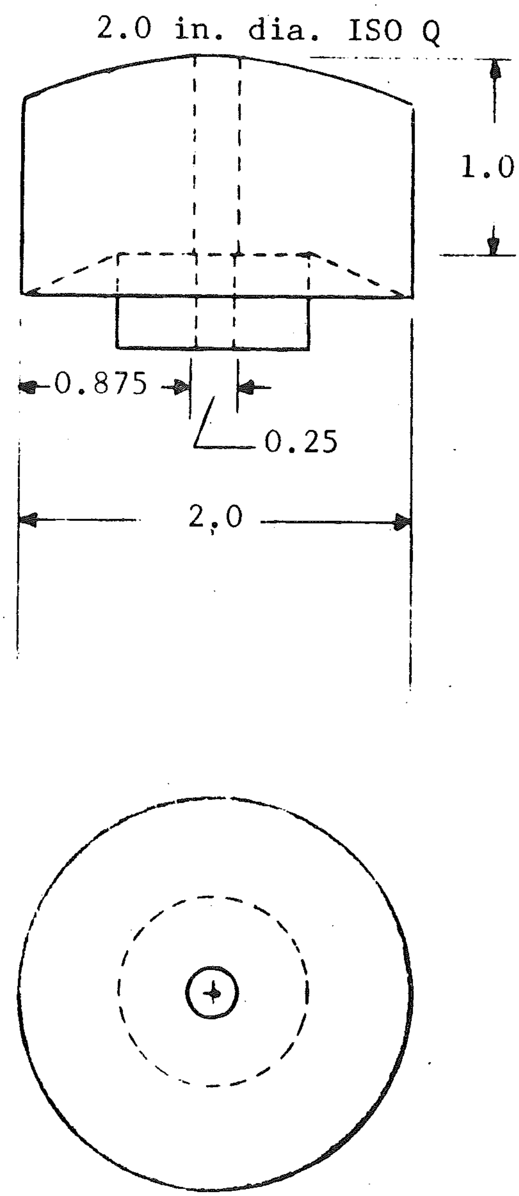

Figure 3. Phenolic Nylon Test Model.

PHENOLIC GRAPHITE

TEST MODEL

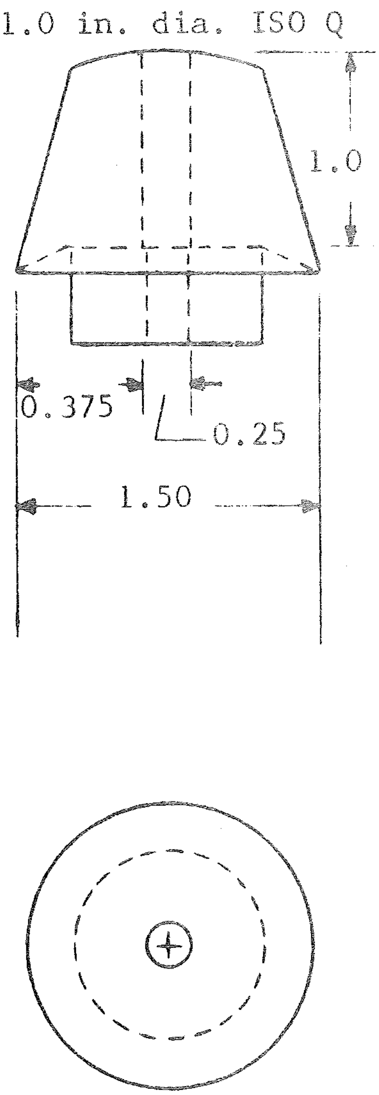

Figure 4. Phenolic Graphite
Test Model.

TEST MODEL HOLDER SCHEMATIC

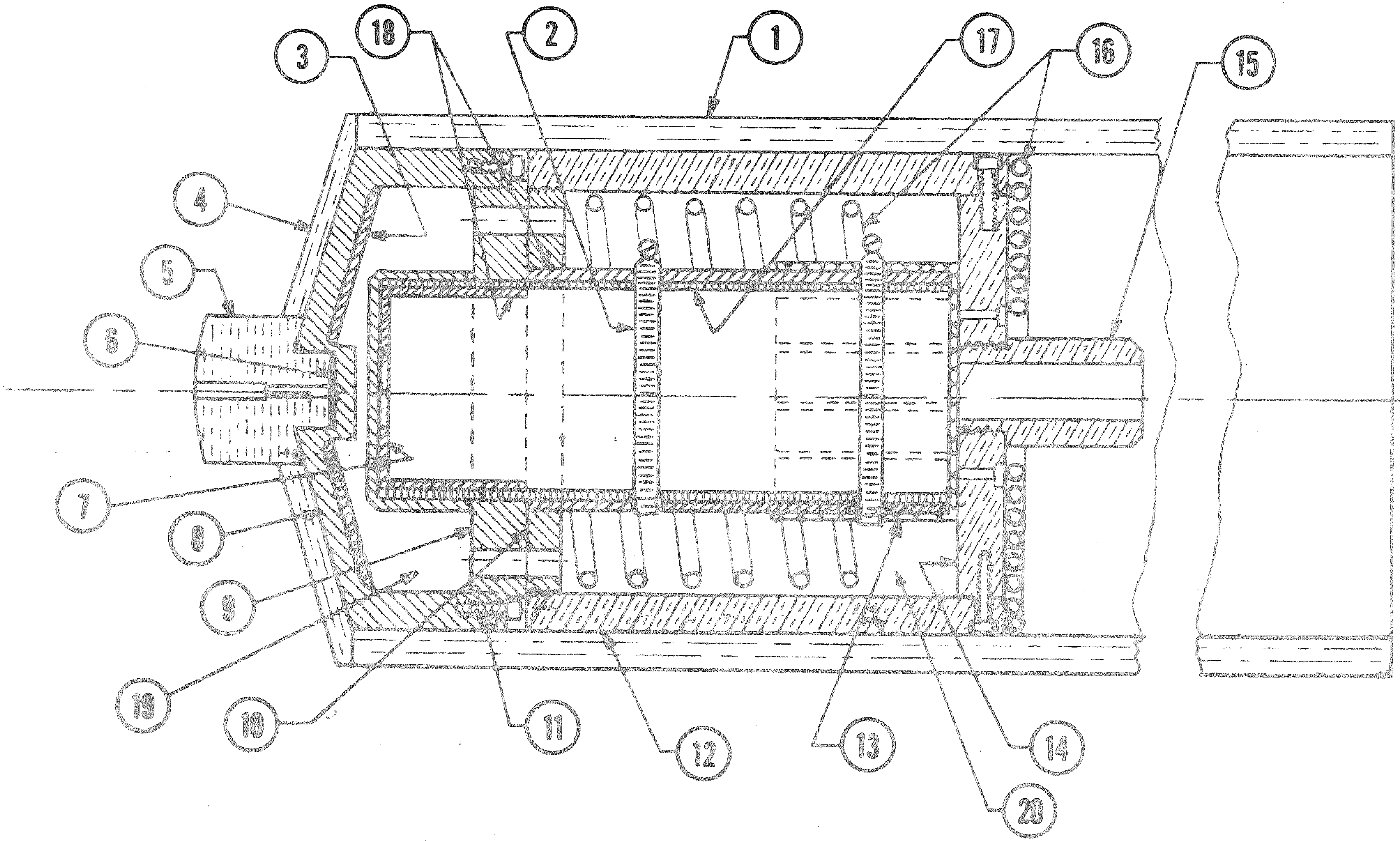

Figure 5. Test Model Holder Schematic.

TEST MODEL HOLDER

LIST OF MATERIALS

1	Thermal Protection Boot	THERMO-LAG T-500-6
2	Clamp, Screwdriver	Standard
3	Nose Cap Shielding	Lead
4	THERMO-LAG Nose Cap	THERMO-LAG T-500-6A
5	Test Model	Phenolic Nylon (Shown) Phenolic Graphite (Not Shown)
6	Contamination Washer	Phenolic Nylon
7	Washer Shield	Lead
8	Front Nose Cap	Copper
9	Rear Nose Cap	Copper
10	Nose Cap Bushing	Copper
11	10-32 X 3/4" Socket Screw	Brass
12	Main Barrel Section	Seamless Steel Tubing
13	Detector Mounting Bracket	Aluminum
14	Back Plate	Steel, Mild
15	Sting	Steel, 4130
16	Coils	Copper Tubing
17	E M Shielding	Netic, Conetic and Copper Foil Layers
18	Detector Shielding	Lead
19	Water Chamber	--
20	Insulation	Rock Wool

holder, assuring the positioning of each test model-sensor plug assembly in precisely the same location with respect to the radiation detector. The design of the test model holder was primarily dictated by the environmental restraints imposed by the radiation detector. Tunnel dimensions and model positioning with respect to the plasma jet nozzle restricted the overall holder length. The test model holder is fully described in Appendix E, with Figures E-1 through E-6 including schematics of the test model holder, the nose cap assembly, the detector shielding, and the hydrostatic test fixture as well as photographs of the radiation detector with and without shielding.

The results of the Phase V test series dictated certain modifications in the holder and detector design. The first modification involved the shielding of the detector assembly from the electromagnetic field within the plasma jet tunnel; the second was a minor change in the front nose cap to prevent water leaks in the holder's cooling chamber; and the third was an extension of the THERMO-LAG shroud and added cooling coils to prevent excessive heating of the back surface plate of the model holder. A description of these modifications is also included in Appendix E.

6.0 DESCRIPTION OF TEST FACILITIES

Two test facilities were used in the performance of Contract NAS1-8221: TSI's radiochemical laboratory at St. Louis University and the Plasmadyne plasma jet facility. TSI's radiochemical laboratory facility was employed for sensor plug impregnations, quality assurance tests, pre-test calibration tests, sensor plug fabrication, model sensor plug sectioning, photographing of sectioned models, and post test calibration tests. All plasma jet tests and some calibration tests were performed at Plasmadyne. Detailed descriptions of equipment employed at each facility are contained in Appendix D.

7.0 TEST PROGRAM

7.1 General

To proof test the dual ablation measurement technique, a test program was performed at a plasma jet facility capable of providing heating environments simulating those of vehicle re-entry. To determine the accuracy of the breadboard and prototype dual ablation measurement systems, a laboratory standard nucleonics system was employed. It was used both to replace the breadboard and prototype electronic processors in measuring material attrition by nucleonic techniques and in parallel with the breadboard electronic processors to simultaneously measure and evaluate the breadboard electronic processor systems during an actual ablation test.

The fully calibrated plasma jet facility at Plasmadyne (a division of Geotel, Inc.) in Santa Ana, California, was employed in the testing of the dual ablation measurement systems. A series of non-radioactive tests to determine the effect of the test environment on the test models and instrumentation and three series of radioactive proof tests were conducted.

Recognizing the potential hazards inherent in the use of radioisotopes, TSI developed safety and handling procedures in accord with AEC guidelines. These procedures were rigidly followed at all times during the handling, installation and use of radioactive sensor plugs for the radioactive type dual ablation measuring system. In addition, TSI required Plasmadyne to submit written procedures to be strictly adhered to in conducting the test program. TSI and Plasmadyne radioactive handling procedures are detailed in Appendix G.

7.2 Plasma Jet Tests

7.2.1 Phase V Calibration Tests

Phase V was devoted to the testing of eight non-radioactive models to determine the test model performance parameters. These parameters included the heating rate, surface temperature and char and virgin material ablation; the effect of the plasma jet test facility on the electronics systems; and the performance of the test model holder-test model test configuration.

Initially, three test points were selected for the plasma jet tests. The third test condition was found to be too severe from the aspect of shearing effects and a fourth test condition's high surface temperature resulted in non-uniform ablation. The fifth test point yielded a satisfactory condition and was designated. These five test conditions are depicted in Table 1. Table 2 describes the test conditions for each model tested.

7.2.2 Phase VIA Concept Accuracy Tests

The first radioactive test series, in Phase VIA, was designed to determine the feasibility of measuring the char and char-virgin material interface recession using the laboratory standard nucleonics system. Six valid tests were performed, two at each test condition, to evaluate the dual ablation measurement technique and determine its feasibility as a means of measuring material attrition by nucleonic techniques. Table 2 shows the test conditions for each model tested.

7.2.3 Phase VIB Concept Accuracy Tests

The second set of concept accuracy tests were used to confirm the Phase VIA test results, using the laboratory standard nucleonics system. Eight tests were conducted with instrumentation identical to that of Phase VIA except in one respect. The two channels' windows were widened to more closely approximate the breadboard and prototype electronic processors to facilitate their evaluation in Phase VII. Test conditions for each model tested are described in Table 2.

Table 1

PERFORMANCE DATA

FACILITY CALIBRATION

Model No.	Point	$\dot{q}$ (Btu/Ft^{2}Sec)	H (Btu/Lbm)	P (atm)	t (Sec.)	x_s (in.)	x_v (in.)
3PN	1	560	21800	.0494	62	.036	.426
6PN	1	563	21940	.0492	45	.010	.295
5PN	2	330	3000	.585	36	.151	.411
1PN	2	326	3020	.592	30	.130	.325
9A30T1	2	315	3120	.578	60	.439	.681
2PG	3	994	3300	4.01	29	.541	.671
1PG	3	993	3292	4.02	20	.424	.517
9A30T3	4	1249	5860	1.96	45	.108	.898
9A30T4	4	1259	5874	1.97	30	.046	.770
9A30T5	5	939	3485	2.97	40	.511	.781
9A30T6	5	943	3492	2.98	30	.382	.682

ENVIRONMENTAL TEST CONDITIONS

Test Model	Phase	Test Point	Cold Wall Heat Flux ($Btu/Ft^2 Sec$)	Stagnation Enthalpy (Btu/Lbm)	Stagnation Pressure (atm)	Test Duration (Seconds)	Surface Temp. (°F)	Avg. Char Recession Rate $\times 10^{+3}$ (In/Sec)	Avg. Char Recession Rate $\times 10^{+3}$ (In/Sec)
3PN	V	1	560	21800	.0494	62.0	4800	.0005806	.006871
6PN	V	1	563	21940	.0492	45.0	4400	.0002222	.006556
9A30C3	VIA	1	541	22432	.0342	50.0	4550	.0005400	.006640
9A30C5	VIA	1	548	22440	.0355	60.0	4450	.0003670	.005750
9A30C6	VIA	1	543	22440	.0355	70.0	4600	.0012430	.006386
9F15C9	VIB	1	542	22400	.0355	45.1	4000	.000643	.008758
9F15C16	VIB	1	535	22380	.0355	45.1	4100	.001264	.007228
9F15C19	VIB	1	542	22410	.0349	45.1	4000	.001220	.006851
9F15C11	VII	1	548	22430	.0355	42.2	4000	.000877	.009242
9F15C23	VII	1	546	22420	.0355	45.2	4100	.000796	.006792
1PN	V	2	326	3020	.592	30.1	3900	.004148	.011291
5PN	V	2	330	3000	.585	36.4	3800	.004319	.010797
9A30T1	V	2	315	3120	.578	60.0	4250	.007317	.011483
9A30C1	VIA	2	308	3084	.578	45.1	4200	.004945	.010665
9A30C4	VIA	2	310	3090	.575	43.8	4300	.004452	.009566
9A30C7	VIA	2	311	3100	.578	45.0	4250	.005578	.010689
9A30C9	VIA	2	312	3121	.576	45.0	4250	.005356	.010467
9F15C17	VIB	2	312	3115	.575	30.1	3900	.005548	.008049
9F15C20	VIB	2	318	3140	.578	45.0	4100	.009667	.013844

Test Model	Phase	Test Point	Cold Wall Heat Flux ($Btu/Ft^2 Sec$)	Stagnation Enthalpy (Btu/Lbm)	Stagnation Pressure (atm)	Test Duration (Seconds)	Surface Temp. (°F)	Avg. Char Recession Rate x 10^{+3} (In/Sec)	Avg. Char Recession Rate x 10^{+3} (In/Sec)
9F15C18	VII	2	314	3128	.575	30.1	4400	.005415	.015382
9F15C21	VII	2	314	3125	.574	31.2	4100	.005417	.012340
9F15C22	VII	2	312	3118	.574	35.1	4000	.005413	.011083
1PG	V	3	993	3292	4.02	20.0	4500	.021200	.025850
2PG	V	3	994	3300	4.01	28.6	4600	.0108916	.023462
9A30T3	V	4	1249	5860	1.96	45.2	5000	.002389	.019425
9A30T4	V	4	1259	5874	1.97	30.2	5300	.001523	.025695
9B04C2	VIA	4	1262	5890	1.98	30.1	5300	.001163	.016678
9B04C3	VIA	4	1260	5885	1.96	45.0	5300	.000778	.016556
9A30T5	V	5	939	3485	2.97	40.2	5250	.012711	.019428
9A30T6	V	5	943	3492	2.98	29.8	5400	.012819	.022215
9B04C4	VIA	5	934	3482	2.99	30.0	5100	.014867	.025290
9B04C6	VIA	5	944	3490	2.97	30.0	5400	.014133	.025467
9D17G1	VIB	5	944	3480	2.98	30.2	5350	.011225	.020497
9D17G2	VIB	5	940	3400	2.97	30.0	5200	.011533	.022067
9D17G3	VIB	5	956	3520	2.98	26.2	5200	.015458	.023626
9F23C23	VII	5	948	3490	2.98	30.0	5200	.011167	.017400
9F23C2	VII	5	950	3510	2.98	30.0	5250	.011367	.015367

7.2.4 Phase VII Breadboard Measuring System Tests

The last plasma jet test series consisted of seven valid radioactive tests serving to evaluate the measurement accuracy of the breadboard and prototype electronic processors. The laboratory standard nucleonics system was run in parallel with the breadboard and prototype electronic processor to simultaneously measure and evaluate the breadboard and prototype electronic processor systems' performance during the actual plasma jet tests.

Because of a malfunction in the manufacturing prototype's radiation detector, only the breadboard system was used. Some of the tests meant for the manufacturing prototype were made with the breadboard unit and some were made with the laboratory system, achieving a comprehensive evaluation of each of the two systems. Table 2 depicts the test conditions for each model tested.

7.3 Test Procedures

The test procedures followed for the Phase V, VIA, VIB, and VII test series were nearly identical. Calibration tests were performed at the radiochemical laboratory before and after each test series and the plasma jet tests were run in precisely the same order and with the same procedures during each test series.

7.3.1 Radiochemical Laboratory Pre-Test Calibrations

Prior to shipping the radioactive test models to Plasmadyne, a series of calibration and quality assurance tests were performed on each of the test models. In addition to those quality assurance tests performed during sensor and test model fabrication (Appendix C), physical measurements, nuclear activity measurements and nuclear spectra of each test and calibration model were taken. These data are shown in Tables 3 and 4 and in Appendices B and H. The pre-test physical measurement data are shown in Table 3; the pre-test nuclear activity measurement data are shown in Table 4; the fabrication quality assurance data are depicted in Table C-1 of Appendix C; and the nuclear pre-test spectra are shown in Figures H-32 to H-67 of Appendix H.

Sensors impregnated with only one isotope were measured. The nuclear spectral overlap data (isotope activity ratios - measuring the millicurie level of one isotope to that of the other) were calculated. The recession calibration measurement data were taken, employing the exact test and electronic configuration used in the plasma jet tests.

Since the test electronics configuration was varied during each test series, the nuclear pre-test activity, nuclear spectral overlap, and recession calibration data were measured for each test electronic configuration. In Phase VIA the laboratory standard nucleonics system

TABLE 3

PRE-TEST DATA

PHYSICAL MEASUREMENTS

Test Point	Test Model	Sensor Plug Diameter (inches)	Sensor Plug Length (inches)	Sensor Plug Weight (grams)	Test Model Front Surface Diameter (inches)	Test Model Rear Flange Diameter (inches)	Test Model Length (inches)	Test Model Weight (grams)
1	9A30C3	.250	0.982	.4302	2.001	2.001	1.499	34.6196
1	9A30C5	.249	0.985	.4303	1.998	1.998	1.491	34.7544
1	9A30C6	.249	0.987	.4345	2.001	2.001	1.497	31.9698
1	9F15C9	.250	1.005	.4450	2.000	2.000	1.500	35.5561
1	9F15C11	.250	1.010	.4644	2.002	2.002	1.503	36.2143
1	9F15C16	.250	0.998	.4401	2.001	2.001	1.499	35.3326
1	9F15C19	.251	1.016	.4657	2.002	2.002	1.504	36.2661
1	9F15C23	.249	1.008	.4453	1.998	1.998	1.449	35.2632
1	3PN	.250	1.001	.4654	2.000	2.000	1.500	34.9114
1	6PN	.251	1.000	.4588	2.000	2.000	1.500	34.5007
2	9A30C1	.250	0.981	.4365	2.000	2.000	1.496	33.1076
2	9A30C4	.250	0.979	.4270	1.999	1.999	1.499	35.1300
2	9A30C7	.250	0.981	.4332	2.001	2.001	1.494	33.5370
2	9A30C9	.251	0.981	.4261	2.001	2.001	1.501	32.0811
2	9A30T1	.251	0.999	.4603	1.999	1.999	1.501	33.1613
2	9F15C17	.248	1.001	.4370	1.999	1.999	1.501	34.6941
2	9F15C18	.250	1.008	.4496	1.998	1.998	1.498	33.1607

Test Point	Test Model	Sensor Plug Diameter (inches)	Sensor Plug Length (inches)	Sensor Plug Weight (grams)	Test Model Front Surface Diameter (inches)	Test Model Rear Flange Diameter (inches)	Test Model Length (inches)	Test Model Weight (grams)
2	9F15C20	.251	1.016	.4657	2.002	2.002	1.504	36.2661
2	9F15C21	.250	1.005	.4420	1.997	1.997	1.498	32.4513
2	9F15C22	.249	1.009	.4521	2.001	2.001	1.498	36.4575
2	1PN	.251	1.000	.5200	2.000	2.000	1.501	34.3856
2	5PN	.251	1.001	.4927	2.000	2.000	1.503	33.2565
3	1PG	.250	0.999	1.0996	1.000	1.500	1.499	30.7319
3	2PG	.249	1.001	1.0956	1.000	1.500	1.506	31.3060
4	9A30T3	.249	0.988	1.0783	1.047	1.500	1.498	33.1773
4	9A30T4	.249	1.001	1.0759	1.049	1.500	1.501	33.6721
4	9B04C2	.251	1.005	1.0785	1.047	1.499	1.501	34.3703
4	9B04C3	.250	1.002	1.0832	1.065	1.500	1.501	35.3885
5	9A30T5	.249	1.001	1.0839	1.050	1.500	1.503	34.1201
5	9A30T6	.250	1.002	1.0972	1.050	1.500	1.500	34.0533
5	9B04C4	.2505	1.006	1.0950	1.030	1.499	1.502	33.8845
5	9B04C6	.250	1.004	1.0637	1.010	1.495	1.501	33.1145
5	9D17G1	.250	0.999	1.0393	1.000	1.500	1.498	34.4350
5	9D17G2	.251	1.012	1.0566	1.001	1.500	1.501	35.4561
5	9D17G3	.251	1.005	1.0616	1.000	1.500	1.500	35.2825
5	9F23C23	.251	1.002	1.0523	1.001	1.499	1.500	35.2372
5	9F23C24	.250	1.001	1.0467	1.001	1.501	1.499	34.9893

TABLE 4

PRE-TEST DATA

NUCLEAR MEASUREMENTS

Test Point	Test Model	Test Model Activity In^{114m} mc	Test Model Activity $ZrNb^{95}$ mc	Test Model Activity Channel 1 cps	Test Model Activity Channel 2 cps	Test Model Activity Channel 3 volts	Test Model Activity Channel 4 volts
1	9A30C3	1.110	.1065	17700	8050	- -	- -
1	9A30C5	1.120	.1080	17300	8750	- -	- -
1	9A30C6	1.121	.1080	18400	10000	- -	- -
1	9F15C9	.811	.0810	13050	15450	6.57	2.68
1	9F15C11	.795	.0800	12750	14750	6.59	2.68
1	9F15C16	.915	.0910	14150	17000	6.86	2.94
1	9F15C19	.912	.0900	14150	16950	6.83	2.92
1	9F15C23	.989	.0990	17250	21950	9.93	3.91
2	9A30C1	1.125	.1085	17800	9500	- -	- -
2	9A30C4	1.100	.1060	16500	9400	- -	- -
2	9A30C7	1.120	.1080	17800	8500	- -	- -
2	9A30C9	1.120	.1080	17700	8500	- -	- -
2	9F15C17	.780	.0800	12150	14150	6.31	2.44
2	9F15C18	.702	.0702	11150	12850	6.04	2.15
2	9F15C20	1.069	.1069	18200	25000	10.50	4.41
2	9F15C21	1.120	.1120	19250	26450	10.72	4.70
2	9F15C22	1.005	.1005	18850	25150	10.59	4.52

Test Point	Test Model	Test Model Activity In^{114m}	Test Model Activity $ZrNb^{95}$	Test Model Activity Channel 1	Test Model Activity Channel 2	Test Model Activity Channel 3	Test Model Activity Channel 4
		mc	mc	cps	cps	volts	volts
4	9B04C2	.658	.0654	15700	6200	- -	- -
4	9B04C3	.653	.0649	16200	8200	- -	- -
5	9B04C4	.664	.0660	16400	7300	- -	- -
5	9B04C6	.605	.0602	13300	6700	- -	- -
5	9D17G1	1.000	.1000	12300	16850	- -	- -
5	9D17G2	1.000	.1000	11820	16700	- -	- -
5	9D17G3	1.000	.1000	10680	13950	- -	- -
5	9F23C23	1.000	.1000	18700	13400	7.84	2.57
5	9F23C24	1.000	.1000	21800	14800	8.18	2.68

was used to measure the char and virgin material attrition histories. Windows were set at 0.15 Mev to 0.23 Mev and 0.65 Mev to 1.00 Mev for the two channels, and all nuclear calibration data employed these settings for the nucleonics.

In Phases VIB and VII, the laboratory standard nucleonics system was used for a portion of the tests and the breadboard dual ablation measurement system in parallel with the laboratory system for the remainder. In order to approximate the breadboard system's electronic windows, the laboratory nucleonics window settings were maintained at 0.15 Mev to 0.25 Mev and 0.30 Mev to 1.00 Mev for all the Phase VIB and VII tests. The gain of the laboratory nucleonics system was adjusted to account for the spectrum shift of the breadboard unit when using the two in parallel.

Essentially, there were four different sets of nuclear calibration data: for Phase VIA, for the singular operation of the laboratory nucleonics system in Phase VIB, for the parallel operation of the laboratory nucleonic and breadboard systems in Phase VII, and for the breadboard nucleonics system in Phase VII.

Upon the completion of the pre-test series measurements at the radiochemical laboratory, the calibration and test models and the test electronics were packaged and shipped to Plasmadyne.

7.3.2 Plasmadyne Pre-Test Procedures and Calibrations

Before actual plasma jet testing, the radiation detector was inserted into the test model holder and the holder assembled. Thermocouples, thermal protection boot, and cooling water coils were attached to the holder and the assembly was placed in the plasma jet tunnel. The nucleonic extension cable was attached to the detector output connectors and the thermocouples were attached to the recorder leads. A cold test model was placed in the test model holder and the configuration was centered with respect to the plasma jet exhaust nozzle.

The electronic-nucleonic systems were then assembled, activated and allowed to warm up for thirty minutes prior to testing. The recorders were then calibrated to determine full scale and zero scale voltage in Channels 1 and 2 for the linear rate meter output and the slope (volts/inches) of Channels 3 and 4 for the breadboard nucleonics system voltage output. Appendix H describes these calibration procedures in detail.

The nuclear spectral overlap data were taken and the recession calibration tests for that day's testing were performed. Calibration data for each electronic configuration were again required. The pre-test pictures, test model weights and measurements were taken and recorded.

7.3.3 Plasmadyne Test Procedures

Prior to beginning the radioactive tests, the following data were taken:

- Background activity data
- Singular isotope test models' activity data
- Test model initial activity data
- Full scale settings on linear rate meters
- Amplification settings on breadboard electronics
- Time constant settings (breadboard and laboratory electronics)
- Test model holder temperature (both thermocouples)
- Test model orientation check.

During testing, the test model was monitored through view points and irregularities were noted on the data sheets. The following data were taken during each test:

- Recorder traces, test model activity history
- Motion pictures
- Test model surface temperature
- Test model holder temperature
- Cold wall heat flux
- Stagnation enthalpy
- Stagnation pressure
- Test duration.

After each test the following data were taken:

- Test model final activity data
- Background activity data

Test model post test pictures

Test model weight and dimensions

Test model holder temperature change (both thermocouples)

Recession calibration test (both isotopes at end of each day's testing).

The test model holder was visually inspected after each test to determine whether or not its thermal protection material required refurbishing.

7.3.4 Radiochemical Laboratory Post Test Calibrations

After the completion of each test series the following measurements were performed at TSI's radiochemical laboratory:

Test model nuclear post test activity data

Nuclear spectral overlap data

Nuclear post test spectra measurements

Sectioned test model physical measurements (virgin and char material thicknesses)

Sectioned model photographs.

As in the previous nuclear measurements, all test electronic configurations were used in determining the post test nuclear data.

The test models were sectioned in a saw fixture within the glove box at the radiochemical laboratory. After sectioning, the models' char and virgin material thicknesses were measured under magnification and the data recorded. The sectioned test models were then photographed and stored.

The post test data measurements are shown in Table 3 (nuclear post test activity and physical measurements) and in Appendix H (post test spectra, Figures H-68 through H-96).

SECTION III

DATA REDUCTION

1.0 INTRODUCTION

During Phase III of Contract NAS1-8221, methods for effectively reducing the nuclear output data from the dual ablation measurement system were developed. The overall measurement technique was analyzed and parameters prerequisite to the accurate representation of the char and virgin material recession were determined. In examining the combined spectra of the In^{114m} and $ZrNb^{95}$ isotopes, a scalar representation of the two individual spectrums was found. This led to the development of a data reduction technique markedly superior to that employed in Contract NAS1-5342.

Through the effective use of the nuclear overlap and singular isotope recession calibration data, the spectrums of each isotope could be separated within each of the windows. The discrimination of the two isotopes in each channel was realized by using the nuclear overlap data to determine the initial distribution of Channel 1 and 2 activity between the two isotopes and then developing a set of recession calibration curves to determine the nuclear overlap and activity of each isotope as functions of sensor length. Since the variation of nuclear overlap with sensor length was substantial, incorporating the nuclear overlap data within the recession calibration data resulted in significantly improved system accuracy. This juxtaposition of data also precluded the necessity of applying the nuclear overlap data at each step in the material recession history solution.

The typical variation of the nuclear overlap between Channels 1 and 2 for each of the two isotopes is depicted in Figures 6 and 7. These figures indicate that the substantial variation at the lower sensor length has a significant effect on the char and virgin material determinations.

2.0 DATA REDUCTION METHODS

The traces from the Midwestern recorder at Plasmadyne were measured, recorded and input to a data reduction computer program especially developed for use with the dual ablation sensor system. The program, described in Appendix K, incorporated the following data into a calibration technique which yielded material recession history as a function of test exposure:

Nuclear overlap data
Raw data trace
Background activity data
Recession calibration data.

An iterative solution to the data at each second of exposure time assured the attainment of valid solutions.

ISOTOPE NUCLEAR OVERLAP DATA

Phenolic Graphite

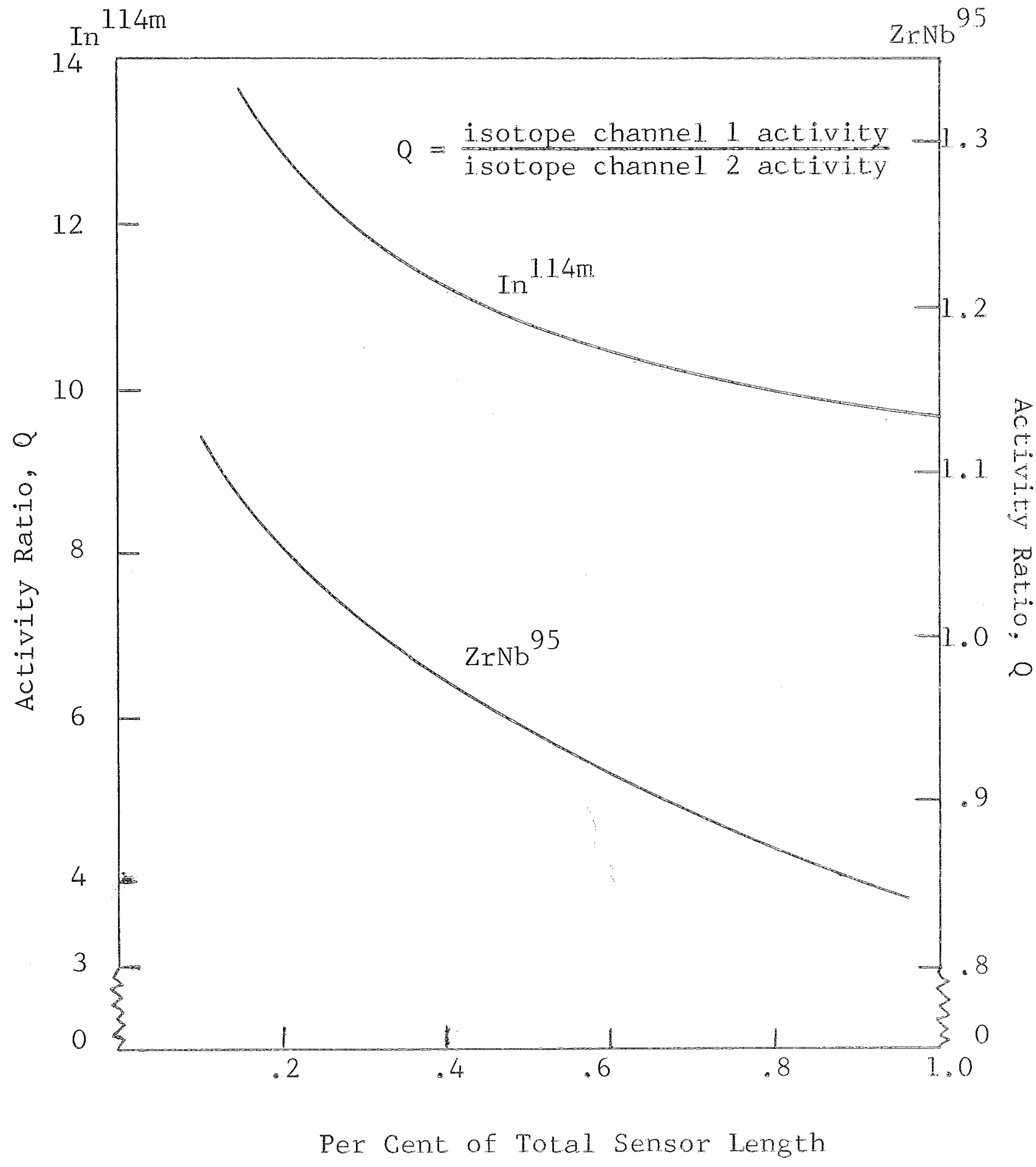

Figure 6

ISOTOPE NUCLEAR OVERLAP DATA

Phenolic Graphite

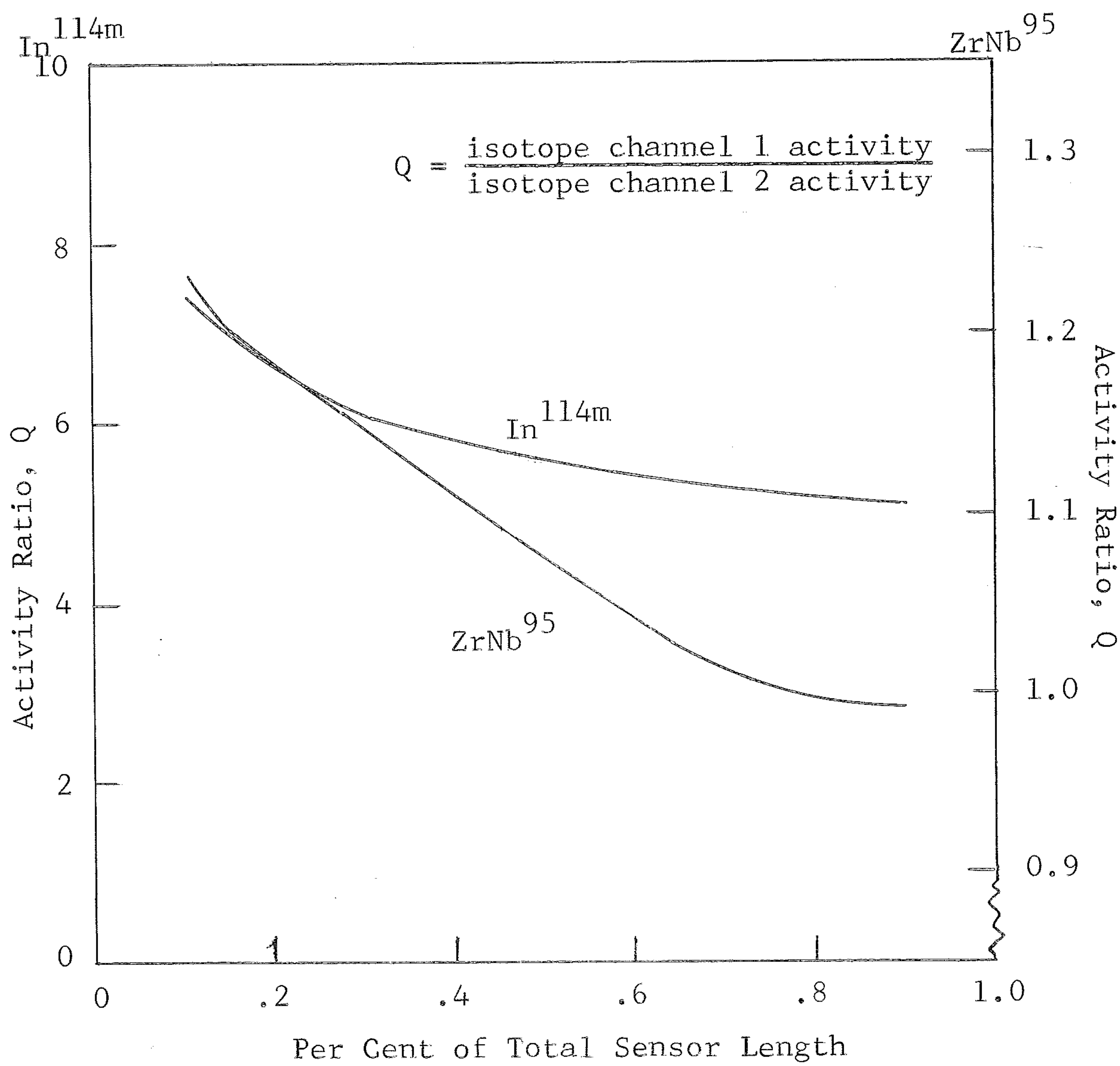

Figure 7

Interpolative routines were incorporated within the recession calibration data tables to allow the computer to step through each plasma jet test history as quickly and accurately as possible.

The material recession histories were plotted as functions of exposure time. The results were compared with the post test measurements of sensor char and virgin material thicknesses. The percentage of measurement error, based on the initial sensor length, was calculated and the data recorded.

In reducing the breadboard electronics voltage history traces (Channels 3 and 4), two assumptions were used in determining the material recession histories. These assumptions were necessitated by the designed circuitry of the electronic processors, which excluded voltages less than 0.45 volts in their measurement. Since the In^{114m} isotope recession calibration sensor's activity in Channel 4 was less than 0.45 volts, no recession calibration data were recorded for the In^{114m} sensor in Channel 4. The laboratory nucleonics system data indicated that the In^{114m} recession sensor was providing some activity in Channel 4. Therefore two data reduction methods were utilized in determining the char and virgin material recession of the breadboard tested sensors. In one method the In^{114m} voltage in Channel 4 was assumed to be zero; in the other, the voltage was assumed to be a function of the In^{114m} voltage in Channel 3. Both assumptions were applied in the data reduction, and both sets of data are reported.

3.0 DATA INPUTS

3.1 Raw Data Traces

The raw data traces were measured at one second intervals and recorded. From these data, the zero output deflections (inches) were subtracted and the results recorded. Using the following equation, the full scale deflections of the linear rate meters were employed to determine the counting rates in Channel 1 and 2:

$$N_i = \frac{(L_i - L_o)}{(L_f - L_o)} * N_f$$

where i is the data measurement at any time, t_i.

The electronic processor output data were recorded on Channels 3 and 4. Their calibrations were not functions of full scale deflections, but straight line curves having slopes of 1.604 volts per inch in Channel 3 and 0.956 volts per inch in Channel 4. When reducing the Channel 3 and 4 data to voltage, the following equations were used:

Channel 3 $\qquad V_i = 1.604 \ (L_i - L_o)$

Channel 4 $\qquad V_i = 0.956 \ (L_i - L_o)$

The Channel 3 and 4 voltages were converted to the same relative gain settings. For gain settings other than coarse 4, fine 6 (available on the electronic processors), a correction factor was applied to the data. For example, the gain settings for Test Model 9F15C11 on Channel 3 were coarse 3, fine 6. A factor of 1.5, obtained from Table H-3 by dividing 8.67 (coarse 4, fine 6) by 5.78 (coarse 3, fine 6), was used to increase the 3.448 volts of the recorder to the 5.712 volts applied in the data reduction. Since the electronic processor output amplifiers lose their linearity above 4.0 volts, the 5.712 voltage was not actually realizable. However, for data reduction purposes the Channel 3 and 4 output voltages were made compatible through conversion to a constant gain setting (coarse 4, fine 6).

3.2 Background Activity Data

The influence of background activity in each channel was subtracted from the raw data to obtain an activity measurement above background in each channel. In some cases the background was appreciable, representing as much as 16 per cent of the total counting rate; however, in thirty-four of thirty-seven Phase VIA, VIB, and VII model tests, the effect of background activity was negligible.

Variation in background activity during testing, which was not measurable with the present system, was disregarded. With the exception of the five graphite tests in Phases VIB and VII, variation had no effect on measurement accuracy.

A more detailed analysis of the effects of background activity on the output data are included in Appendix H.

3.3 Model Activity Histories

The data, corrected for background effects, were ratioed to the initial test model activity in each channel. A fraction of the initial activity above background for each test model was obtained for each second of elapsed time. Appendix I includes data for each test model.

SECTION IV

DISCUSSION OF RESULTS

1.0 ACCURACY OF NUCLEONIC SYSTEMS MEASUREMENT

Post test data for each model are depicted in Table 5. System performance data for the Phase VIA, VIB and VII test series are presented in Table 6. As depicted, measurement accuracy was greatest when the laboratory nucleonics system was most nearly optimized.

In Phase VIA, where the laboratory nucleonics system was optimized to achieve maximum system accuracy, the average overall errors were 1.4 per cent for the char recession measurement and 2.2 per cent for the virgin material recession measurement in the phenolic nylon model tests. In the phenolic graphite tests, average overall errors were 3.1 per cent for the char recession measurement and 3.2 per cent for the virgin material recession measurement. Since a portion of the measurement inaccuracy is attributable to the radiation detector and the fabrication and impregnation of the sensors, these results indicate remarkable system accuracy.

In Phase VIB, the laboratory standard nucleonics system was optimized except that the windows approximated the breadboard electronic processors' configuration. Measurement errors were less than 4 per cent for both of the recession (char and char-virgin material interface) in each of the two materials. The laboratory nucleonics

TABLE 5

POST-TEST DATA

Test Point	Test Model	Sensor Plug Length (inches)	Virgin Material Thickness (inches)	Test Model Activity Channel 1 (cps)	Test Model Activity Channel 2 (cps)	Test Model Activity Channel 3 (volts)	Test Model Activity Channel 4 (volts)
1	9A30C3	0.955	0.650	14700	7800	- -	- -
1	9A30C5	0.963	0.640	13800	8400	- -	- -
1	9A30C6	0.900	0.540	14200	9250	- -	- -
1	9F15C9	0.976	0.610	8100	13600	5.40	1.80
1	9F15C11	0.973	0.620	7300	9400	4.65	1.35
1	9F15C16	0.941	0.672	10100	14400	6.23	2.15
1	9F15C19	0.961	0.707	10000	14300	6.08	2.10
1	9F15C23	0.972	0.701	12600	17200	7.28	2.80
1	3PN	0.965	0.575	- -	- -	- -	- -
1	6PN	0.990	0.705	- -	- -	- -	- -
2	9A30C1	0.758	0.500	12200	7200	- -	- -
2	9A30C4	0.784	0.560	12500	8000	- -	- -
2	9A30C7	0.730	0.500	12250	6650	- -	- -
2	9A30C9	0.740	0.510	11300	6851	- -	- -
2	9A30T1	0.560	0.310	- -	- -	- -	- -
2	9F15C17	0.834	0.638	7200	8800	4.28	1.06
2	9F15C18	0.845	0.545	7200	8700	4.43	1.30
2	9F15C20	0.560	0.372	9600	14100	B	B

Test Point	Test Model	Sensor Plug Length (inches	Virgin Material Thickness (inches)	Test Model Activity Channel 1 (cps)	Test Model Activity Channel 2 (cps)	Test Model Activity Channel 3 (volts)	Test Model Activity Channel 4 (volts)
2	9F15C21	0.836	0.620	12500	17200	7.43	2.95
2	9F15C22	0.819	0.620	12200	16800	7.20	2.80
2	1PN	0.870	0.675	- -	- -	- -	- -
2	5PN	0.850	0.590	- -	- -	- -	- -
3	1PG	0.575	0.482	- -	- -	- -	- -
3	2PG	0.460	0.330	- -	- -	- -	- -
4	9A30T3	0.880	0.110	- -	- -	- -	- -
4	9A30T4	0.955	0.225	- -	- -	- -	- -
4	9B04C2	0.810	0.520	9200	5700	- -	- -
4	9B04C3	0.690	0.257	6200	5900	- -	- -
5	9A30T5	0.490	0.220	- -	- -	- -	- -
5	9A30T6	0.620	0.340	- -	- -	- -	- -
5	9B04C4	0.602	0.312	10100	5200	- -	- -
5	9B04C6	0.580	0.260	7250	4400	- -	- -
5	9D17G1	0.660	0.380	6200	10700	4.58	1.40
5	9D17G2	0.666	0.350	6000	9500	4.35	1.30
5	9D17G3	0.600	0.386	6050	9100	4.13	1.15
5	9F23C23	0.667	0.480	6500	7100	3.90	0.95
5	9F23C24	0.660	0.540	6000	7600	4.43	1.00

Table 6

SYSTEM PERFORMANCE DATA SUMMARY

Test Model	Test Point	Nucleonic System		Sensor Length			Virgin Material Thickness		
		Type	Phase	Measured (inches)	Nucleonic (inches)	Percent Error (%)	Measured (inches)	Nucleonic (inches)	Percent Error (%)
9A30C3	1	LAB	VIA	.955	.936	1.93	.650	.652	0.20
9A20C5	1	LAB	VIA	.963	.929	3.45	.640	.620	2.03
9A30C6	1	LAB	VIA	.900	.895	0.51	.540	.565	2.55
9F15C9	1	LAB	VIB	.976	.971	0.51	.610	.569	4.18
9F15C11	1	BB-1	VII	.973	.985	1.19	.620	.602	1.78
	1	BB-2	VII	.973	.913	5.94	.620	.626	0.59
	1	BB-3	VII	.973	.934	3.86	.620	.650	2.97
9F15C16	1	LAB	VIB	.941	.969	2.81	.672	.716	4.41
9F15C19	1	LAB	VIB	.961	1.009	4.72	.707	.737	2.95
9F15C23	1	BB-1	VII	.972	.996	2.38	.701	.766	6.45
	1	BB-2	VII	.972	.953	1.88	.701	.797	9.52
	1	BB-3	VII	.972	.960	0.79	.701	.815	11.31
9A30C1	2	LAB	VIA	.758	.701	5.81	.510	.517	0.71
9A30C4	2	LAB	VIA	.784	.781	0.31	.560	.564	0.41
9A30C7	2	LAB	VIA	.730	.731	0.10	.500	.529	2.96
9A30C9	2	LAB	VIA	.740	.746	0.61	.510	.541	3.16
9F15C17	2	LAB	VIB	.834	.864	3.00	.638	.517	11.89

Test Model	Test Point	Nucleonic System Type	Nucleonic System Phase	Sensor Length Measured (inches)	Sensor Length Nucleonic (inches)	Sensor Length Percent Error (%)	Virgin Material Thickness Measured (inches)	Virgin Material Thickness Nucleonic (inches)	Virgin Material Thickness Percent Error (%)
9F15C18	2	BB-1	VII	.845	.841	0.40	.545	.533	1.19
	2	BB-2	VII	.845	.717	12.70	.545	.485	5.95
	2	BB-3	VII	.845	.729	11.51	.545	.507	3.77
9F15C20	2	LAB	VIB	.560	.597	3.72	.372	.363	0.90
9F15C21	2	BB-1	VII	.836	.831	0.50	.620	.653	3.28
	2	BB-2	VII	.836	.773	6.27	.620	.747	12.64
	2	BB-3	VII	.836	.772	6.37	.620	.766	14.53
9F15C22	2	BB-1	VII	.819	.853	3.37	.620	.598	2.18
	2	BB-2	VII	.819	.791	2.78	.620	.620	0
	2	BB-3	VII	.819	.801	1.78	.620	.606	1.39
9B04C2	4	LAB	VIA	.810	.870	5.97	.520	.518	0.20
9B04C3	4	LAB	VIA	.690	.735	4.49	.257	.110	14.67
9B04C4	5	LAB	VIA	.602	.636	3.39	.312	.348	3.59
9B04C6	5	LAB	VIA	.580	.551	2.90	.260	.289	2.90
9D17G1	5	LAB	VIB	.660	.671	1.10	.380	.402	2.20
9D17G2	5	LAB	VIB	.666	.665	0.10	.350	.384	3.36
9D17G3	5	LAB	VIB	.600	.627	2.69	.386	.467	8.06

Test Model	Test Point	Nucleonic System		Sensor Length			Virgin Material Thickness		
		Type	Phase	Measured (inches)	Nucleonic (inches)	Percent Error (%)	Measured (inches)	Nucleonic (inches)	Percent Error (%)
9F23C23	5	BB-1	VII	.667	.646	2.08	.480	.481	0.10
	5	BB-2	VII	.667	.620	4.66	.480	.415	6.45
	5	BB-3	VII	.667	.622	4.46	.480	.456	2.38
9F23C24	5	BB-1	VII	.660	.629	3.10	.540	.547	0.70
	5	BB-2	VII	.660	.661	0.10	.540	.418	12.19
	5	BB-3	VII	.660	.668	0.80	.540	.460	7.99

NOTE: LAB = laboratory standard nucleonics output data system

BB-1 = laboratory and breadboard system in parallel, laboratory output data

BB-2 = laboratory and breadboard system in parallel, laboratory output data with $In^{114m} = F(In^{114m})$

BB-3 = laboratory and breadboard system in parallel, laboratory output data with $In^{114m} = 0$.

system established that it could track the sensor's surface and its char-virgin material interface within an accuracy of 96 per cent even in a non-optimized configuration.

Phase VII was utilized to establish the measurement accuracy of the breadboard processors. In this phase the breadboard and laboratory systems were run in parallel in order to evaluate the performance of the breadboard nucleonics system during each second of test exposure. The laboratory nucleonics system was adjusted to simulate the reported window locations of the breadboard system as closely as possible. The overall measurement error of the breadboard system was almost 6 per cent for the char recession measurement and almost 7 per cent for the char-virgin material recession measurement. These measurements were within acceptable limits for a non-optimized system, but could have been considerably improved with the addition of a gain adjustment to the breadboard system. This adjustment, which was not available, would have made it possible to correct the shifts in apparent energy level to maintain effective discrimination between the fixed window locations. In most instances the laboratory system was superior to the breadboard system in measurement accuracy; however, the performance of both electronic processors was degraded because of circuitry difficulties in the breadboard system.

2.0 RESULTS OF PLASMA JET TESTS

2.1 General

Four series of tests were performed at the Plasmadyne plasma jet facility. Phase V was devoted to calibration tests; Phases VIA and VIB to establishing and proving the accuracy of the dual ablation concept; and Phase VII to evaluating the measurement accuracy of the breadboard dual ablation measurement system. Table 1 depicts facility calibration data; Table 2, the environmental test conditions; and Table 3, pre-test physical measurements comprised of sensor plug length and diameter. Table 4 contains before test nuclear measurements used in the initial data reduction. Post test data for each of the models tested, including sensor plug length, virgin material thickness and activities in the two channels as measured in cps and volts, are depicted in Table 5. The summary of system performance in terms of sensor lengths and virgin material thicknesses (measured physically and nucleonically) and corresponding per cent errors between the two systems are presented in Table 6. Material recession histories for models not specifically discussed in the following paragraphs are depicted at the end of this section. (Figures 16-51). Test model temperature and nucleonic data histories are contained in Appendix I; and the before test, after test and sectioned model pictures comprise Appendix J.

Because of the relatively small surface recession experienced at test point 1, radioactive tests proved least accurate in predicting surface recession of the test models at this test point. On the other hand, virgin material recession predictions were accurate at this test condition, particularly in Phase VIA.

Char-surface recession measurement inaccuracies at test point 1 were chiefly attributable to the relatively slight depletion of the $ZrNb^{95}$ activity in Channel 2. Since background activity measurements were equal to as much as 60 per cent of the total activity loss of the $ZrNb^{95}$ isotope in Channel 2, the background activity uncertainty contributed significantly to the measurement errors. As shown in Table H-2 of Appendix H, the magnitude of the background activity was approximately 300 cps in Phase VIA and approximately 600 cps in Phase VIB and VII, representing uncertainties due to background activity of 20 and 50 cps. In addition, the counting rate uncertainty in Channel 2 was circa 320 cps, making a total uncertainty of 340 to 370 cps for the tests. With these counting rates greater than the total $ZrNb^{95}$ depletion, the char-surface measurements were actually surprisingly accurate.

An example of a model tested at test point 1 is model 9A30C3, a phenolic nylon model which was exposed to a heat flux of 541 Btu/sec/ft^2 for a period of 50 seconds. It exhibited a surface temperature of 4550°F. The real time recessions for the virgin and char phases of the model as obtained by laboratory nucleonic measurements during test, in concert with physical measurements after test, are depicted in Figure 8. The dimensions of the sensor plug after test were physically measured at .955", yielding a 1.93 per cent error. The

TEST MODEL PERFORMANCE DATA

MATERIAL RECESSION HISTORY

Phase VIA

Laboratory Nucleonics System

Model No. 9A30C3

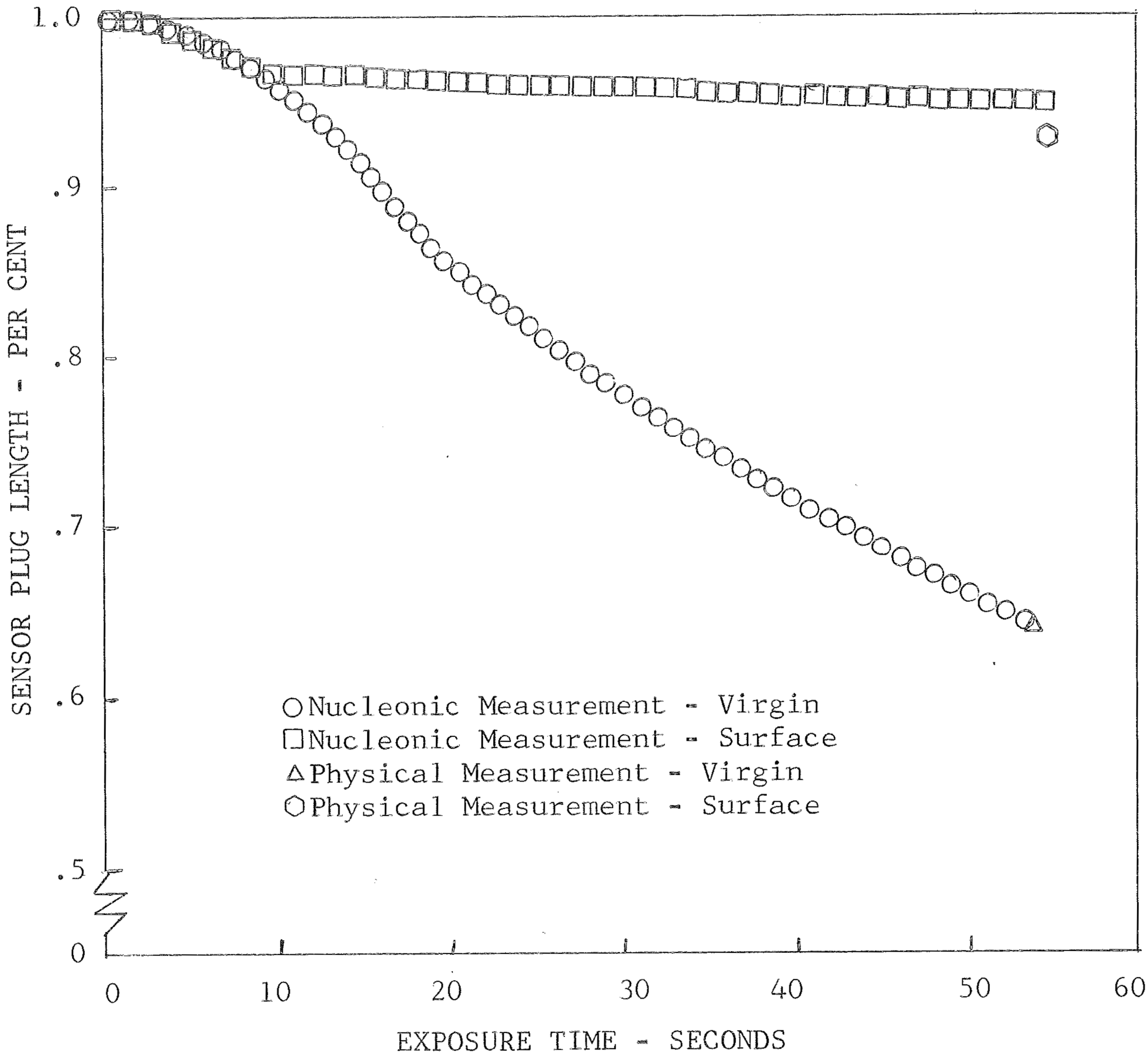

Figure 8

virgin material was measured physically at .650" in comparison with the nucleonic measurement of .652", for a 0.020 per cent error. This data is found in Table 6 and is in concert with data obtained in Tables 3, 4 and 5. Before and after test photographs of Model 9A30C3, including a cross section, are depicted in Figure 9.

Test point 2 proved easier for both the char and virgin material recession measurements. In general, the measurement accuracy was consistently higher than that obtained at test point 1. An examination of the depletion of both isotopes' activity in both channels shows that measurement uncertainties represent only a fraction of the total count rate loss due to material attrition.

An example of a model tested at Test point 2 was Model 9F15C18, a phenolic nylon model which was exposed to a heat flux of 314 Btu/SecFt^2 for a period of 30.1 seconds. The measured surface temperature was 4400°F. The real time recessions for the virgin and char systems as obtained by the breadboard measurements and compared with physical measurements obtained after test are depicted in Figure 10. The sensor plug length after test was .845" as physically measured and .841" as measured by the breadboard, for a 0.040 per cent error between the two measurements. At the end of the test the physically measured virgin material was .545", compared

TEST MODEL PERFORMANCE DATA

TEST MODEL PHOTOGRAPHS

MODEL 9A30C3

TEST POINT 1

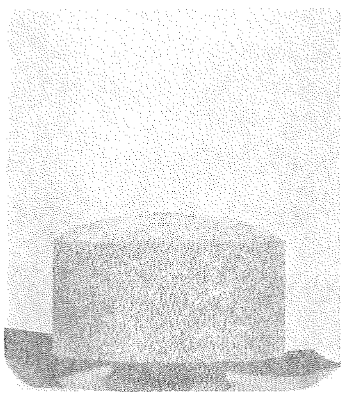

BEFORE TEST

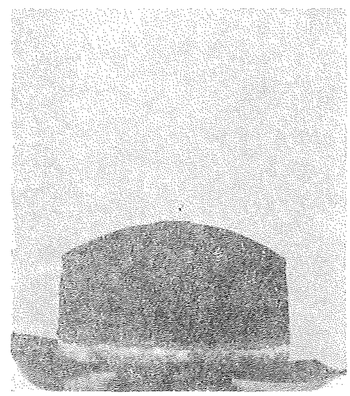

AFTER TEST

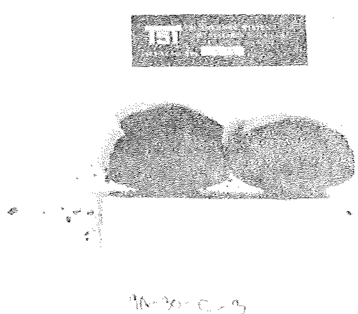

SECTIONED

FIGURE 9

TEST MODEL PERFORMANCE DATA

MATERIAL RECESSION HISTORY

Phase VII

Laboratory and Breadboard Nucleonics System in Parallel

Laboratory Output

Model No. 9F15C18

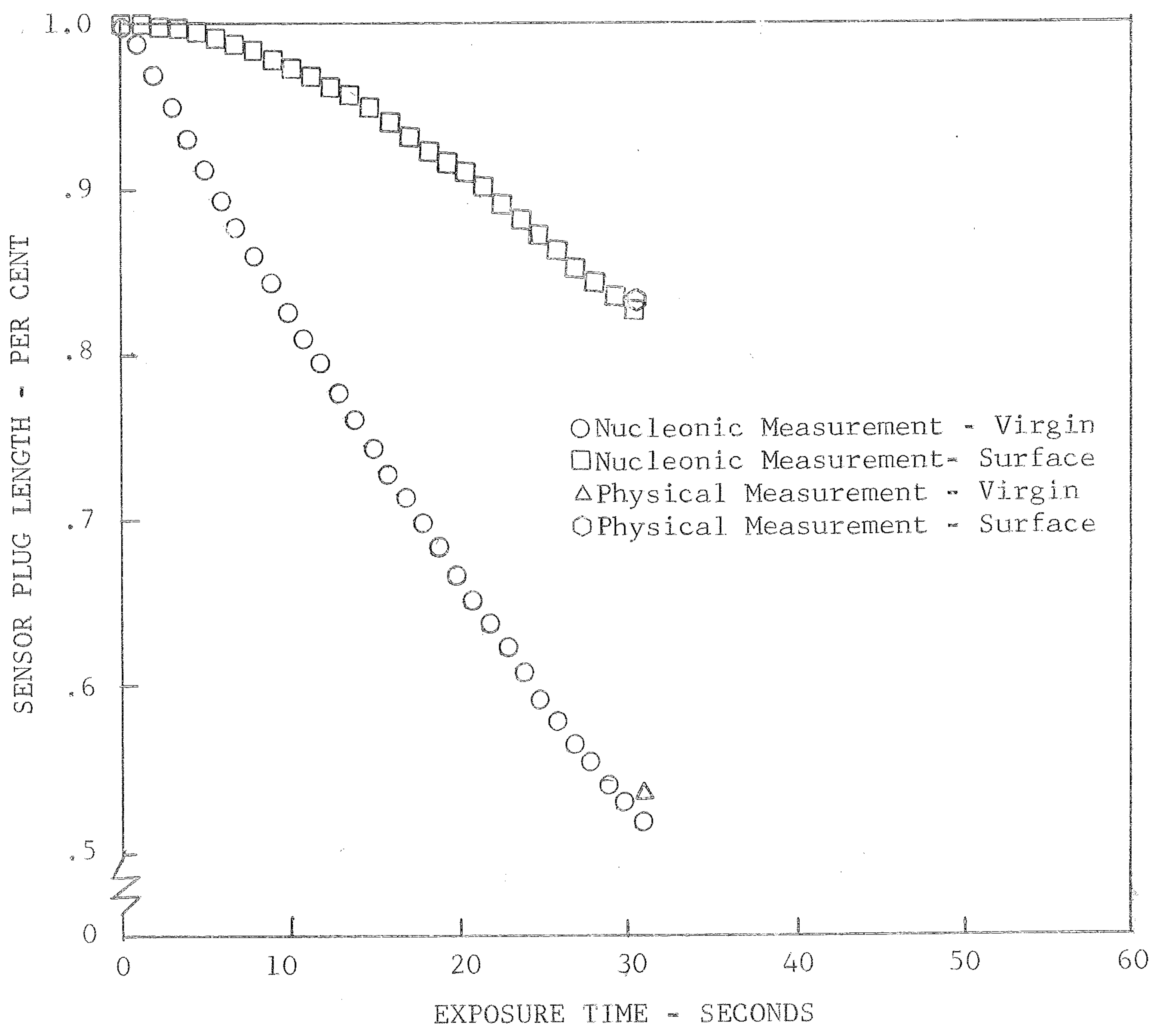

Figure 10

with .533" as measured by the breadboard system, yielding a 1.19 per cent error. This data can be found in Table 6 and is in concert with data obtained in Tables 3, 4 and 5. Before and after test photographs of Model 9F15C18 including a cross section, are depicted in Figure 11.

The measurement accuracy at test point 5 (used for phenolic graphite tests) was lower than that of the first two test points (used for phenolic nylon). Since the phenolic graphite impregnations were more uniform than the phenolic nylon, this greater system inaccuracy was almost entirely attributable to the test conditions. Ablation rates and surface temperatures of the conical test model fluctuated during each test (as indicated in Appendix I temperature histories). In addition, the plasma stream tended to dish out the middle of the model and the heating at the sensor location was greater than anticipated.

Both char and virgin material recession were more than adequate for good system resolution regardless of the heating rate fluctuation; nevertheless, the system accuracy at test point 5 was consistently lower for both the laboratory and breadboard dual ablation measurement systems than at test points 1 and 2.

For example, the real time recessions for the virgin and char phases of Model 9F23C23 as measured by the breadboard system in parallel with the laboratory nucleonic system are depicted in Figure 12. The model was exposed

TEST MODEL PERFORMANCE DATA

TEST MODEL PHOTOGRAPHS

MODEL 9F15C18

TEST POINT 2

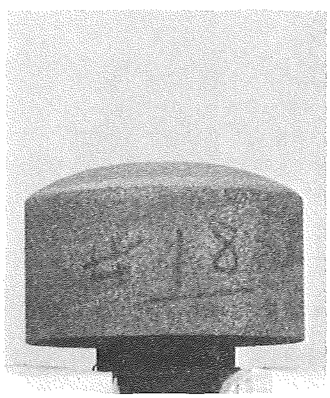

BEFORE TEST

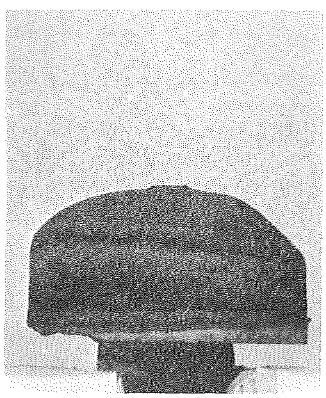

AFTER TEST

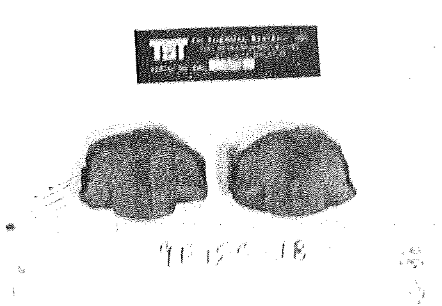

SECTIONED

FIGURE 11

TEST MODEL PERFORMANCE DATA

MATERIAL RECESSION HISTORY

Phase VII

Laboratory and Breadboard Nucleonics System in Parallel

Laboratory Output

Model No. 9F23C23

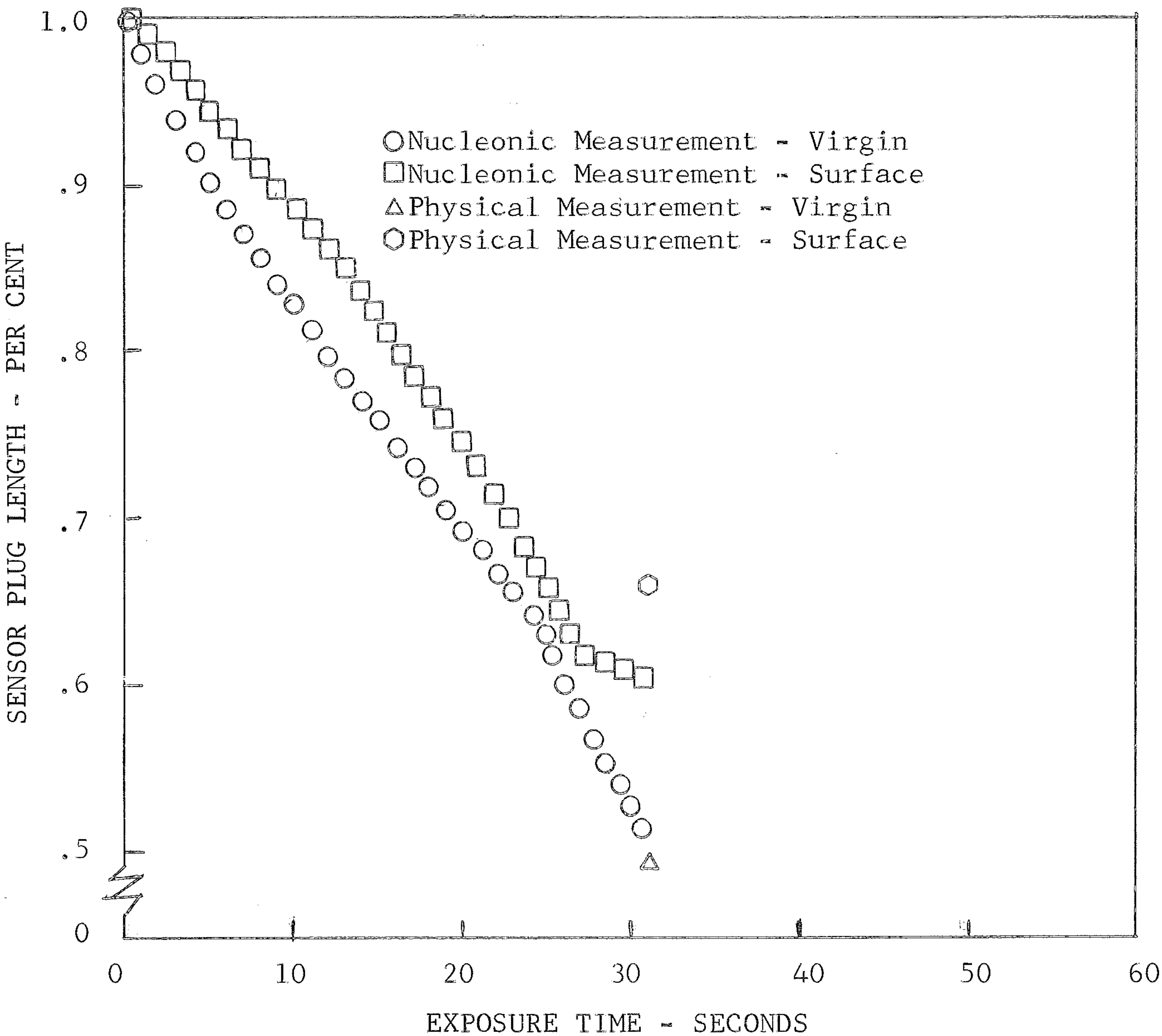

Figure 12

to a heat flux of 948 Btu/SecFt^2 for a period of 30 seconds. The surface temperature was 5200°F. The dimensions of the sensor plug after test were physically measured at .667" and nucleonically measured at .646", yielding a 2.08 per cent error. The virgin material was measured physically at .480" in comparison with the .481" nucleonic measurement, for a per cent error of 0.020. This data is found in Table 6 and is in concert with data obtained in Tables 3, 4 and 5. Before and after test photographs of Model 9F23C23, including a cross section, are depicted in Figure 13.

Another phenolic graphite model tested at Test Point 5 was 9D17G1. It was exposed to a heat flux of 944 BTU/Ft^{2}Sec for a period of 30.2 seconds. It exhibited a surface temperature of 5350°F. The real time recessions for the virgin and char phases of the model as measured by the laboratory nucleonic system are depicted in Figure 14. The sensor plug length after test was physically measured at .660" and nucleonically measured at .671", yielding a per cent error of 1.10. The virgin material was physically measured at the end of testing at .380", in comparison with the .402" nucleonic measurement, for a per cent error of 2.20. This data is found in Table 6 and is in concert with data obtained in Tables 3, 4 and 5. Before and after test photographs of Model 9D17G1, including a cross section, are depicted in Figure 15.

2.2 Non-Radioactive Calibration Tests

To establish three test conditions for the valid measurement of the three dual ablation sensor systems,

TEST MODEL PERFORMANCE DATA

TEST MODEL PHOTOGRAPHS

MODEL 9F23C23

TEST POINT 5

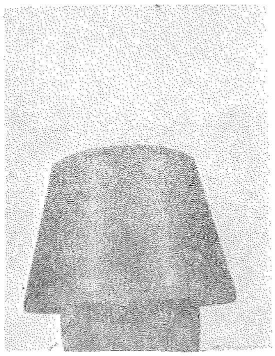

BEFORE TEST

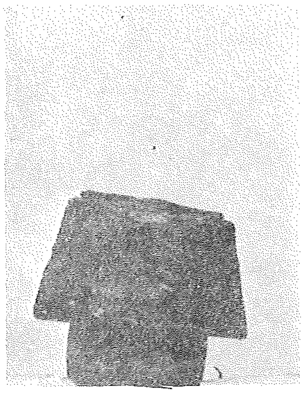

AFTER TEST

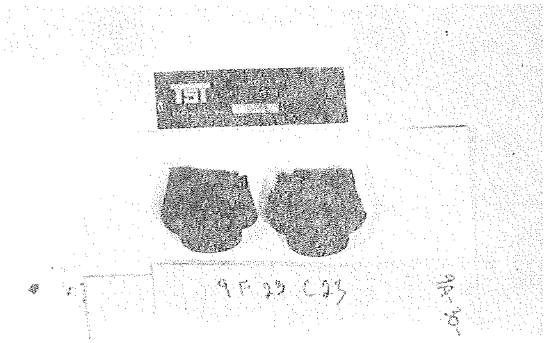

SECTIONED

FIGURE 13

TEST MODEL PERFORMANCE DATA

MATERIAL RECESSION HISTORY

Phase VIB

Laboratory Nucleonics System

Model No. 9D17G1

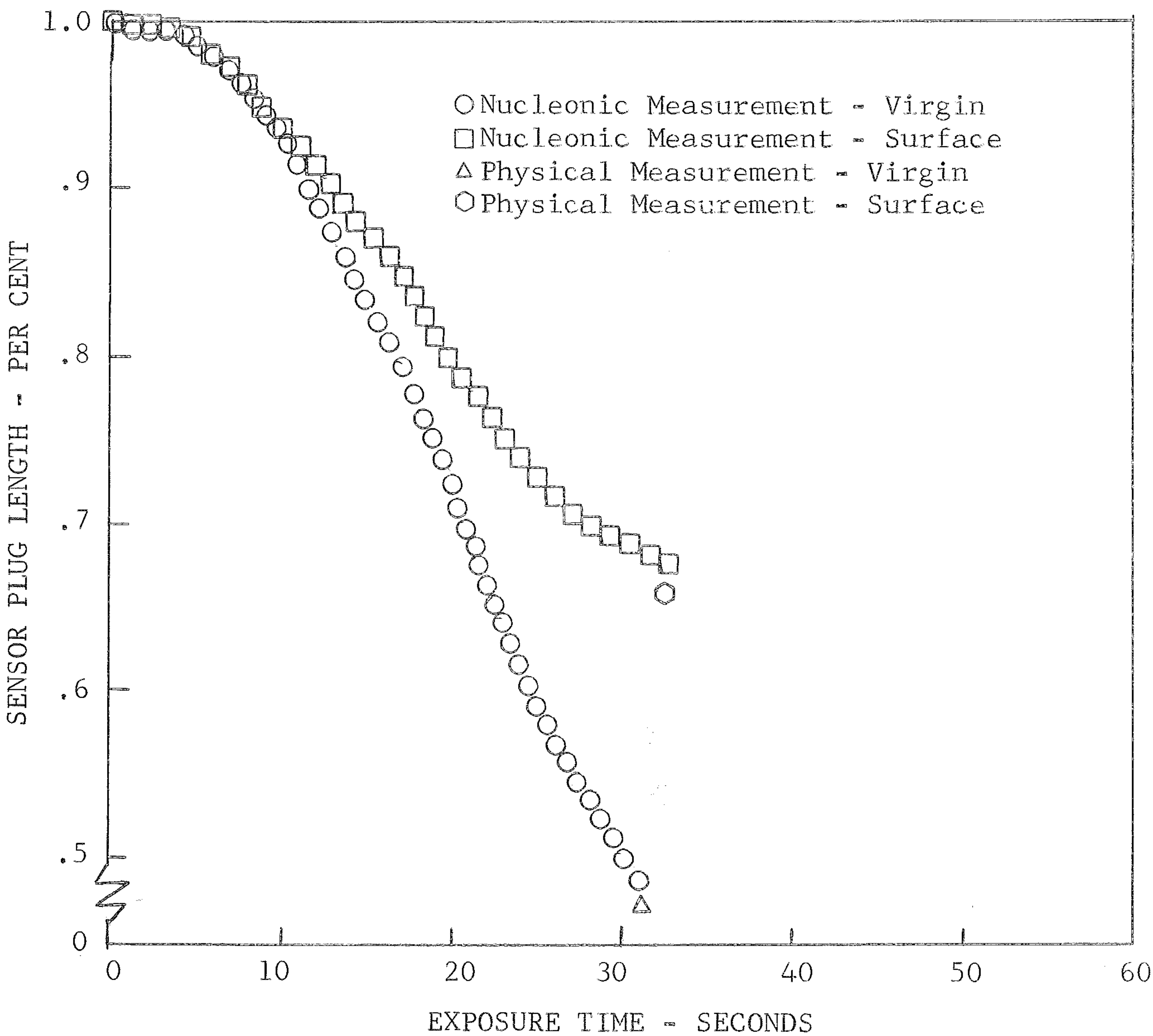

Figure 14

TEST MODEL PERFORMANCE DATA

TEST MODEL PHOTOGRAPHS

MODEL 9D17G1

TEST POINT 5

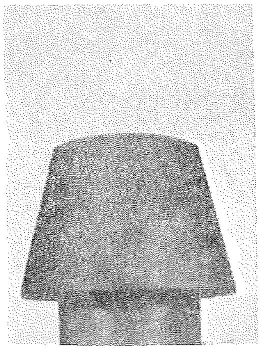

BEFORE TEST

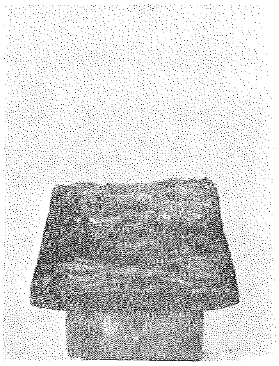

AFTER TEST

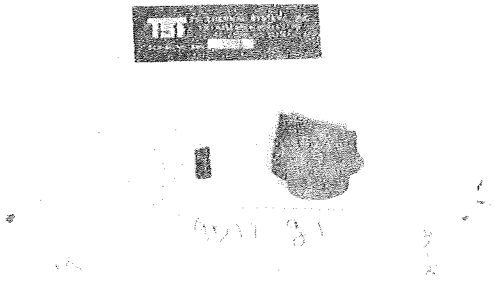

SECTIONED

FIGURE 15

eleven calibration tests were performed during Phase V. Tests were run at different time intervals within each test point to establish the recession rate as a function of exposure time. These data are summarized in Table 1. An examination of the model pictures for the Phase V tests shown in Appendix J and of the test model temperature histories of Appendix I illustrates the results of the Phase V calibration tests. The ablation rates of the char and virgin material as well as the test durations and conditions are summarized in the performance data (Table 2).

Test points 1 and 2 were established for the phenolic nylon test models. The test conditions at test point 3 were initially selected for the phenolic graphite; however, because of the high stagnation pressure (4 atm), the recession of the phenolic graphite test model was primarily due to shearing rather than heating effects. The next selection, test point 4, was much lower in stagnation pressure (2 atm) but higher in enthalpy, giving a cold wall heat flux of 1300 Btu/ft^2 sec. The surface temperature of 5800°F was found to be too high, the char recession proving too small and in general nonuniform. Test conditions were then established to form a compromise between test points 3 and 4. The cold wall heat flux at test point 5 was reduced to 940 Btu/ft^2 sec and the stagnation pressure set at 3 atm., which resulted in a surface temperature of 5200°F. With these conditions, the material recession was uniform, not subject to large shearing effects, and great enough to adequately test the performance of the dual ablation measurement systems.

Allied to the test results were the performance of the test model holder and radiation detector within the severe plasma jet heating environments. During the first of the two Phase V testing sessions, the radiation detector was significantly affected by the magnetic field used to stabilize the plasma arc (measured to be 1000 Gauss at the plasma jet nozzle exit). An electromagnatic-electrostatic shield was designed and fabricated to protect the detector from the magnetic field for the final Phase V and subsequent tests. After some minor modifications, the test model holder performed well, maintaining temperature control within the holder to 75°F ± 5°F during testing and providing a stable platform on which to affix the test models. The test model holder modifications and radiation detector magnetic shielding are discussed in detail in Appendix E.

2.3 Concept Accuracy Tests

2.3.1 Phase VIA Tests

A laboratory standard nucleonics system was employed along with the breadboard and prototype radiation detector as the Phase VIA dual ablation measurement system. Isotope activity levels, isotope activity ratios, impregnation and fabrication procedures, and electronic discrimination settings had been established during Phase III laboratory tests to provide the optimum system for measuring material attrition by nucleonic techniques. Eleven radioactive tests using the optimized laboratory nucleonics system were performed in Phase VIA, three at test point 1, four at test point 2, two at test point 4, and two at test point 5. The results (data traces) were recorded on the Midwestern Recorder, reduced with an SDS time-sharing computer, and presented to the Government in an oral briefing in March, 1969.

The optimized laboratory nucleonics system resulted in better than 97 per cent system accuracy for all tests, with 99.4 per cent or better accuracy for most tests. Virgin material and surface recession of the radioactive sensors were accurately predicted.

The Phase VIA testing was performed in a ten day period, with an average of four radioactive models tested per day at the Plasmadyne facility. The tests were run with minimum difficulty; no problems with instrumentation or the facility were experienced. The radiation dose rate exposures experienced during the testing and clean up procedures were minimum (less than a total of 100 millirems of whole body exposure) for the most part and confirmed that the testing of radioactive models could be accomplished without excessive radiation exposure. The radiation dose exposures are shown in Table G-1 of Appendix G.

The removal of the test models from the plasma jet tunnel presented the only difficulties of the Phase VIA test series. When the model was ablated too much (as was 9A30T1, a calibration model), it had to be broken for removal. In some cases the char material was impossible to keep intact, making post test physical measurements difficult. Shorter test durations provided the solution to this problem.

In summary, the Phase VIA tests were successful, both from the aspect of system measurement accuracy and in the ease of their execution. The feasibility of measuring char and virgin material recession by nucleonic techniques was established and the dual ablation measurement system concept was shown to be an accurate method of determining char and virgin material recession histories.

2.3.2 Phase VIB Tests

In Phase VIB, the laboratory nucleonics system was arranged to simulate the window locations of the electronic processors (breadboard and manufacturing prototype). Eight radioactive tests were performed in this test series, three at test point 1, two at test point 2, and three at test point 5. Even with non-optimum window settings, the laboratory nucleonics system tracked the material recession of the eight test models within a 95 per cent system accuracy. Due to the window change in the laboratory system, errors increased by a factor of from two to ten over those experienced with the optimized laboratory system. However, even with this increase, errors were maintained within the original dual ablation system specification of 5 per cent.

No problems were experienced with either the models or the facility during this test phase. The radiation dose exposures and the overall testing experience were similar to those of Phase VIA.

2.4 Breadboard Measuring System Tests

The Phase VII plasma jet tests affirmed that the dual ablation measuring system could measure material ablation by nucleonic techniques. The breadboard system employed was less accurate, however, than the laboratory standard nucleonics system. The plasma jet tests indicated that certain minor improvements in its overall design could significantly improve the breadboard system accuracy.

Phase VII tests originally scheduled for the manufacturing prototype's matched detector (which was damaged) were transferred to Phase VIB and to the Phase VII breadboard tests. Seven valid radioactive tests, two at test point 1, three at test point 2, and two at test point 5, were performed with the laboratory standard nucleonics and breadboard dual ablation measurement systems in parallel. The laboratory system was adjusted to compensate for the spectrum shifts and signal attenuation difficulties evaluated in using the two systems in parallel.

(See Appendix A for a detailed discussion of signal attenuation and spectrum shift effects.) Calibrations and tests were then performed simultaneously with the two units.

The breadboard system's output was recorded on Channels 3 and 4 of the recorder; the laboratory system's output on Channels 1 and 2. The laboratory system provided 94-99 per cent system accuracy for all Phase VII tests even though the spectrum of measurement was significantly altered by the breadboard electronics and the discrimination windows were not optimized.

The breadboard system performance was not consistent for all test models. Its prediction of the surface recession of the sensor was accurate within 7 per cent (except for test model 9F15C18); however, the virgin material recession tracking was less accurate. This was caused primarily by the breadboard's signal attenuation difficulties and partially by data reduction difficulties. The signal attenuation problems seriously affected the system measurement accuracy. The shift in the spectra within the electronic windows caused the spectra to move toward the lower energy levels. The $ZrNb^{95}$ emission peak was shifted from 0.75 to 0.35 Mev. The breadboard's Channel 2 window location of between 0.3 and 0.85 Mev was fortuitous, preventing the $ZrNb^{95}$ spectrum from shifting completely into the low energy channel. The In^{114m} spectrum's exact shift was not determined. However, a part of the Channel 1 discrimination area was shifted below 0.1 Mev and out of the low energy channel window (0.1 to 0.3 Mev). These combined effects hampered the virgin material recession measurement while not greatly affecting the char-surface recession measurement.

Problems in data reduction originated in the breadboard electronic processors' exclusion of voltages of less than 0.45 volts. Background activity measurements in both channels and In^{114m} singular isotope recession measurements in Channel 2 did not attain this voltage cut off level and thus were not recorded by the breadboard instrumentation. In the data reduction process, this problem was avoided through a mathematical technique. Two assumptions were employed for the data. In the first, the voltage outputs for the In^{114m} isotope activity in Channel 2 were assumed to be zero. In the second, the assumed value for the In^{114m} activity in Channel 2 was a function of the In^{114m} activity in Channel 1. Table 6 presents the results attained with each of these methods. The former solution showed equal or better measurement accuracy than the latter in two out of the seven tests for the virgin material recession.

In summary, the Phase VII tests indicated that the breadboard system could, with minor design modifications, be an effective instrument in the measurement of char-surface and char-virgin material interface recession.

3.0 EVALUATION OF THE BREADBOARD NUCLEONIC SYSTEM

The three nucleonic systems used in this test program were the breadboard dual ablation measurement system, manufacturing prototype dual ablation measurement system and laboratory standard nucleonics system. Each of these systems is discussed in detail in Appendix B. In general, all three systems demonstrated the efficacy of the dual ablation measurement technique. Certain advantages inherent to the laboratory nucleonics system resulted in superior system accuracy. A comparable level of accuracy could be approached with the breadboard electronic processor systems through the incorporation of minor design modifications.

The two nucleonic systems tested at Plasmadyne were the laboratory standard and the breadboard. Damage to the manufacturing prototype system's matched detector procluded its inclusion in the plasma jet tests. In Phase VIA, the laboratory system was tested singularly at optimized gain adjustment and window settings. In Phase VIB, the laboratory system was tested singularly with window settings simulating the reported breadboard's and with optimized gain adjustments. In Phase VII, the breadboard system was tested in parallel with the laboratory standard system, which was adjusted to simulate the electronic windows of the breadboard. In this manner, a simultaneous evaluation of the breadboard dual ablation measurement could be made utilizing the laboratory standard system's test results. A comparison of these results with those of the Phase VIA and VIB tests gives a comprehensive evaluation of the breadboard electronic processor systems.

The breadboard system accuracy in Phase VII was lower than that of the laboratory system in any of the test phases. This lower accuracy (significant when compared with the optimized laboratory system of Phase VIA) could be attributed to several items. The major difficulty was that neither the gain or window settings could be adjusted in the breadboard electronic processors. The shift in electronic window locations due to signal attenuation, further compounded by the unadjustable gain and windows, had significant effects upon the breadboard system's measurement accuracy. Window locations for each system are depicted in Table 7.

During the pre-test calibration for Phase VII, it was discovered that the high energy emission peak ($ZrNb^{95}$ isotope) had been shifted from 0.75 to 0.35 Mev because of signal attenuation, part of which was the result of the breadboard circuitry. The problems associated with the breadboard circuitry were traced to three major areas: the pulse amplification network, the pulse shaping circuitry, and the power supply circuitry. Each of these is examined in detail in Appendix B.

The effect of signal attenuation was detrimental to the breadboard system accuracy in that the lower energy emission peak (In^{114m} isotope) was also shifted downward

TABLE 7

WINDOW LOCATIONS

Nucleonic System	Isotope Activity Ratio	In^{114m} Activity (mc)	$ZrNb^{95}$ Activity (mc)	Window Locations Channel 1 Lower (Mev)	Window Locations Channel 1 Upper (Mev)	Window Locations Channel 2 Lower (Mev)	Window Locations Channel 2 Upper (Mev)
Laboratory	8	.8	.1	.15	.22	.64	1.00
Laboratory	10	0.8-1.0	0.08-0.1	.15	.23	.65	1.00
Breadboard	10	1.0-1.2	0.1-0.12	.10*	.30*	.30*	0.85*
Manufacturing Prototype	10	1.0-1.2	0.1-0.12	.10*	.30*	.30*	0.85*

*Original Window Locations chosen in NAS1-5342.

(although to a lesser amount) and some, if not all, of the Channel 1 discrimination area was shifted below the cut off energy of 0.1 Mev, which was fixed in the breadboard system. Isotope discrimination was therefore seriously degraded and system accuracy greatly impaired, particularly in the measurement of the virgin material recession. Fortunately, the shift from 0.75 to 0.35 Mev of the high energy channel did not shift the $ZrNb^{95}$ peak out of the upper window (set at 0.03 to 0.85 Mev), and the char surface recession measurement of the breadboard system was generally unimpaired.

Another major problem of the breadboard system could not be evaluated due to the signal attenuation difficulties. It is important, however, to consider. The breadboard system was inflexible in its adjustment of windows and gain and no electronic optimization of the breadboard system could be made. In comparing the results of the Phase VIB laboratory tests, which utilized non-optimum window settings with those results obtained from the optimum settings in Phase VIA, it is evident that the system measurement accuracy was significantly affected. Instead of 98-99½ per cent accuracy, the accuracy was reduced to 95 per cent, which was in some cases an increase in system error by a factor of ten. These results are significant, indicating that the flexibility required for optimization of discrimination is a prerequisite for dual ablation measurement system accuracy.

TEST MODEL PERFORMANCE DATA

MATERIAL RECESSION HISTORY

Phase VIA

Laboratory Nucleonics System

Model No. 9A30C5

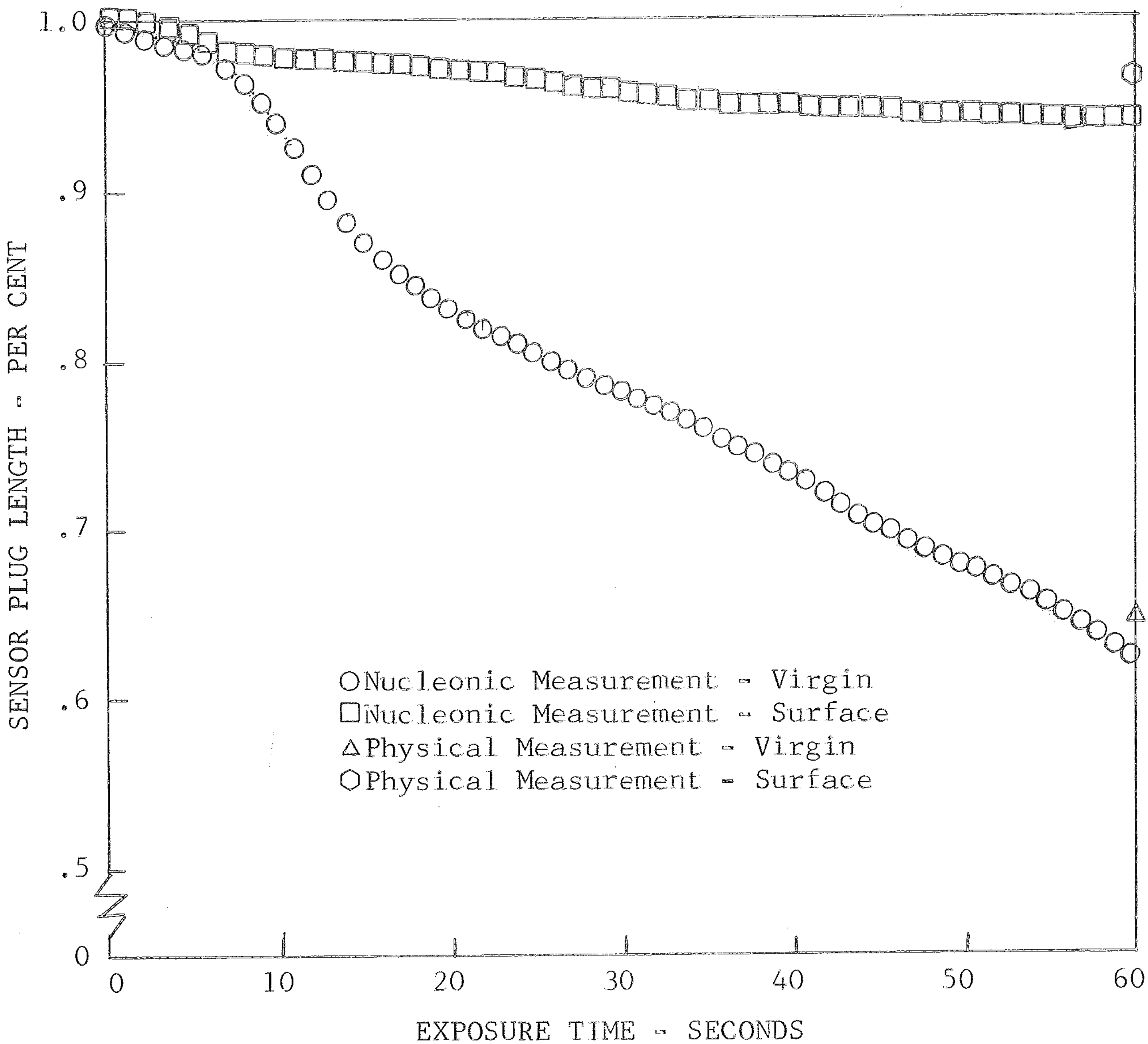

Figure 16

TEST MODEL PERFORMANCE DATA

MATERIAL RECESSION HISTORY

Phase VIA

Laboratory Nucleonics System

Model No. 9A30C6

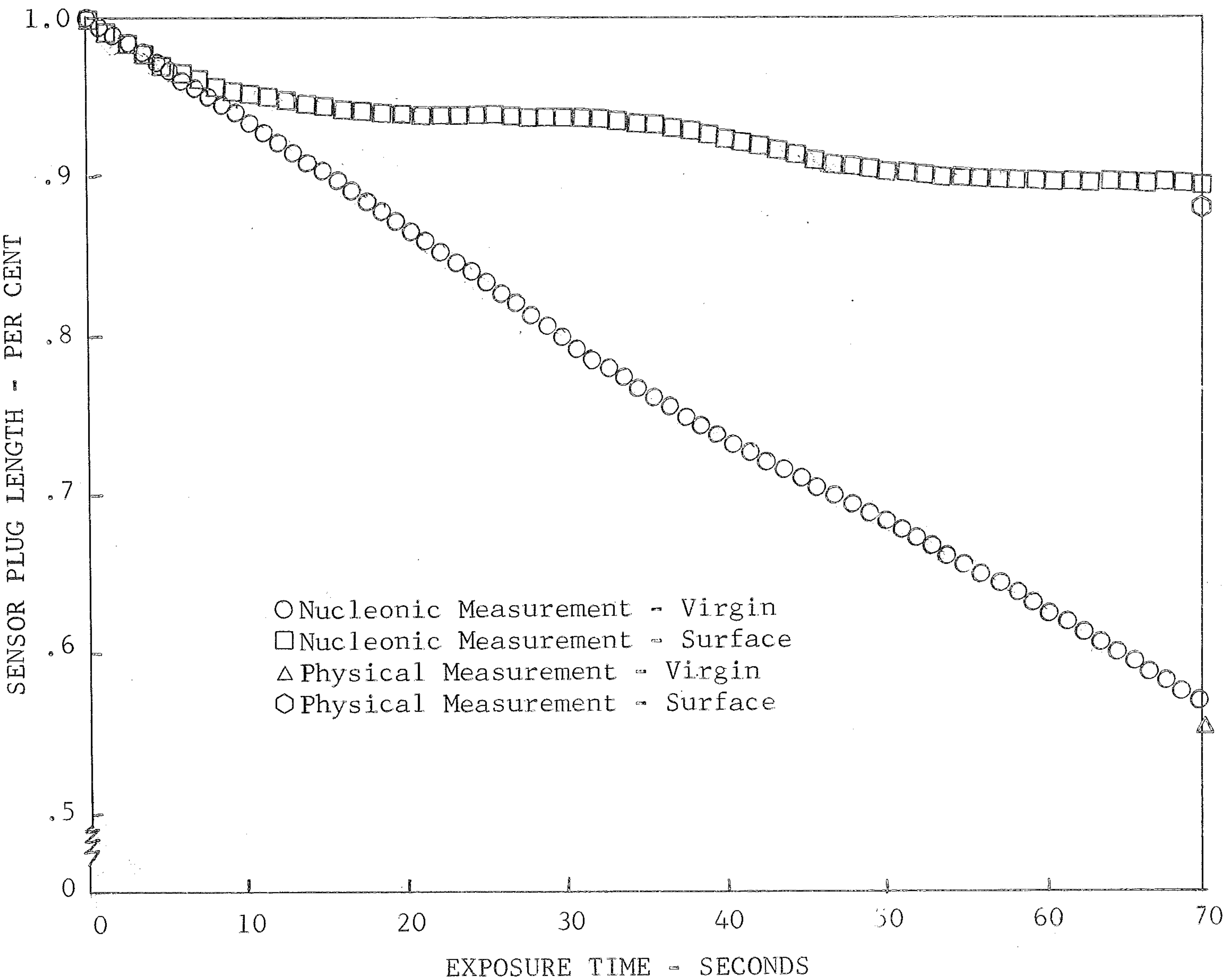

Figure 17

TEST MODEL PERFORMANCE DATA

MATERIAL RECESSION HISTORY

Phase VIB

LABORATORY NUCLEONICS SYSTEM

Model No. 9F15C9

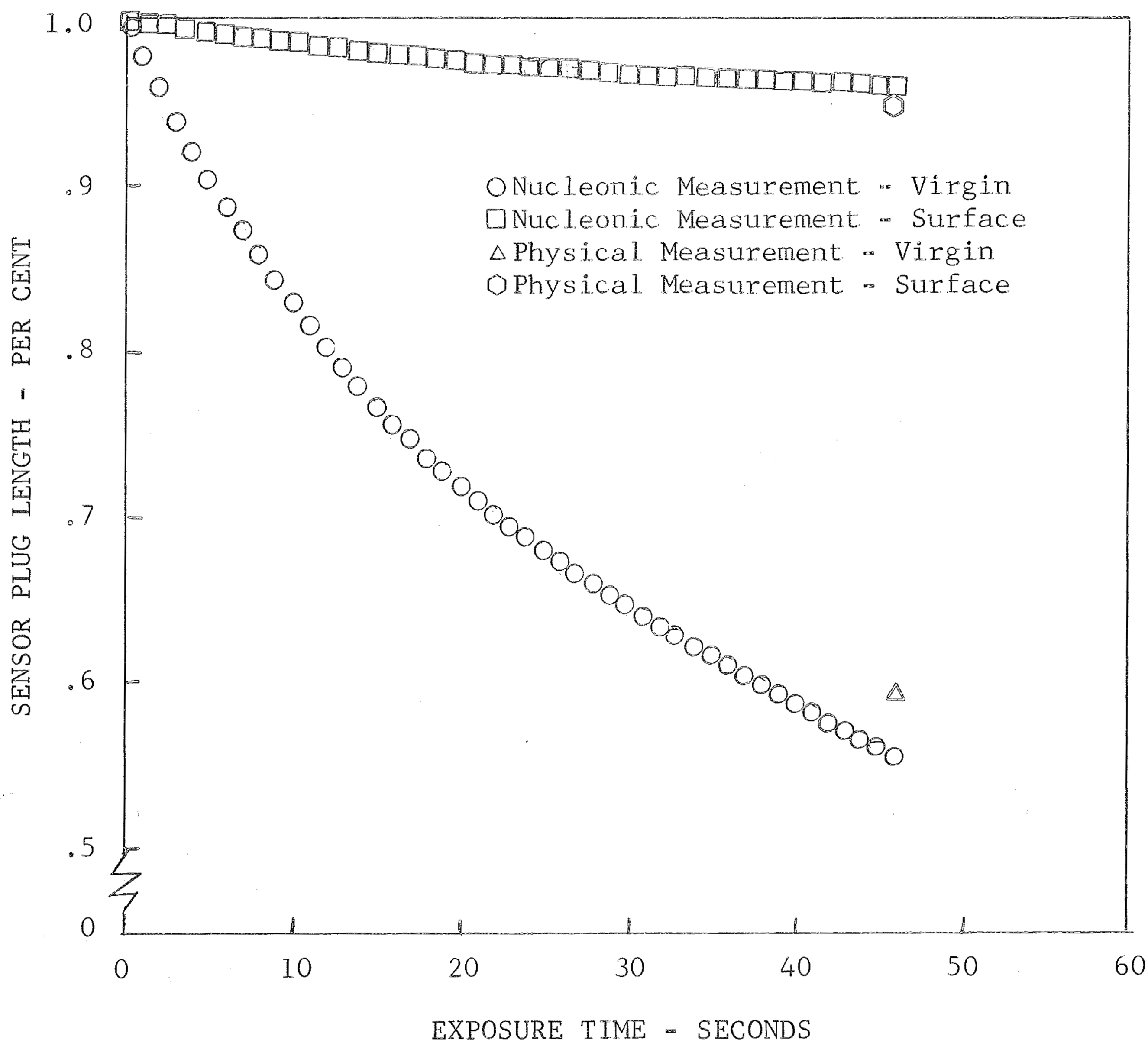

Figure 18

TEST MODEL PERFORMANCE DATA

MATERIAL RECESSION HISTORY

Phase VII

Laboratory and Breadboard Nucleonics System in Parallel

Laboratory Output

Model No. 9F15C11

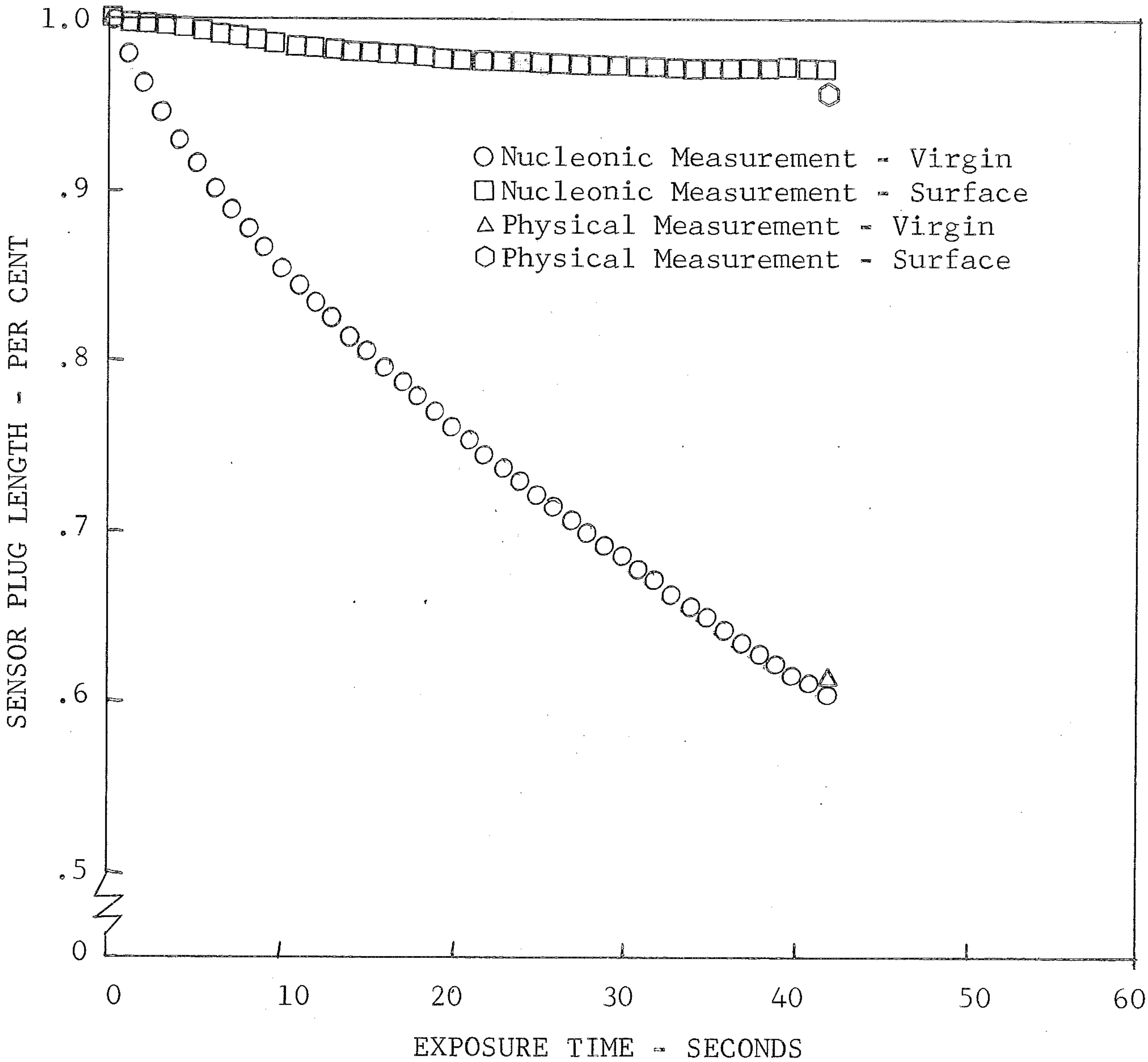

Figure 19

TEST MODEL PERFORMANCE DATA

MATERIAL RECESSION HISTORY

Phase VII

Laboratory and Breadboard Nucleonics System in Parallel

Breadboard Output with $In_2^{114m} = f(In_1^{114m})$

Model No. 9F15C11

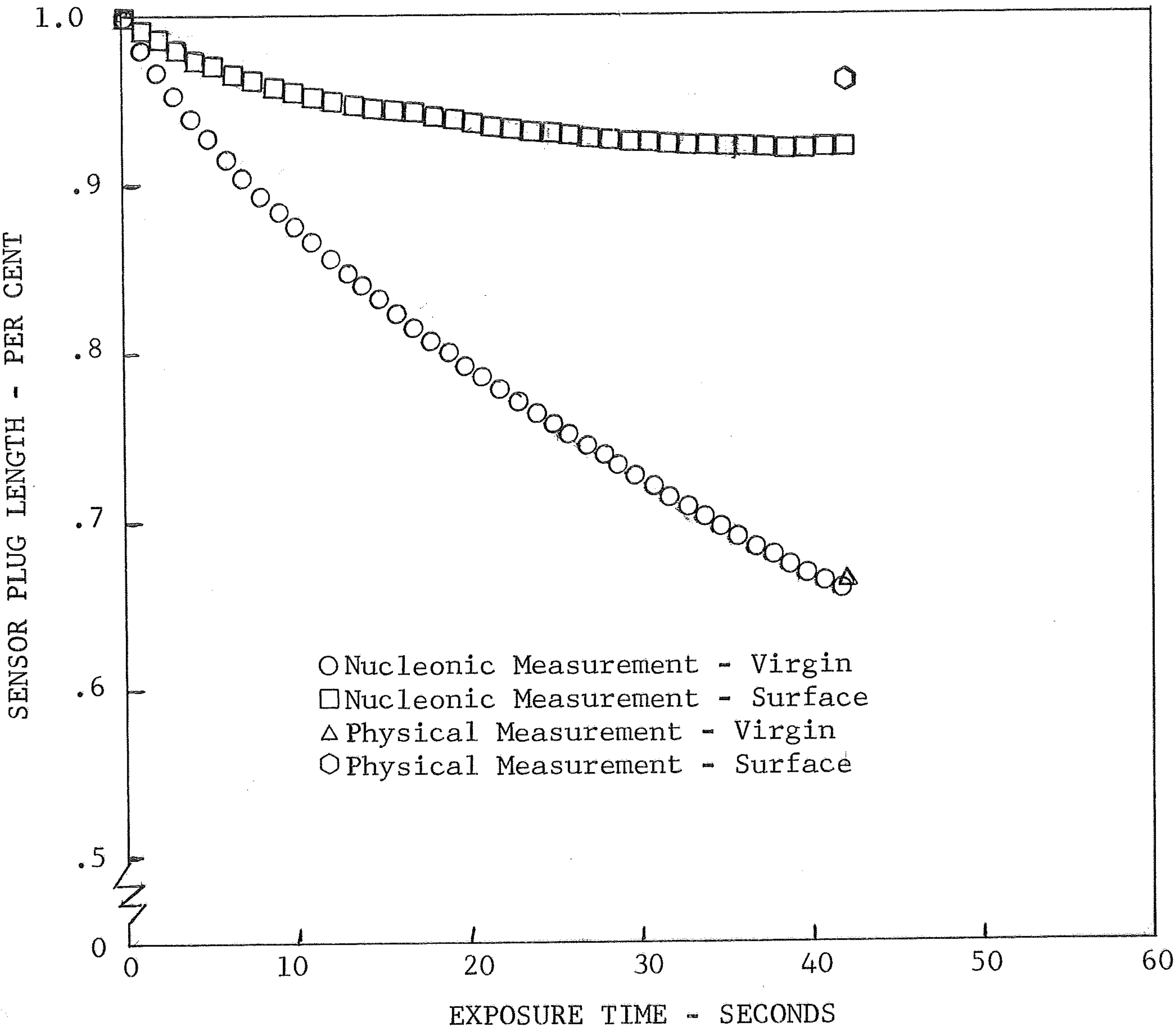

Figure 20

TEST MODEL PERFORMANCE DATA

MATERIAL RECESSION HISTORY

Phase VII

Laboratory and Breadboard Nucleonic System in Parallel

Breadboard Output with $In_2^{114m} = 0$

Model No. 9F15C11

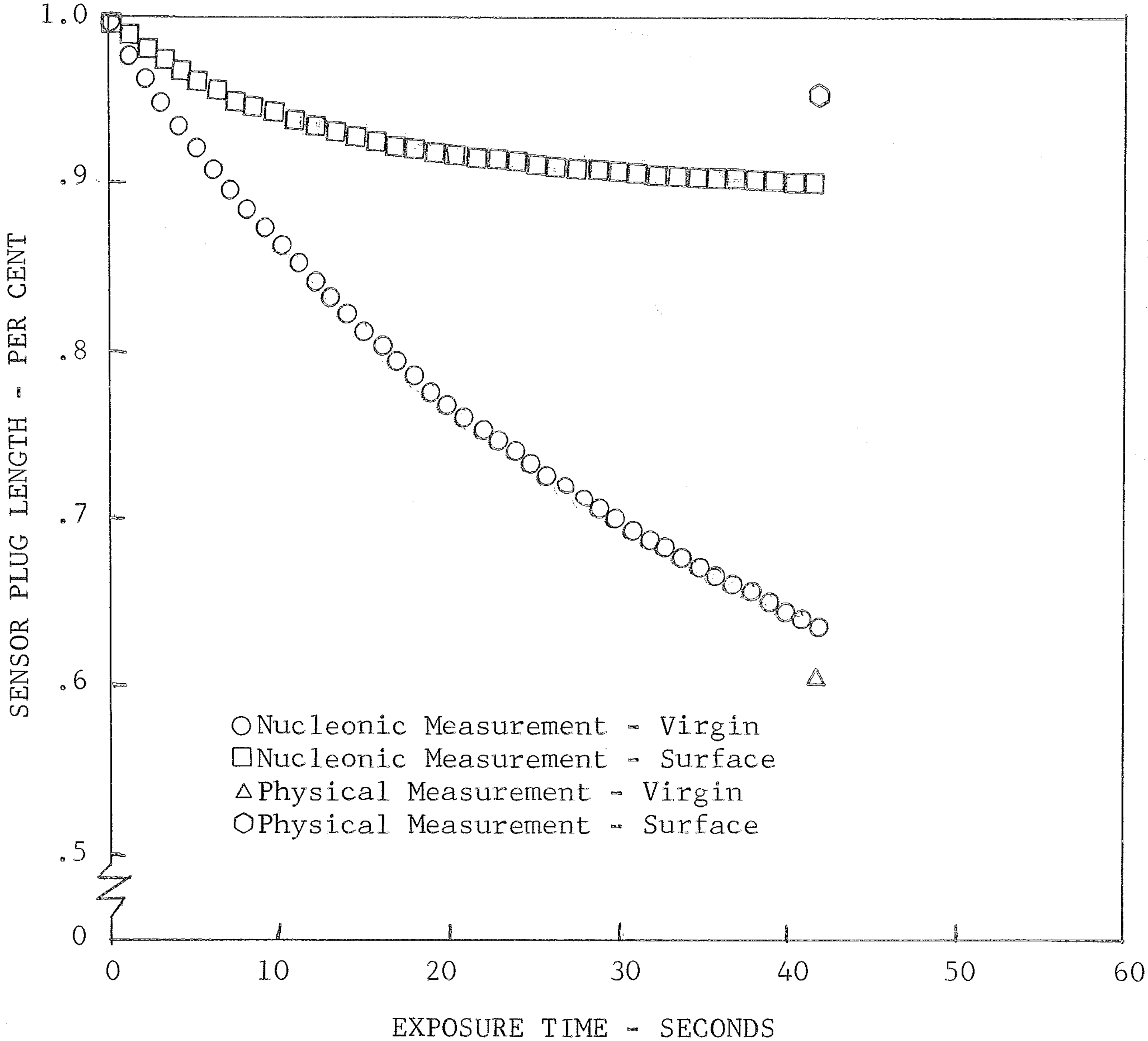

Figure 21

TEST MODEL PERFORMANCE DATA

MATERIAL RECESSION HISTORY

Phase VIB

Laboratory Nucleonics System

Model No. 9F15C16

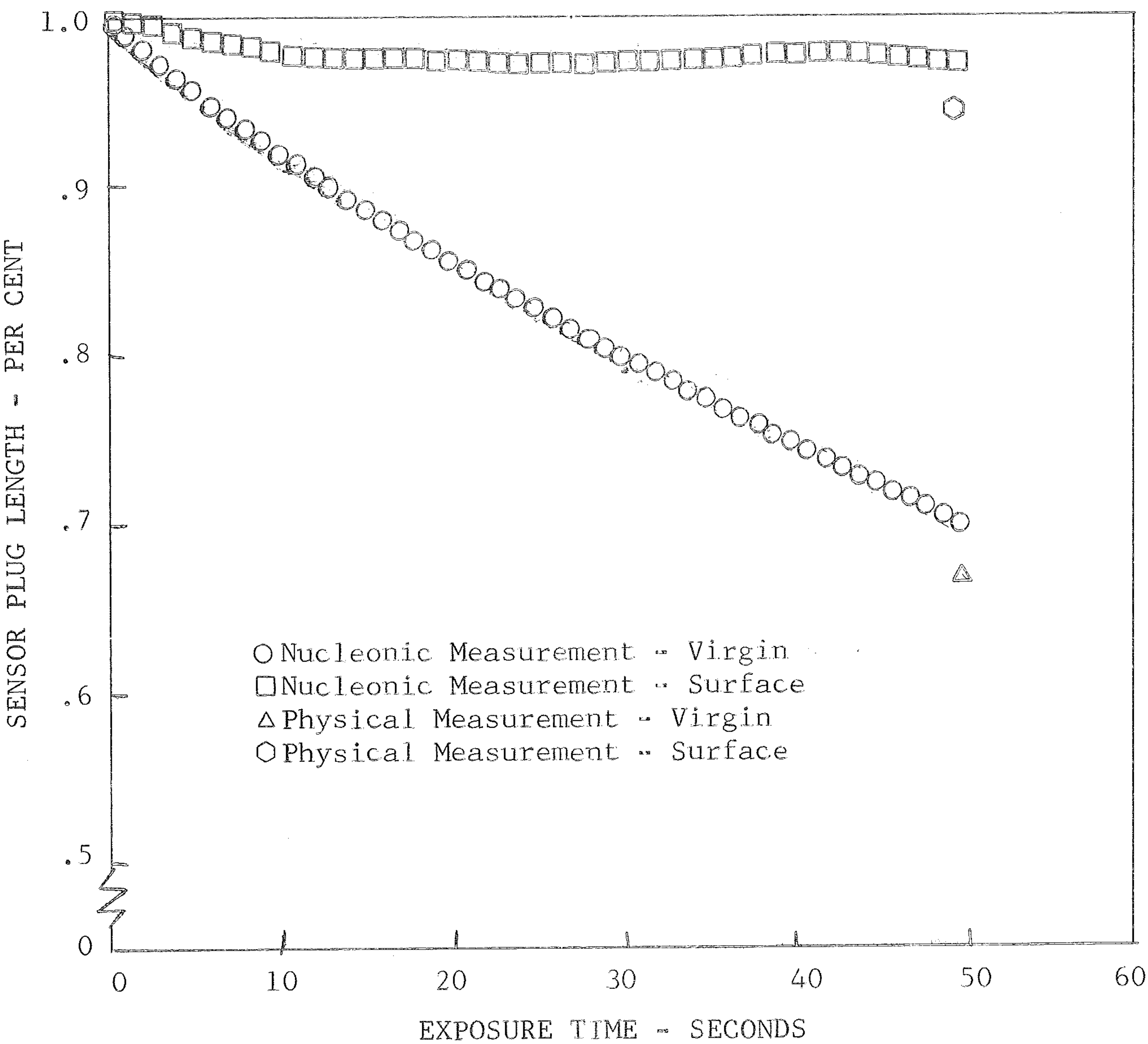

Figure 22

TEST MODEL PERFORMANCE DATA

MATERIAL RECESSION HISTORY

Phase VIB

Laboratory Nucleonics System

Model No. 9F15C19

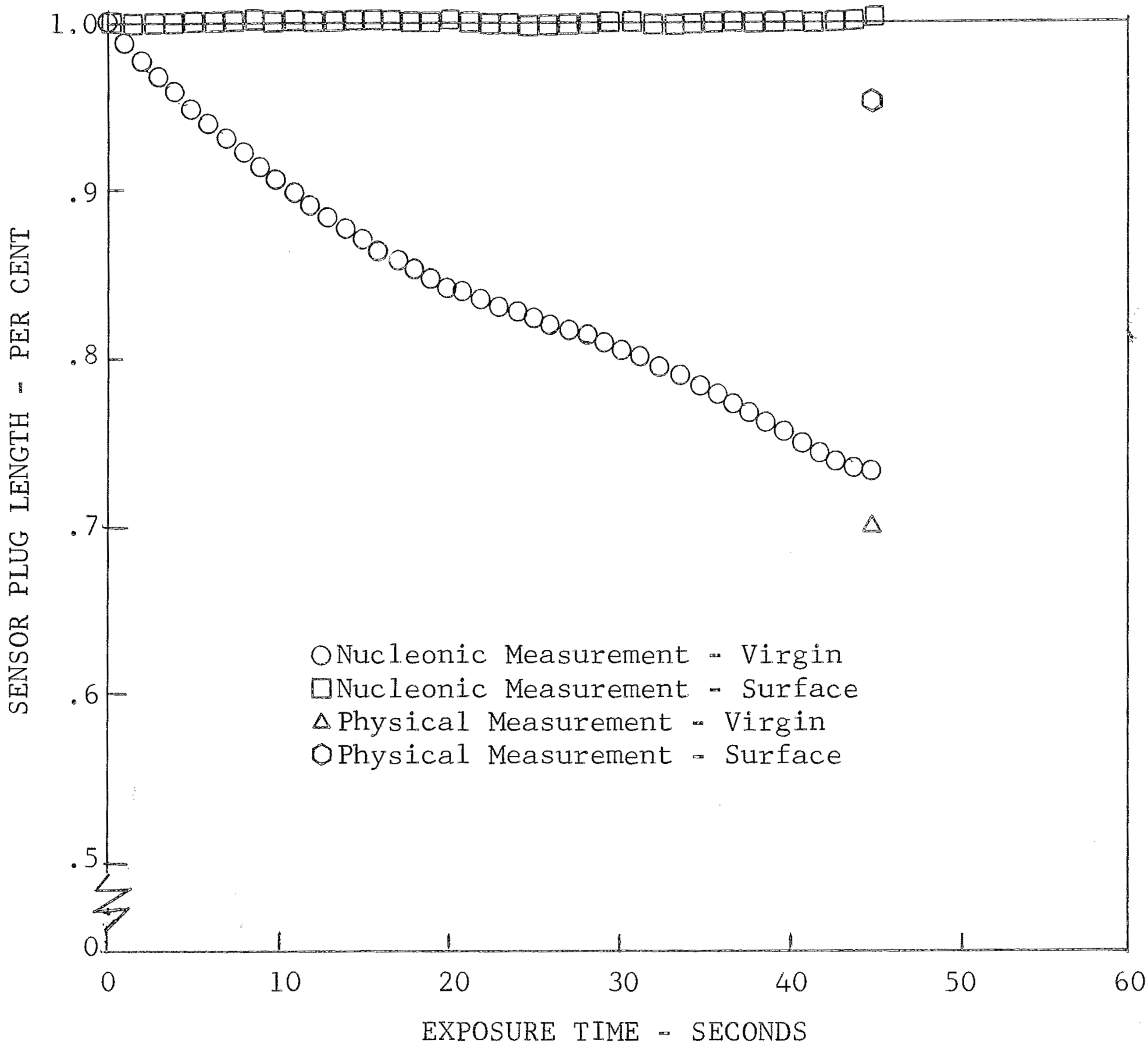

Figure 23

TEST MODEL PERFORMANCE DATA

MATERIAL RECESSION HISTORY

Phase VII

Laboratory and Breadboard Nucleonics System in Parallel

Laboratory Output

Model No. 9F15C23

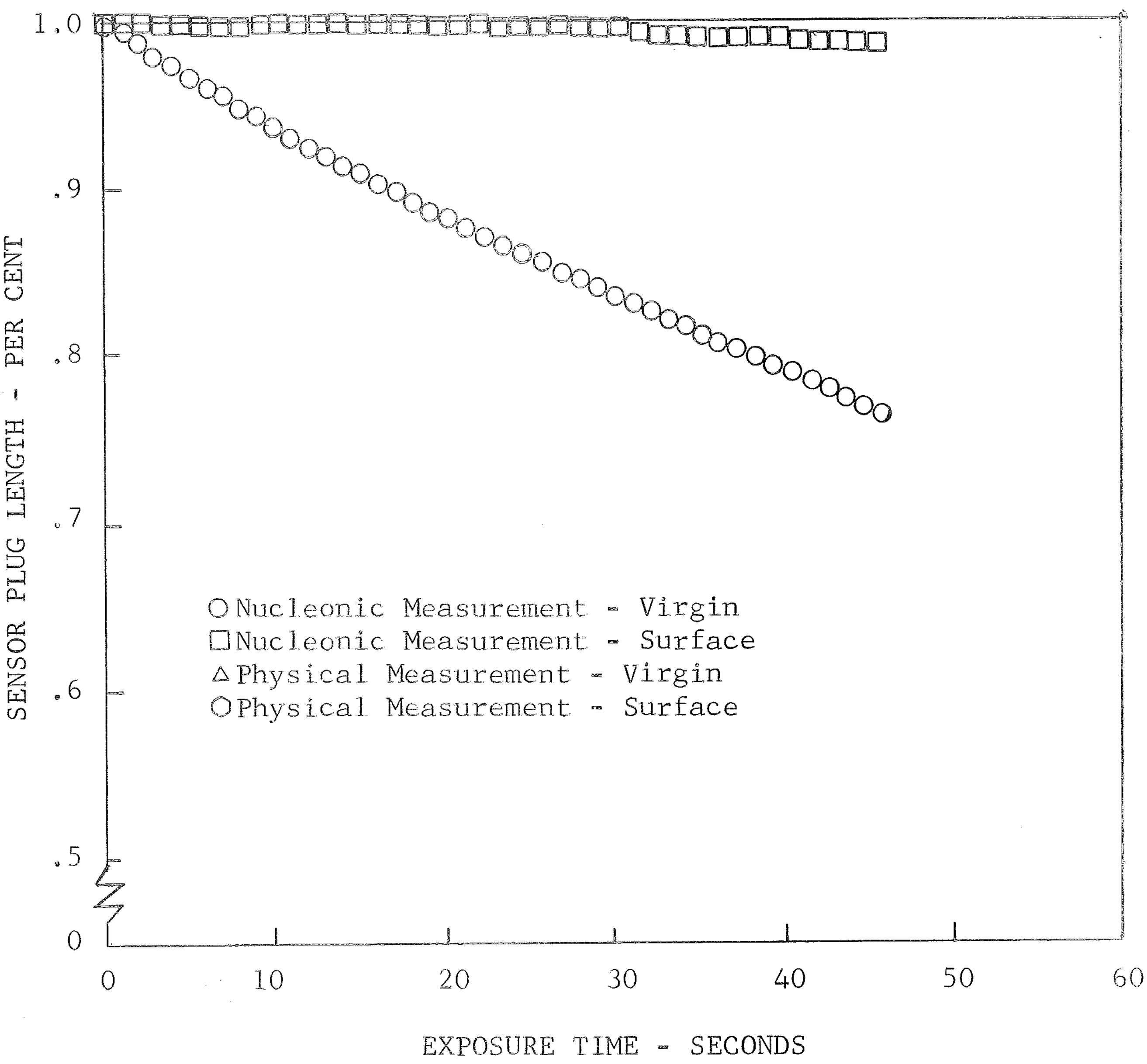

Figure 24

TEST MODEL PERFORMANCE DATA

MATERIAL RECESSION HISTORY

Phase VII

Laboratory and Breadboard Nucleonic System in Parallel

Breadboard Output with $In_2^{114m} = f(In_1^{114m})$

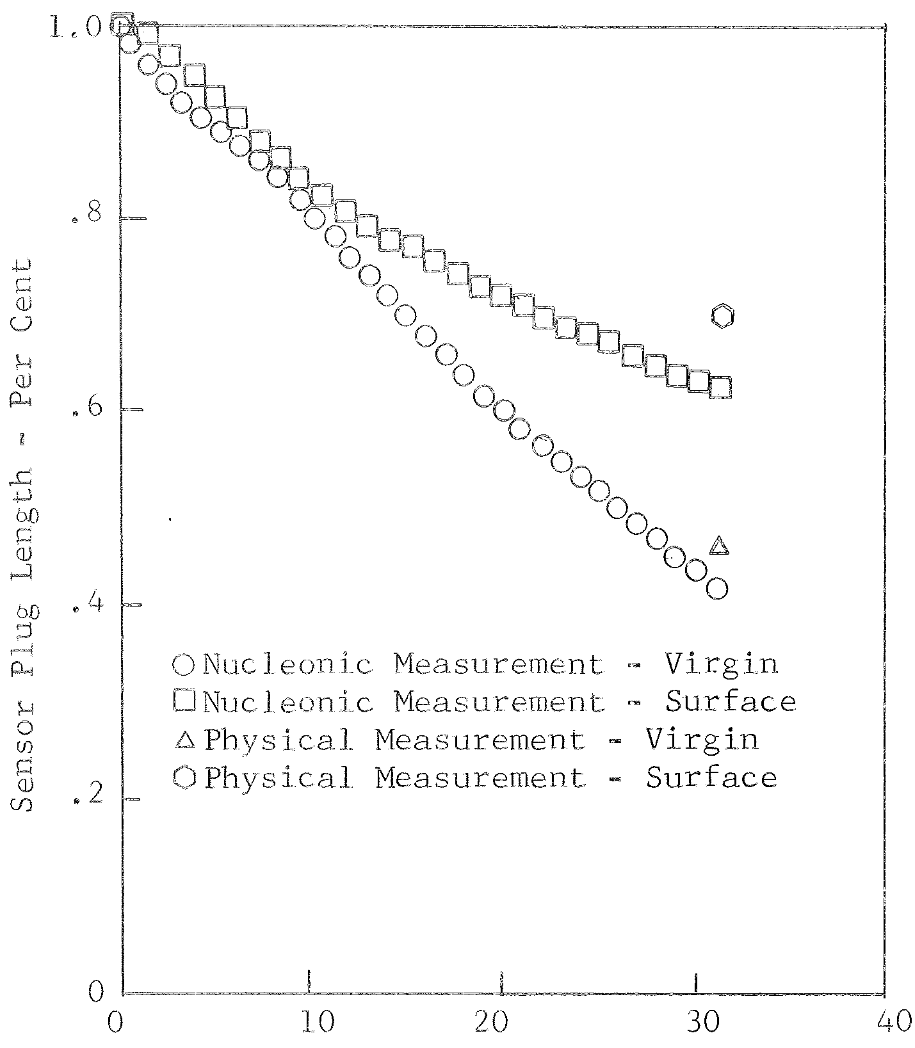

Figure 25

TEST MODEL PERFORMANCE DATA

MATERIAL RECESSION HISTORY

Phase VII

Laboratory and Nucleonics System in Parallel

Breadboard Output with $In_2^{114m} = 0$

Model No. 9F15C23

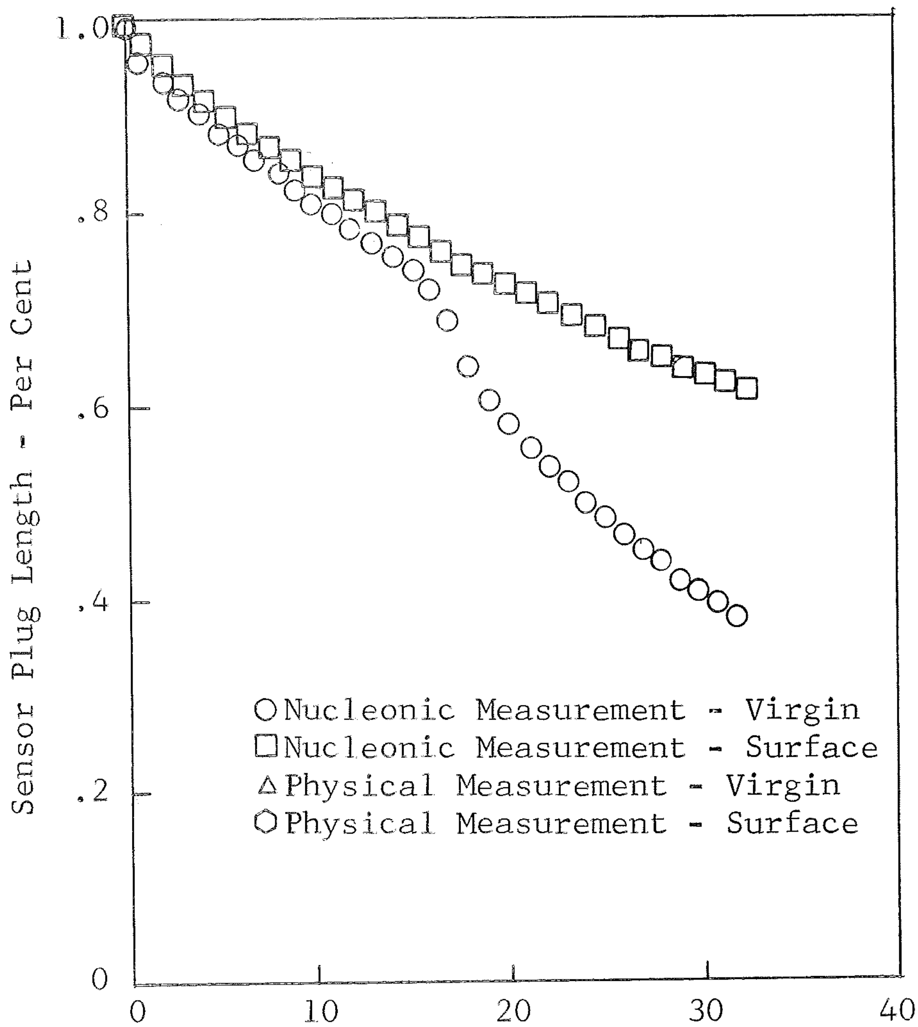

Figure 26

TEST MODEL PERFORMANCE DATA

MATERIAL RECESSION HISTORY

Phase VIA

Laboratory Nucleonics System

Model No. 9A30C1

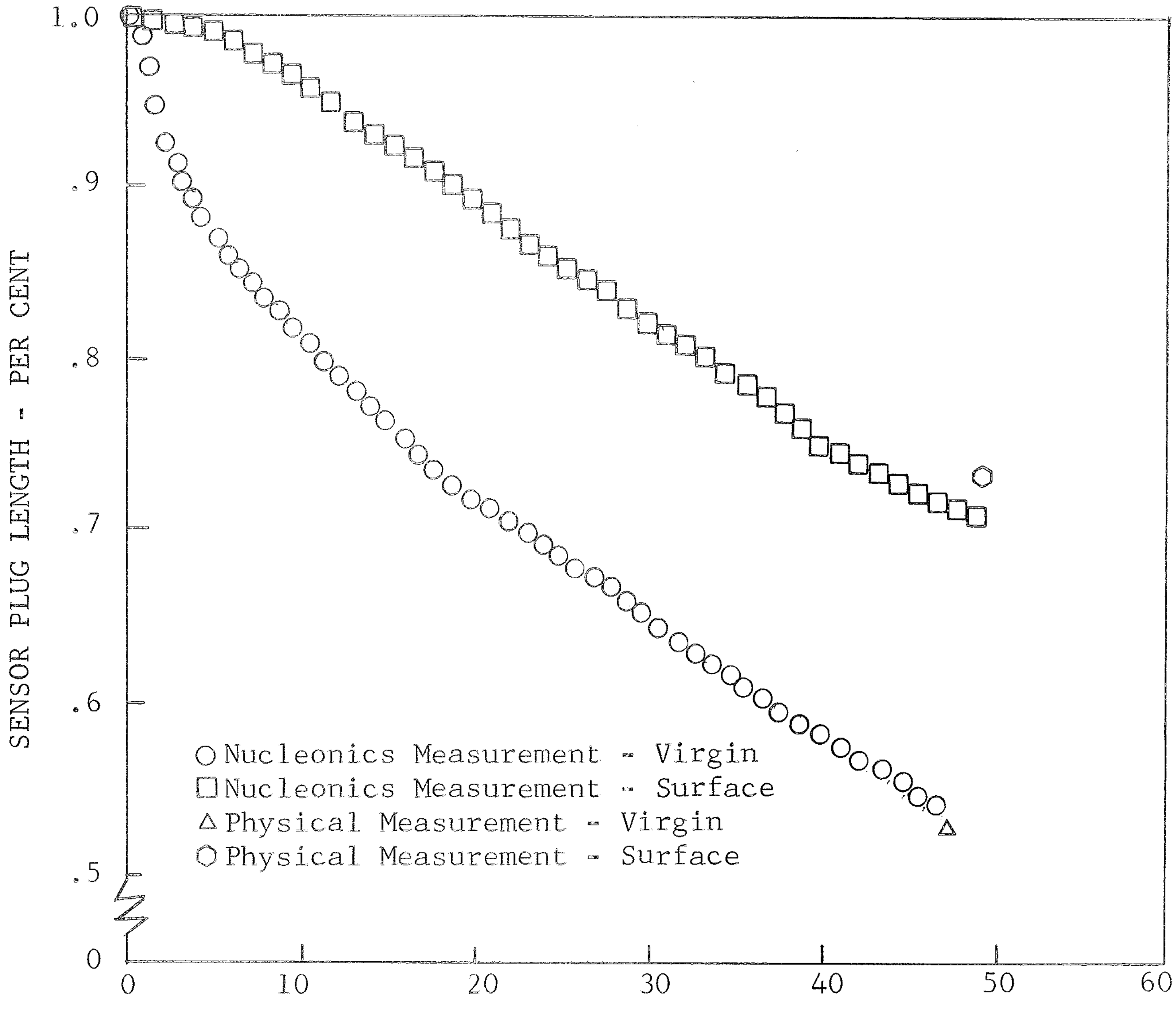

Figure 27

TEST MODEL PERFORMANCE DATA

MATERIAL RECESSION HISTORY

Phase VIA

Laboratory Nucleonics System

Model No. 9A30C4

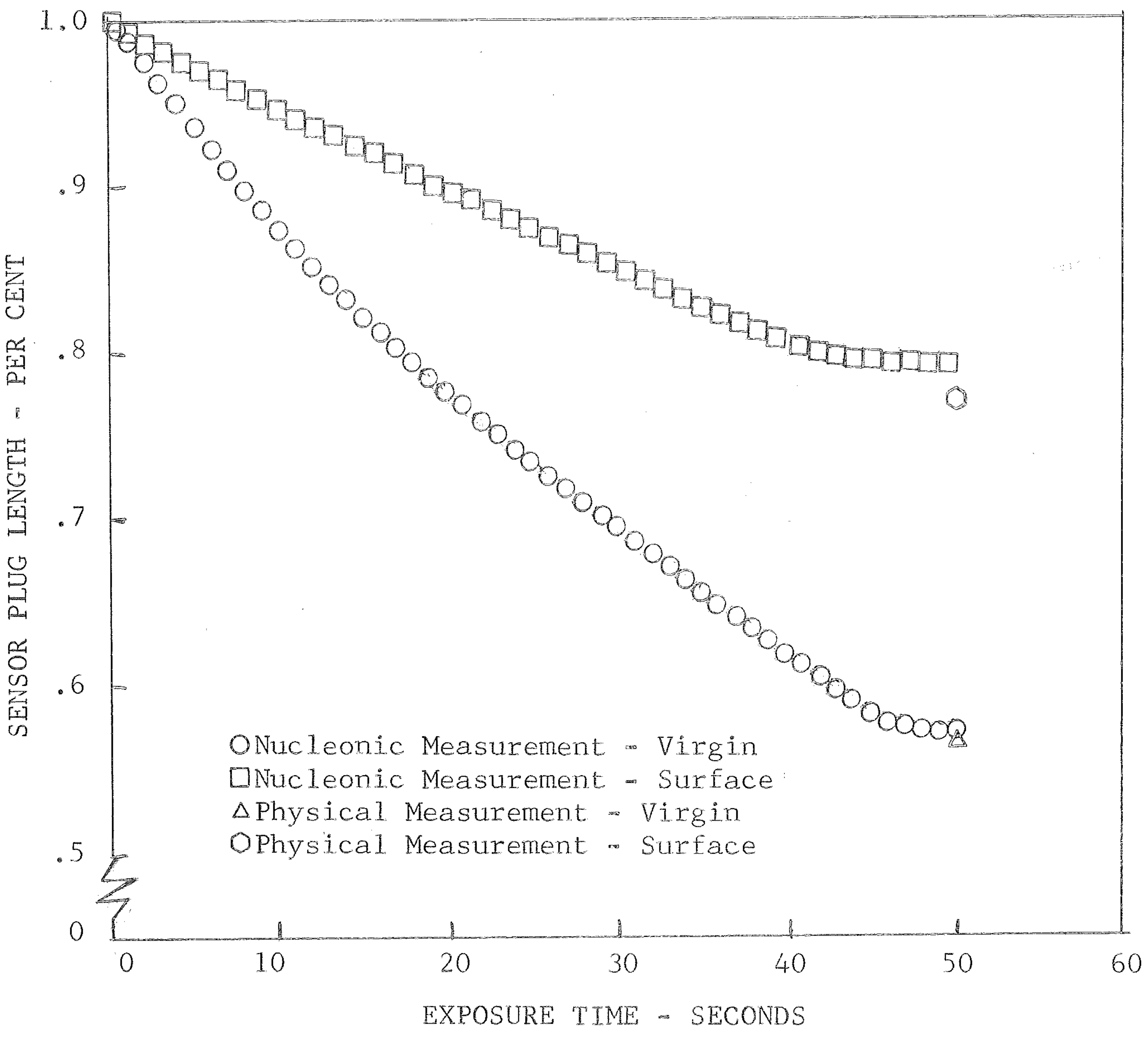

Figure 28

TEST MODEL PERFORMANCE DATA

MATERIAL RECESSION HISTORY

Phase VIA

Laboratory Nucleonics System

Model No. 9A30C7

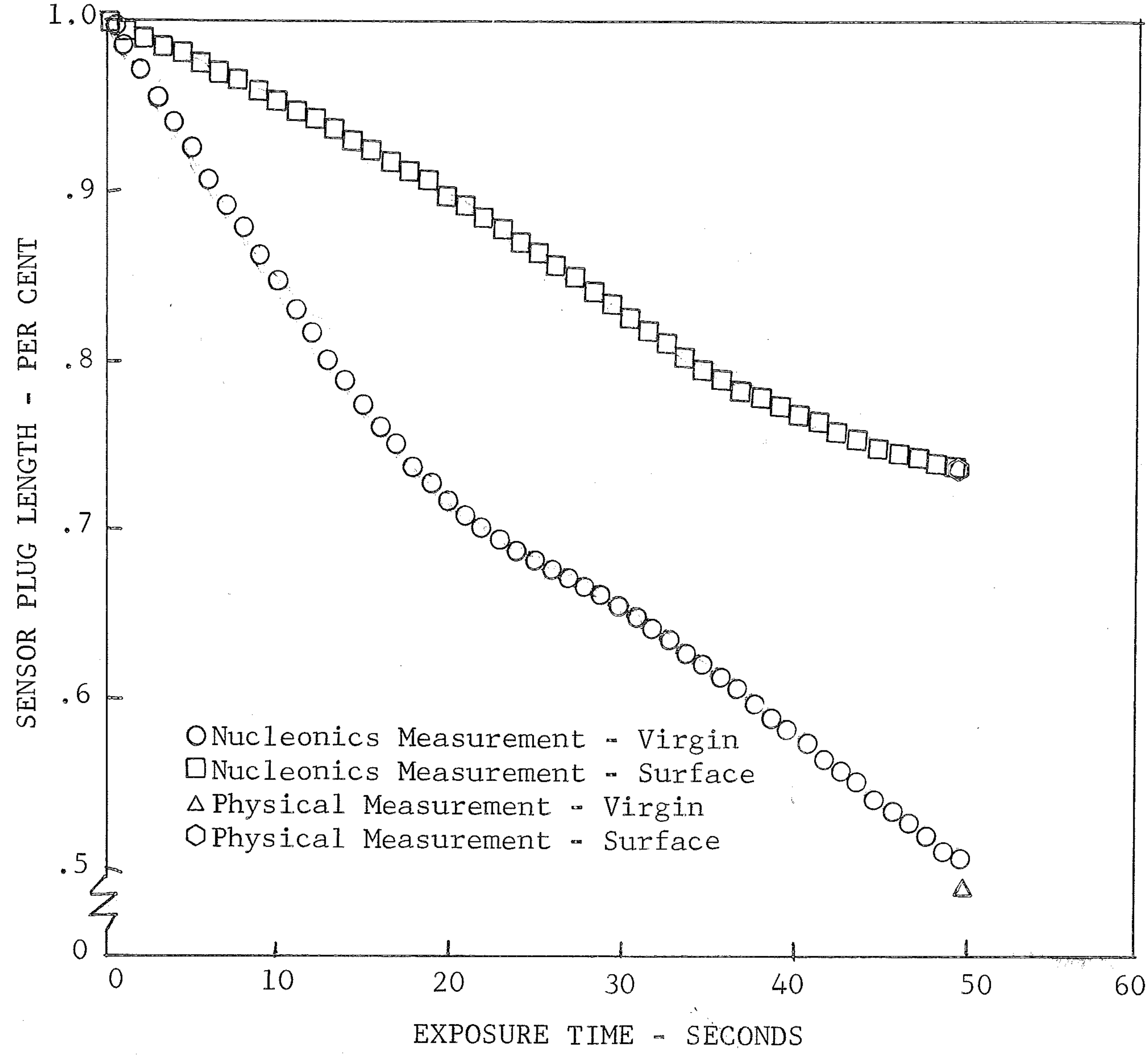

Figure 29

TEST MODEL PERFORMANCE DATA

MATERIAL RECESSION HISTORY

Phase VIA

Laboratory Nucleonic System

Model No. 9A30C9

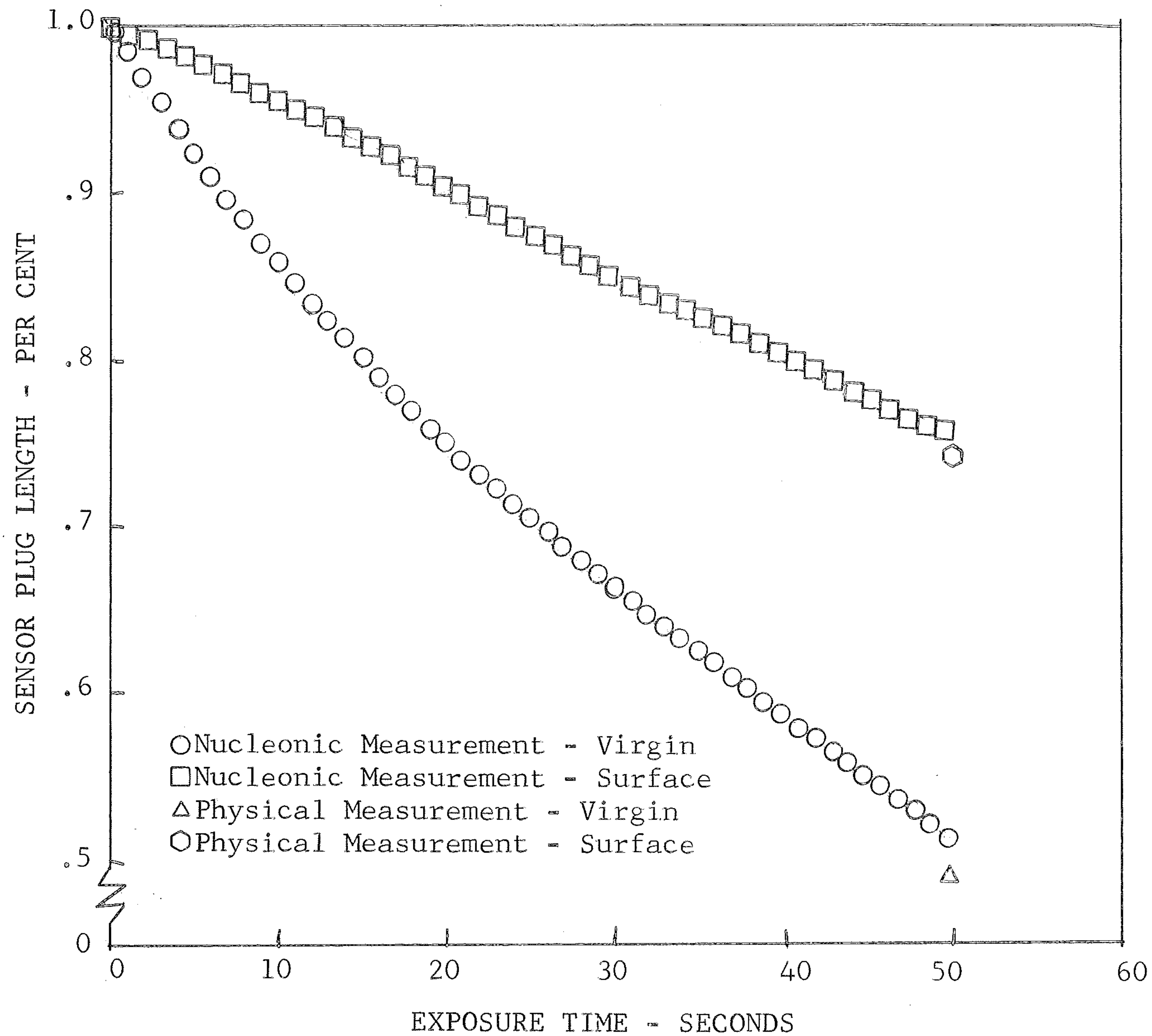

Figure 30

TEST MODEL PERFORMANCE DATA

MATERIAL RECESSION HISTORY

Phase VIB

Laboratory Nucleonics System

Model No. 9F15C17

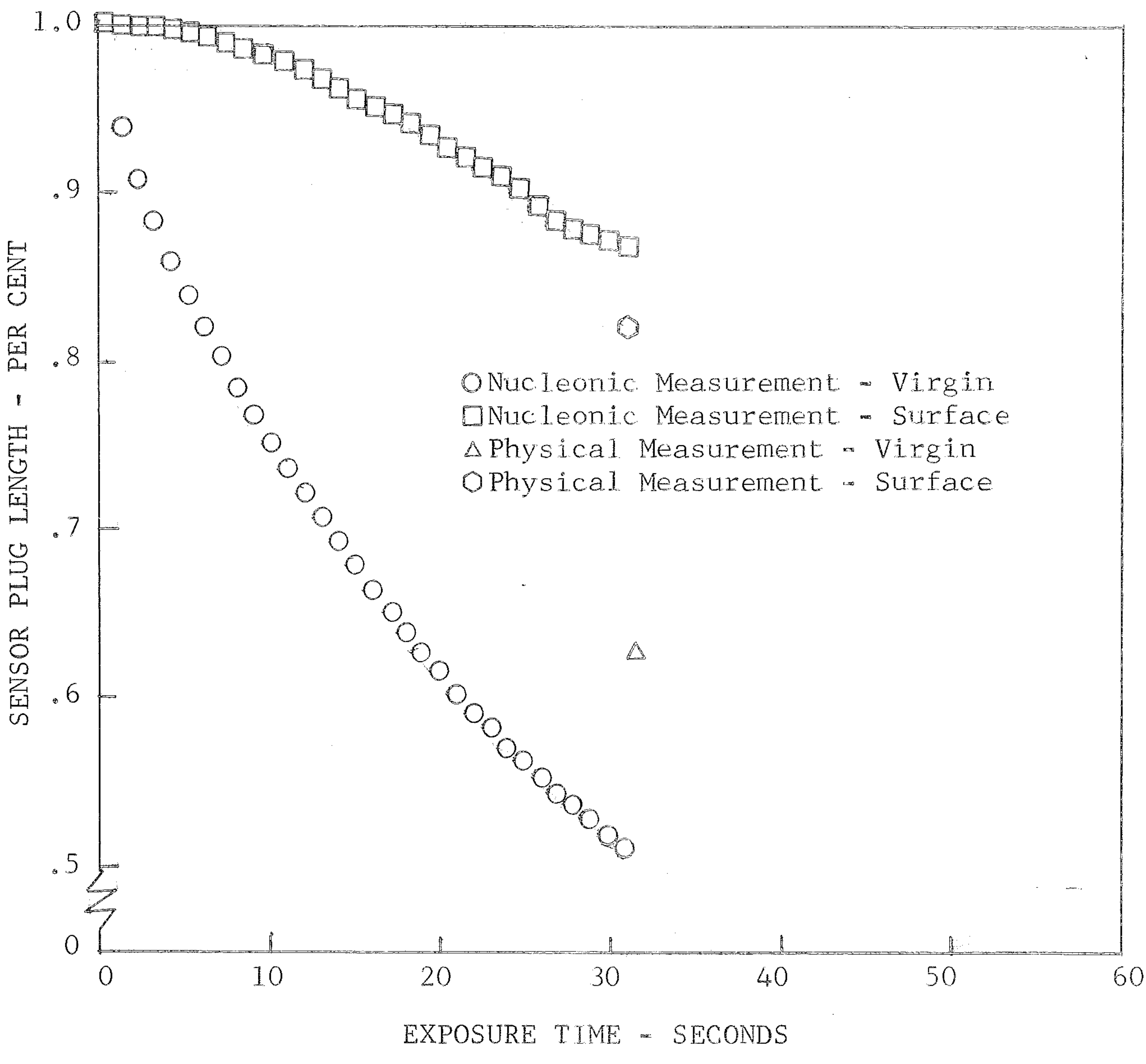

Figure 31

TEST MODEL PERFORMANCE DATA

MATERIAL RECESSION HISTORY

Phase VII

Laboratory and Breadboard Nucleonics System in Parallel

Breadboard Output with $In_2^{114m} = f(In_1^{114m})$

Model 9F15C18

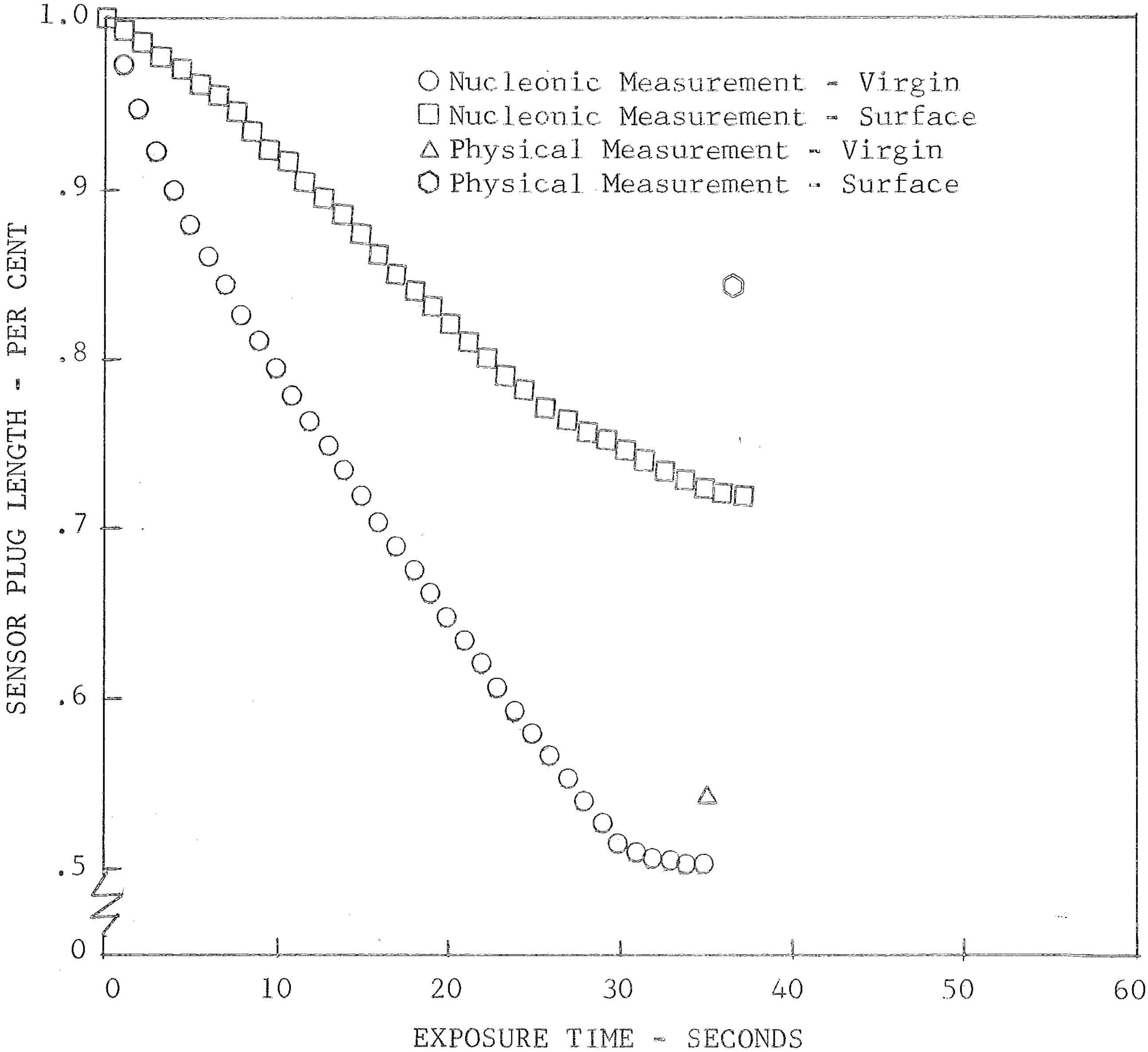

Figure 32

TEST MODEL PERFORMANCE DATA

MATERIAL RECESSION HISTORY

Phase VII

Laboratory and Breadboard Nucleonic System in Parallel

Breadboard Output with $In_2^{114m} = 0$

Model No. 9F15C18

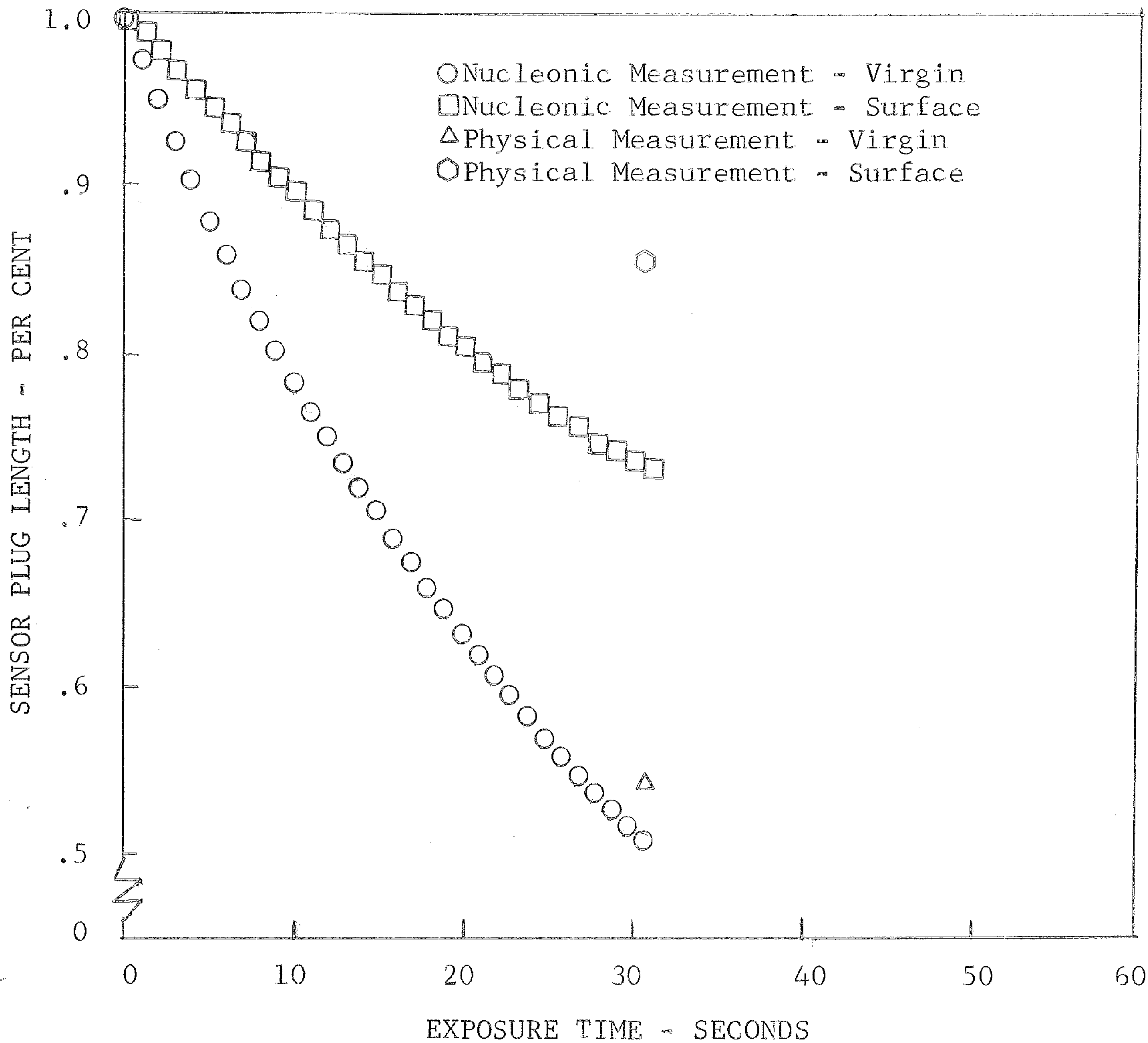

Figure 33

TEST MODEL PERFORMANCE DATA

MATERIAL RECESSION HISTORY

Phase VIB

Laboratory and Nucleonics System

Model No. 9F15C20

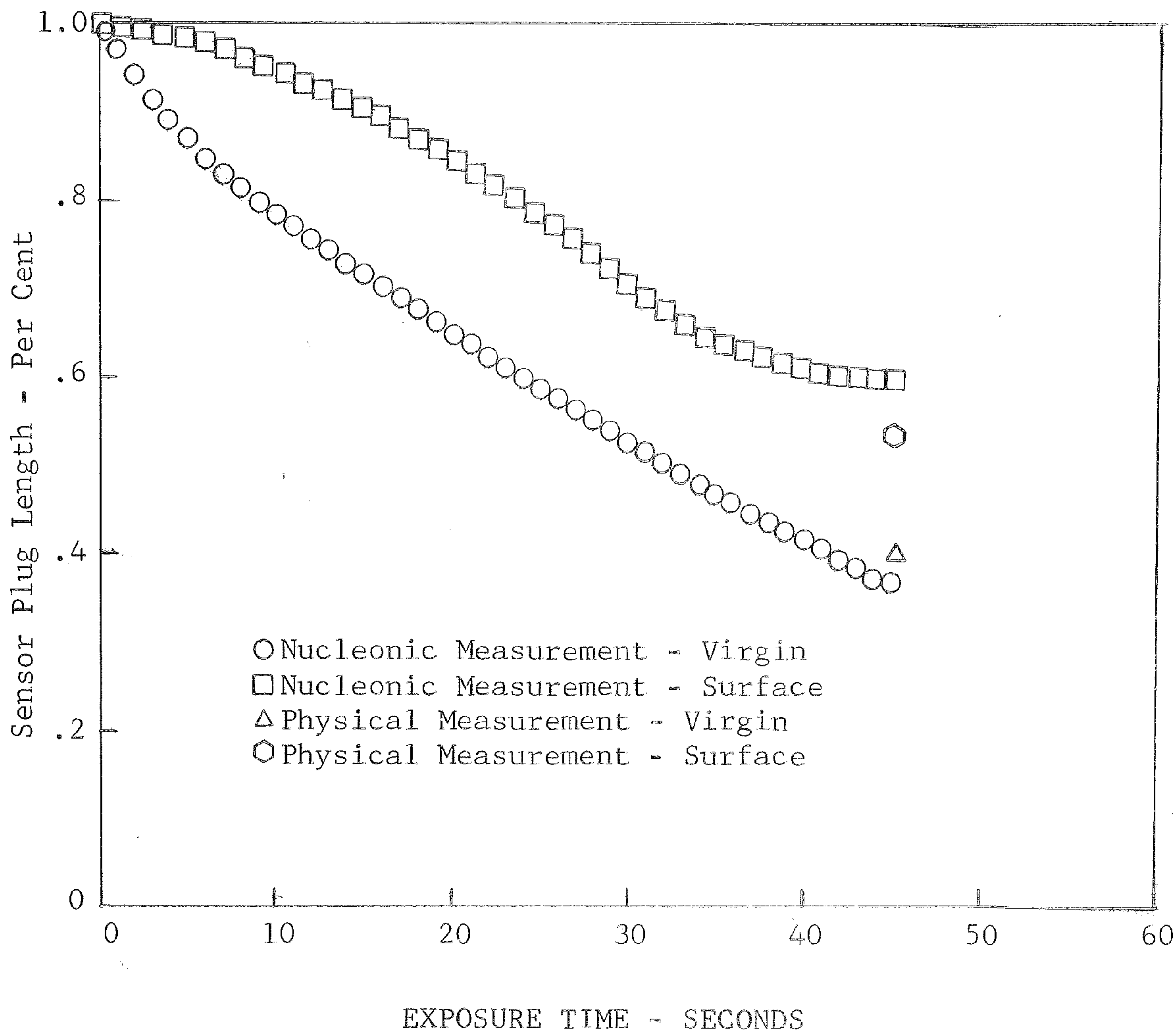

Figure 34

TEST MODEL PERFORMANCE DATA

MATERIAL RECESSION HISTORY

Phase VII

Laboratory and Breadboard Nucleonics System in Parallel

Laboratory Output

Model No. 9F15C21

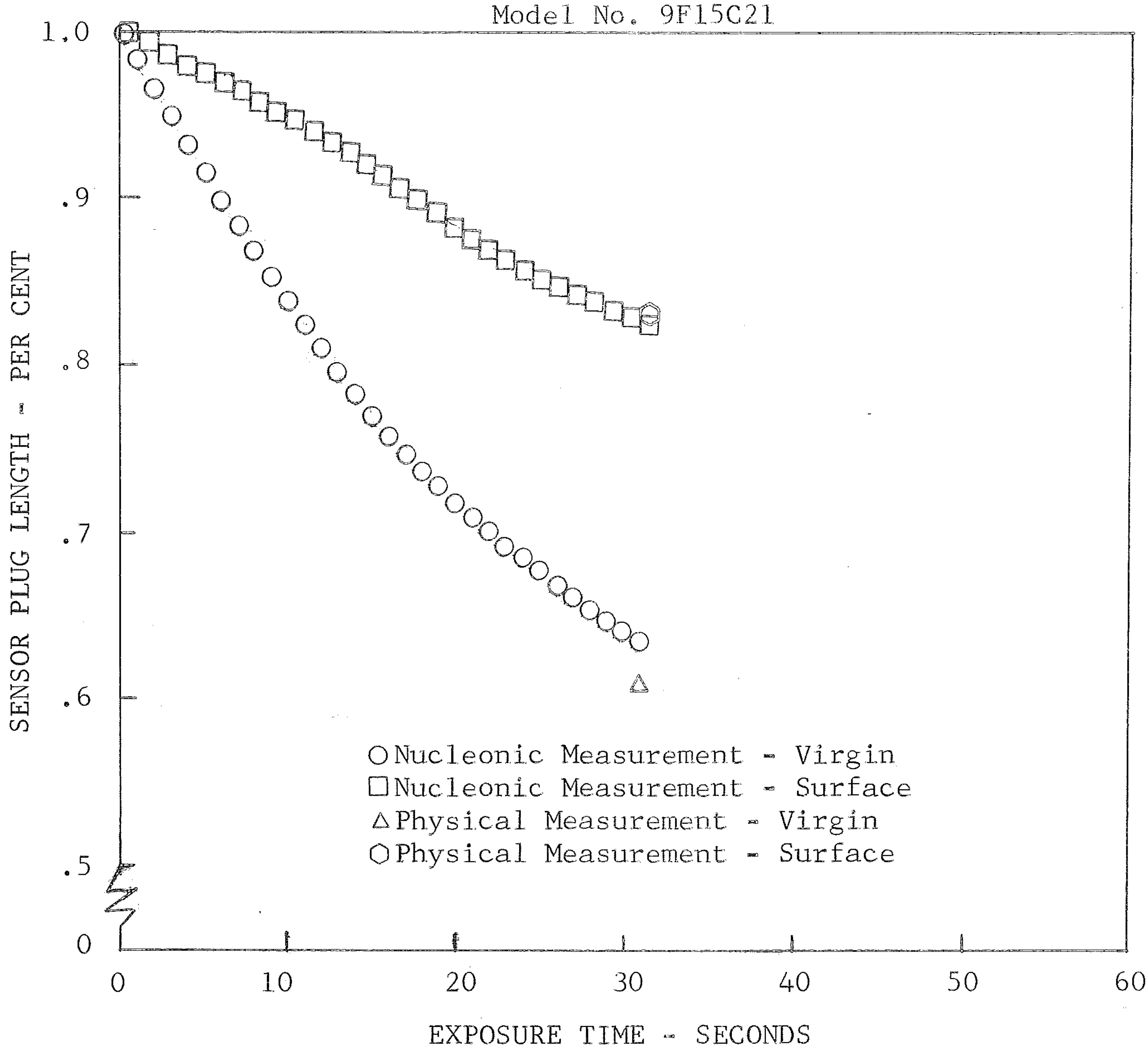

Figure 35

TEST MODEL PERFORMANCE DATA

MATERIAL RECESSION HISTORY

Phase VII

Laboratory and Breadboard Nucleonic System in Parallel

Breadboard Output with $In_2^{114m} = f(In_1^{114m})$

Model No. 9F15C21

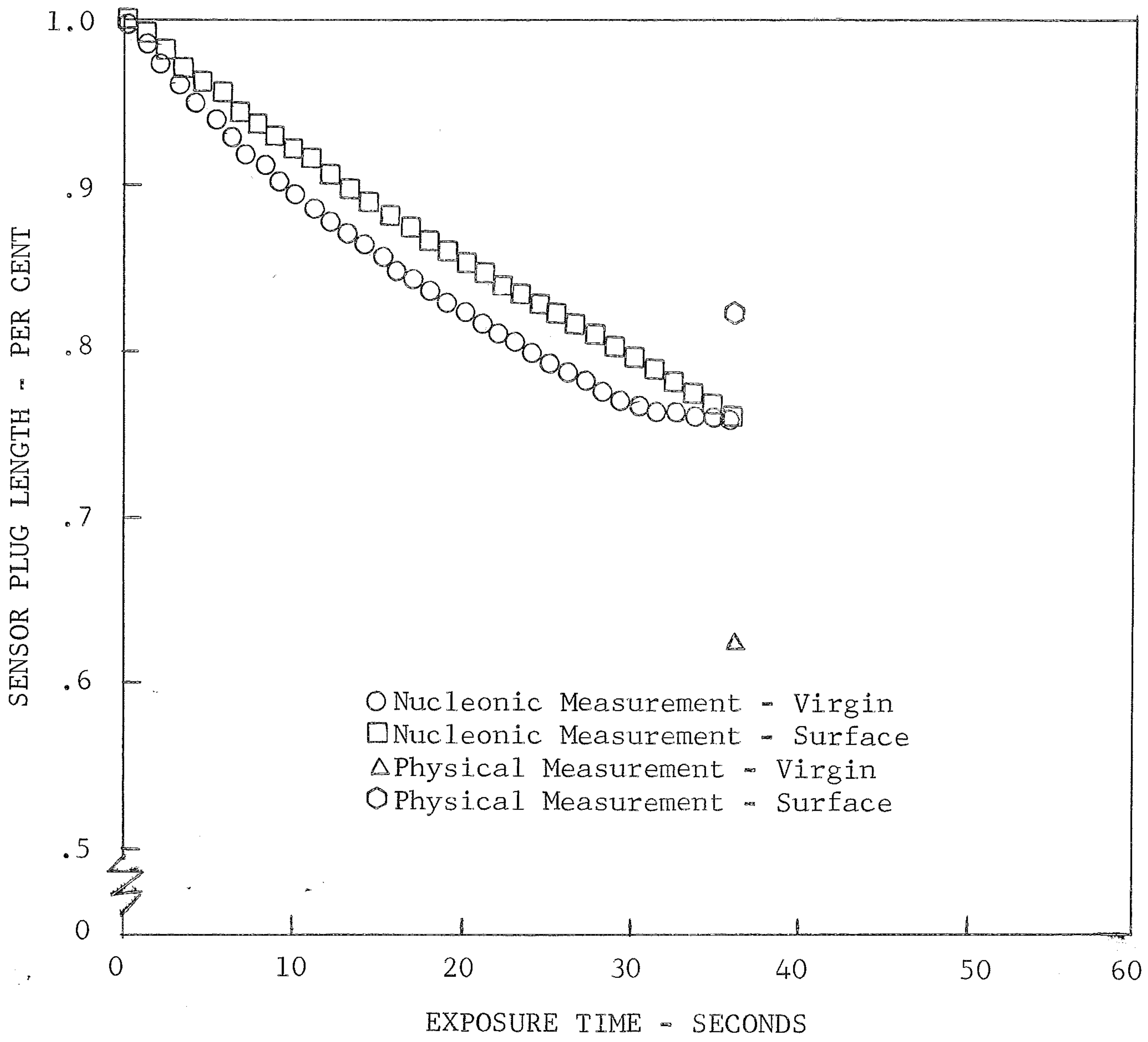

Figure 36

TEST MODEL PERFORMANCE DATA

MATERIAL RECESSION HISTORY

Phase VII

Laboratory and Breadboard Nucleonic System in Parallel

Breadboard Output with $In_2^{114m} = 0$

Model No. 9F15C21

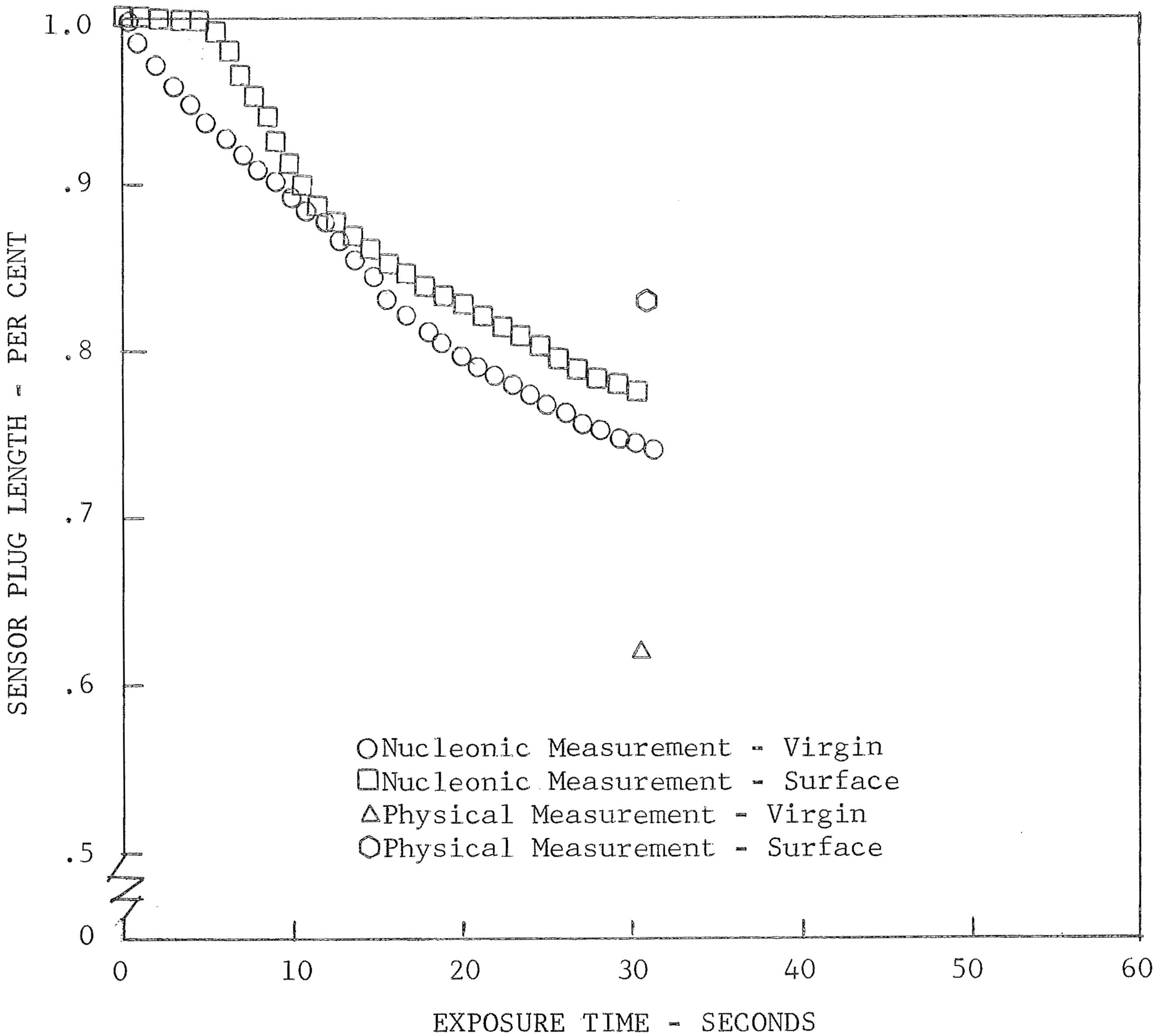

Figure 37

TEST MODEL PERFORMANCE DATA

MATERIAL RECESSION HISTORY

Phase VII

Laboratory and Breadboard Nucleonics System in Parallel

Laboratory Output

Model No. 9F15C22

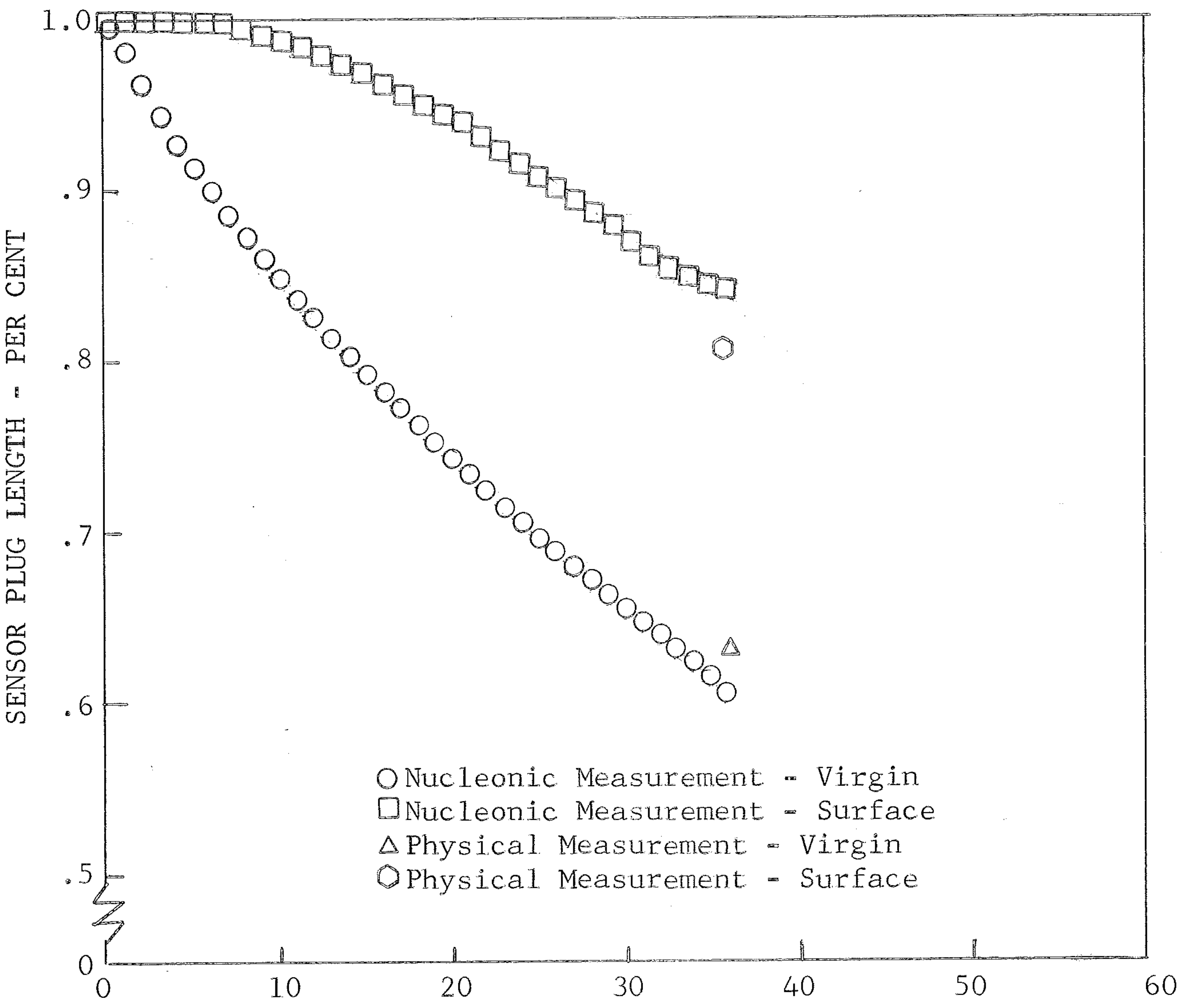

Figure 38

TEST MODEL PERFORMANCE DATA

MATERIAL RECESSION HISTORY

Phase VII

Laboratory and Breadboard Nucleonic System in Parallel

Breadboard Output with $In_2^{114m} = f(In_1^{114m})$

Model No. 9F15C22

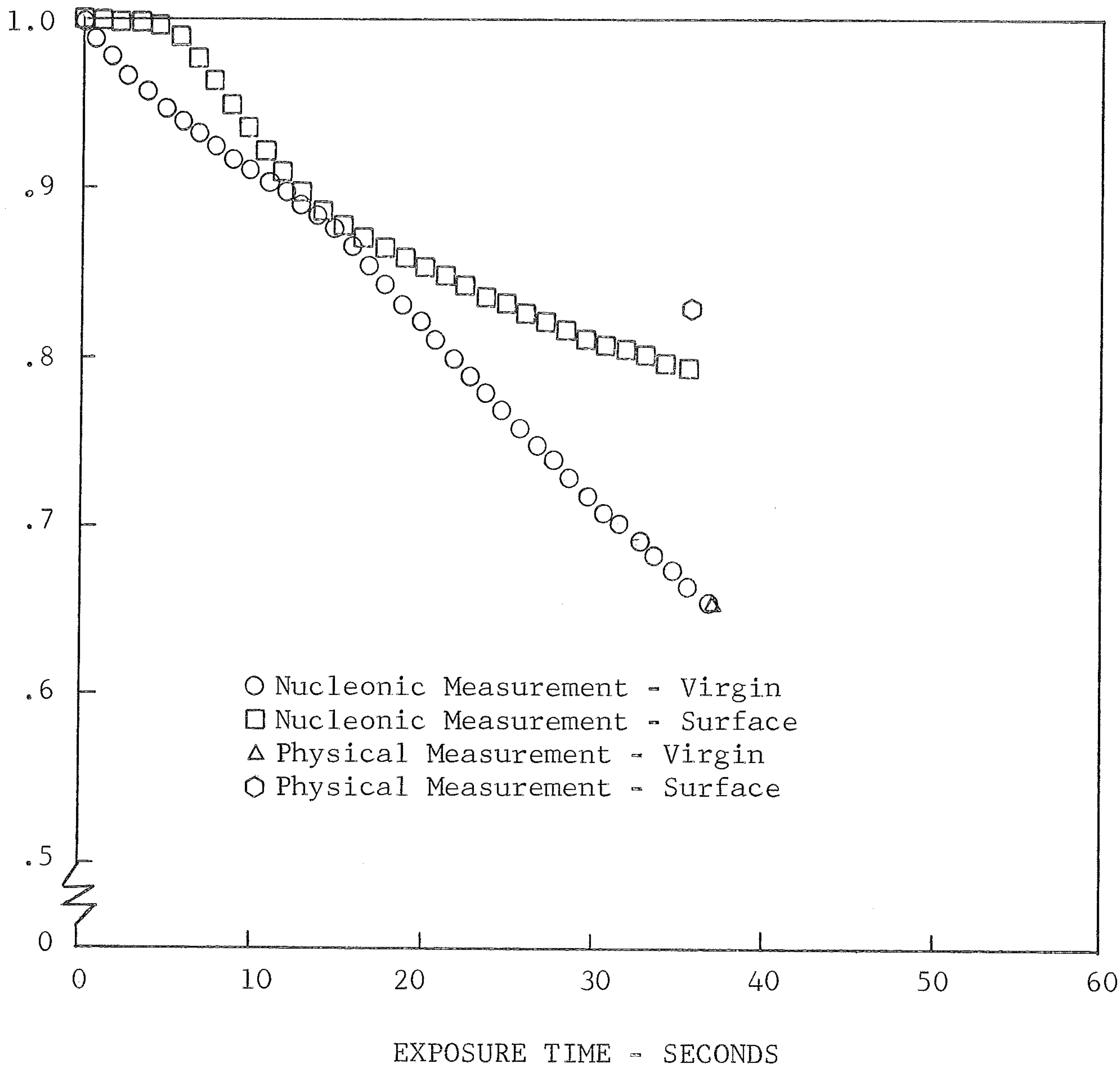

Figure 39

TEST MODEL PERFORMANCE DATA

MATERIAL RECESSION HISTORY

Phase VII

Laboratory and Breadboard Nucleonic System in Parallel

Breadboard Output with $In_2^{114m} = 0$

Model No. 9F15C22

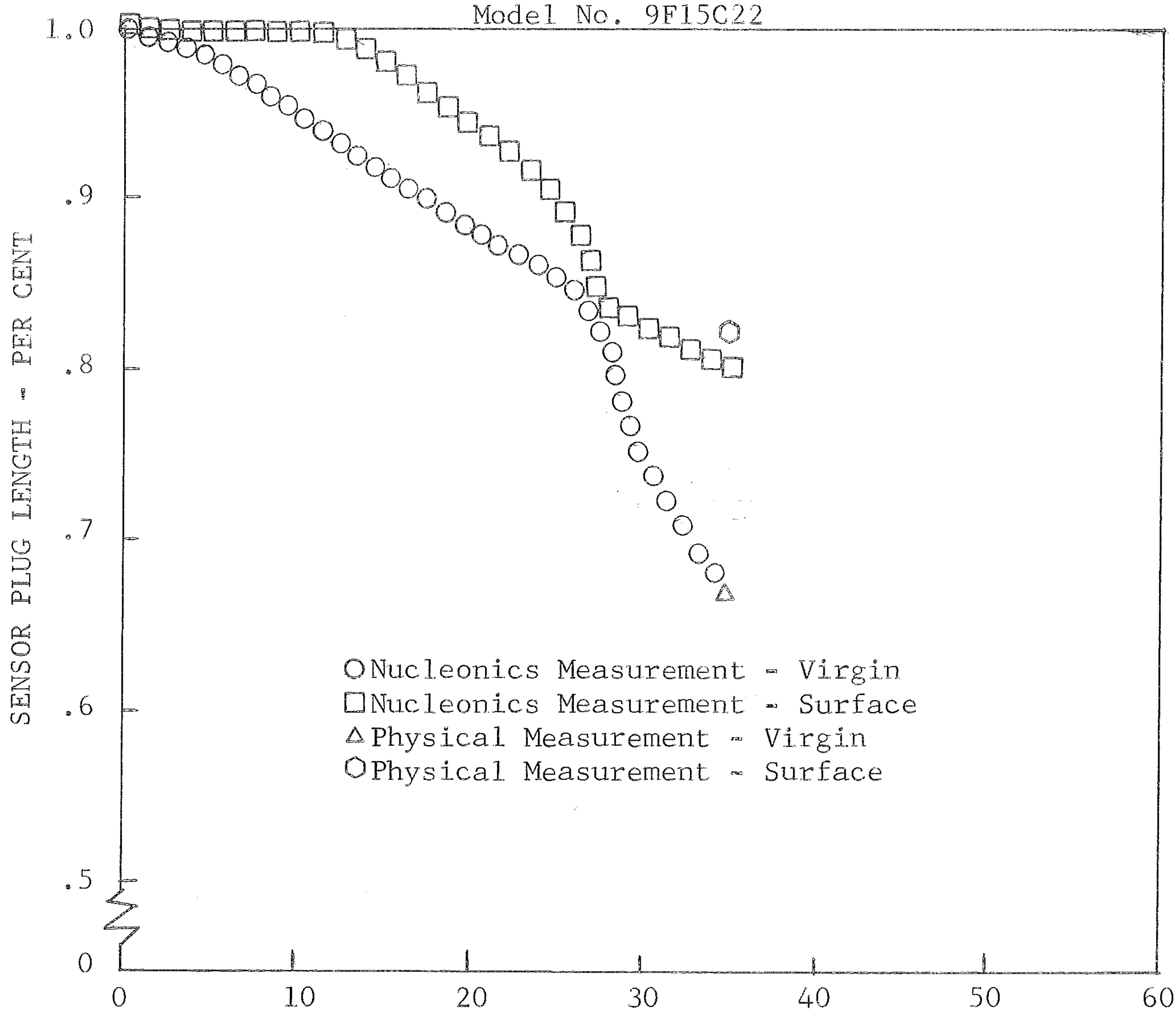

Figure 40

TEST MODEL PERFORMANCE DATA

MATERIAL RECESSION HISTORY

Phase VIA

Laboratory Nucleonics System

Model No. 9B04C2

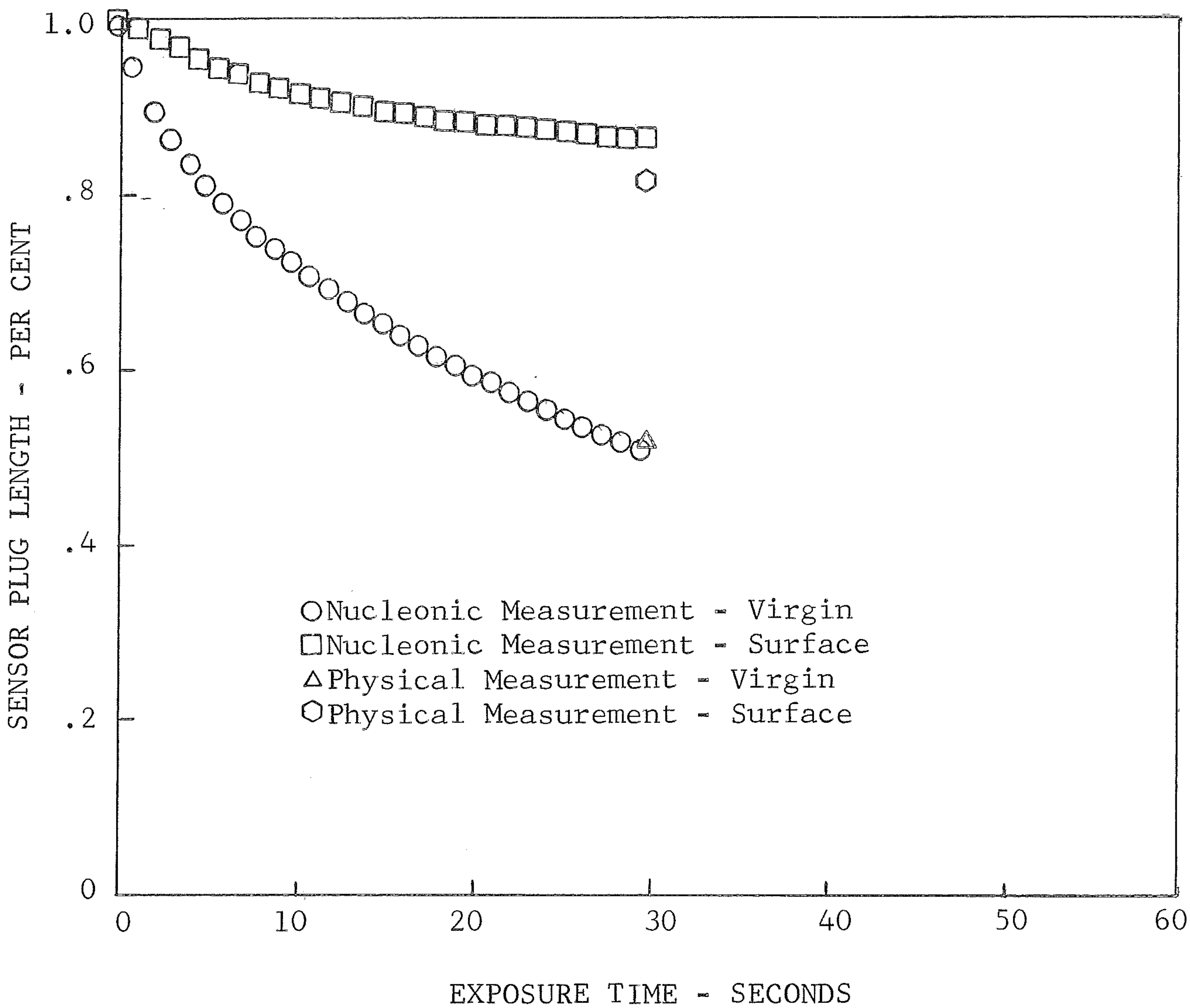

Figure 41

TEST MODEL PERFORMANCE DATA

MATERIAL RECESSION HISTORY

Phase VIA

Laboratory Nucleonics System

Model No. 9B04C3

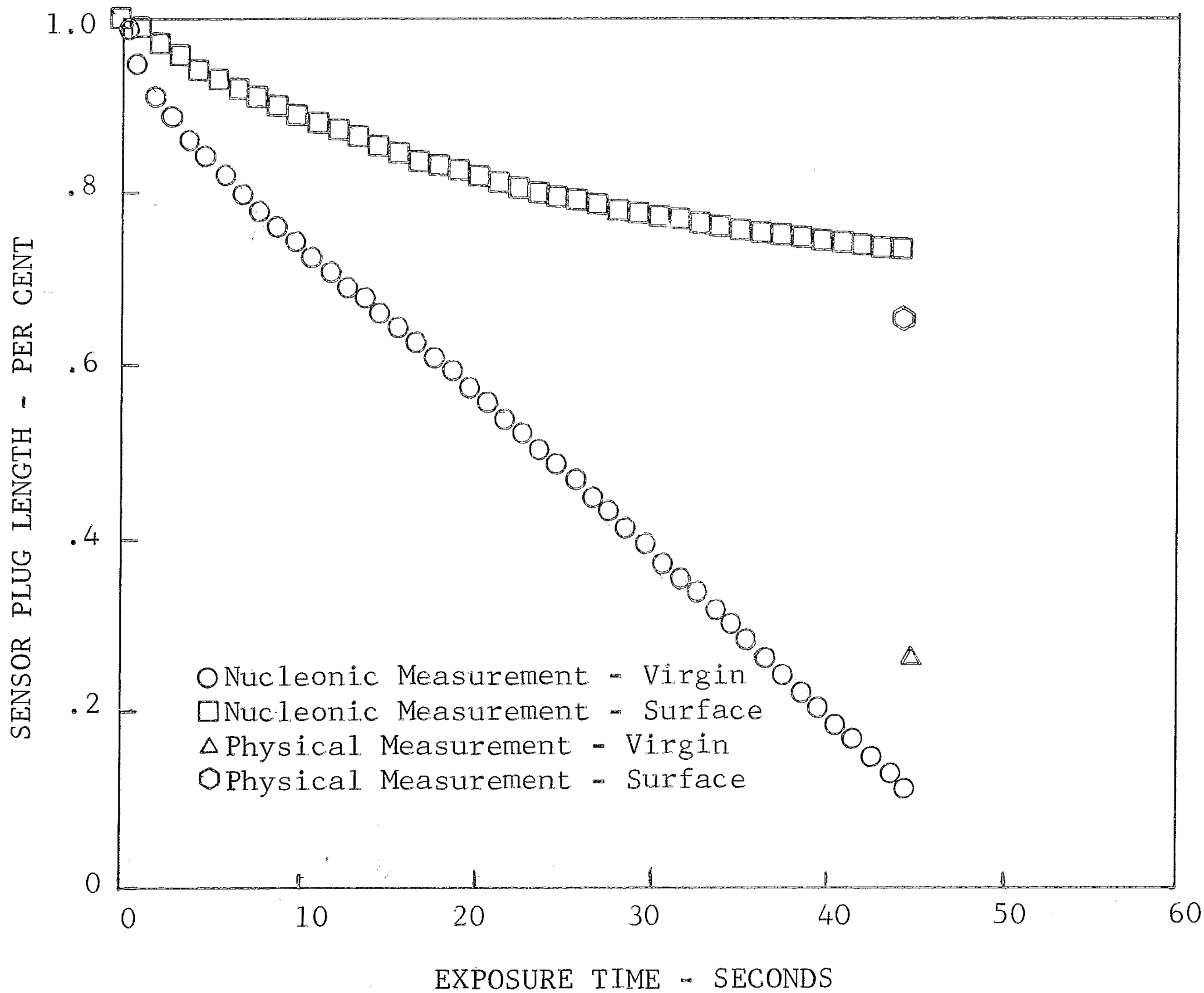

Figure 42

TEST MODEL PERFORMANCE DATA

MATERIAL RECESSION HISTORY

Phase VIA

Laboratory Nucleonics System

Model No. 9B04C4

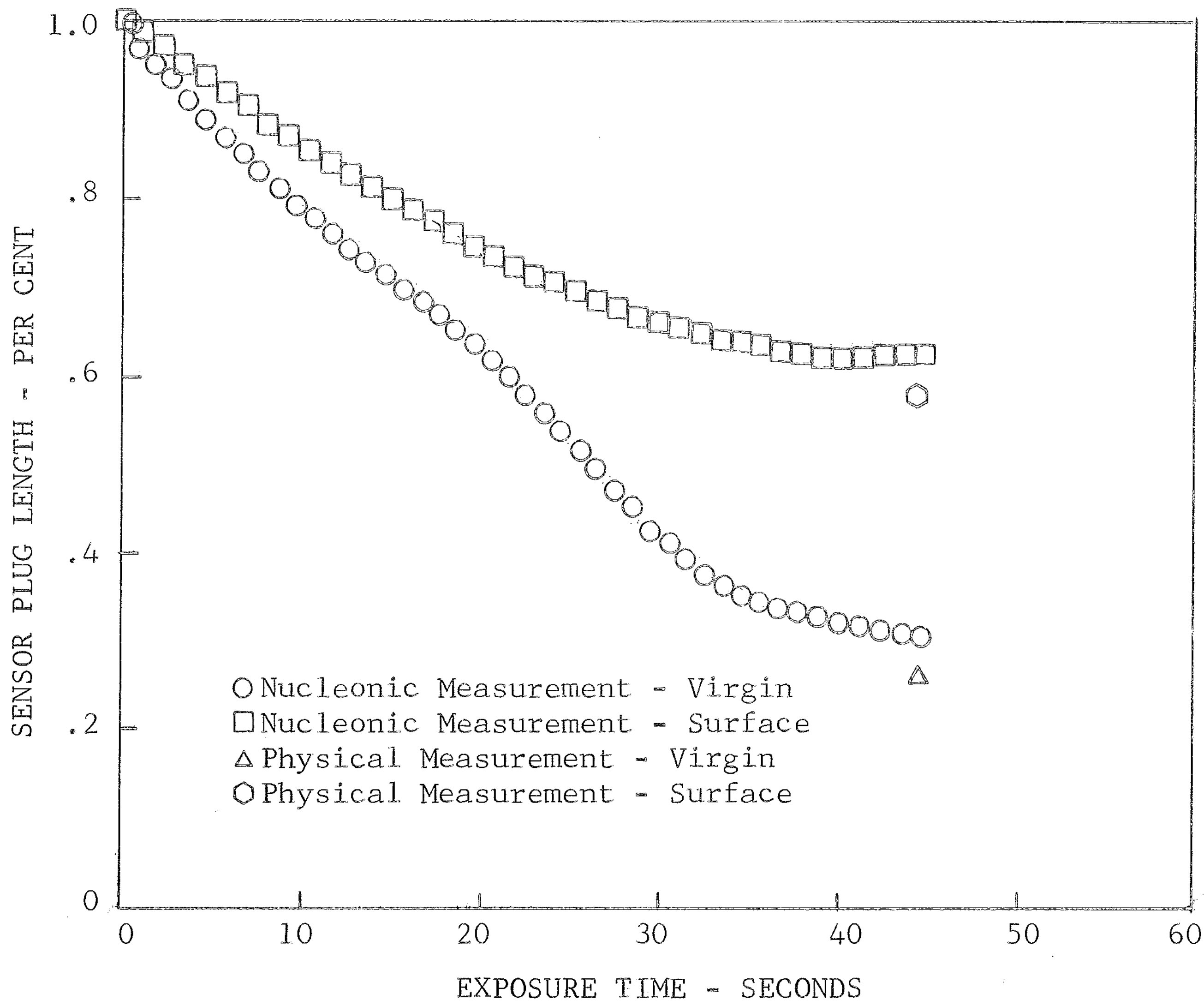

Figure 43

TEST MODEL PERFORMANCE DATA

MATERIAL RECESSION HISTORY

Phase VIA

Laboratory Nucleonics System

Model No. 9B04C6

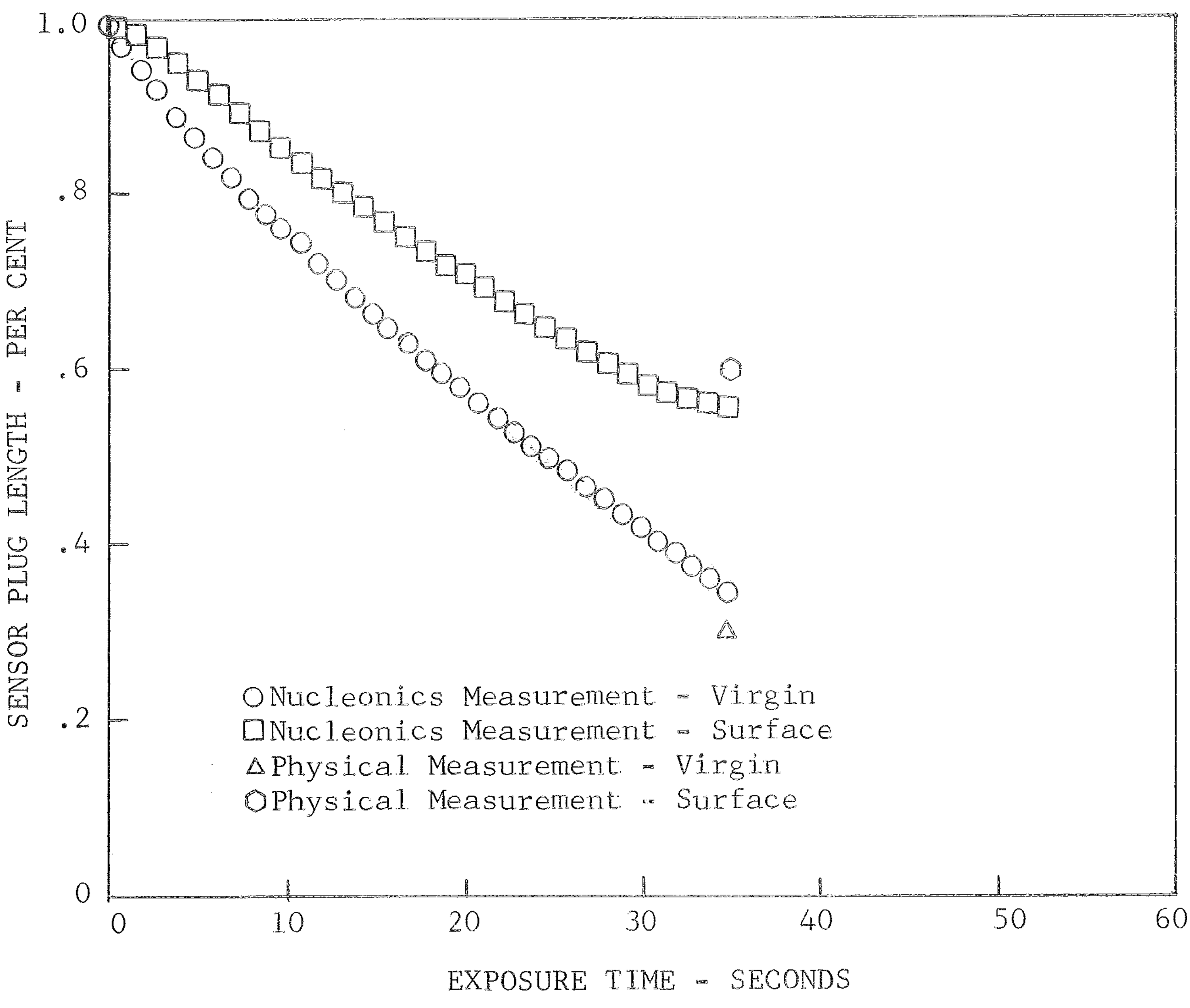

Figure 44

TEST MODEL PERFORMANCE DATA

MATERIAL RECESSION HISTORY

Phase VIB

Laboratory Nucleonics System

Model No. 9D17G2

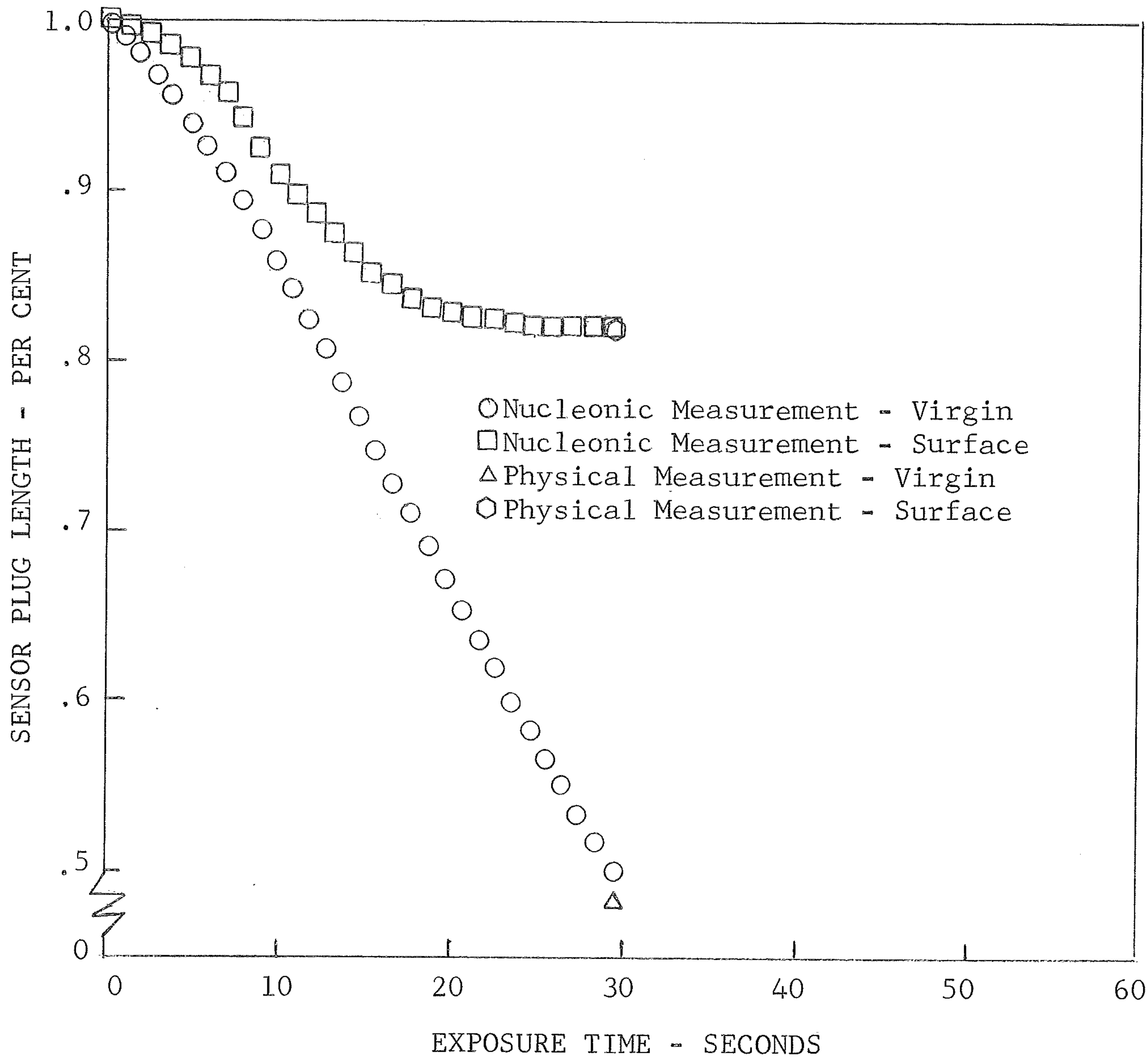

Figure 45

TEST MODEL PERFORMANCE DATA

MATERIAL RECESSION HISTORY

Phase VIB

Laboratory Nucleonics System

Model No. 9D17G3

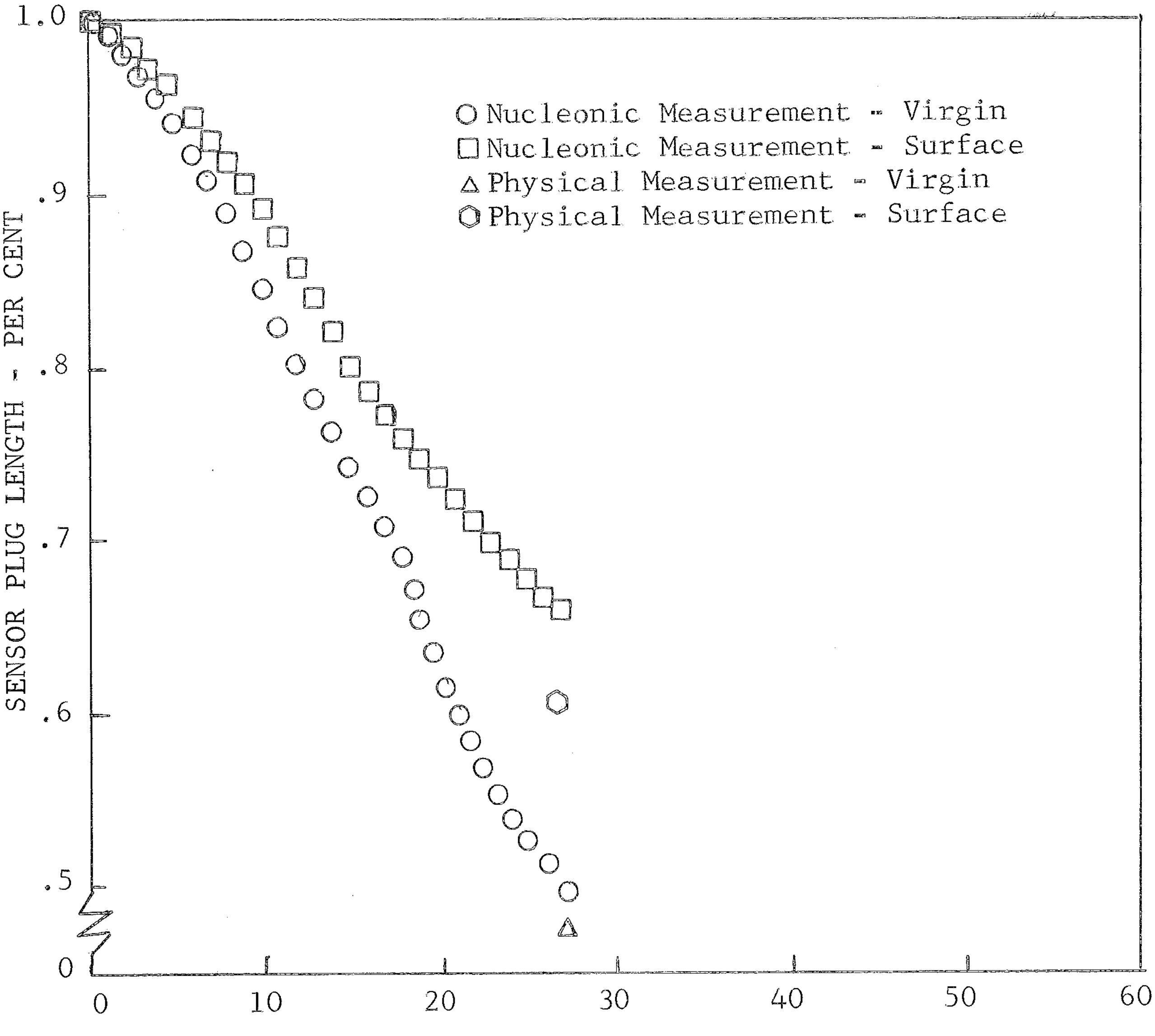

Figure 46

TEST MODEL PERFORMANCE DATA

MATERIAL RECESSION HISTORY

Phase VII

Laboratory and Breadboard Nucleonics System in Parallel

Breadboard Output with $In_2^{114m} = 0$

Model No. 9F15C23

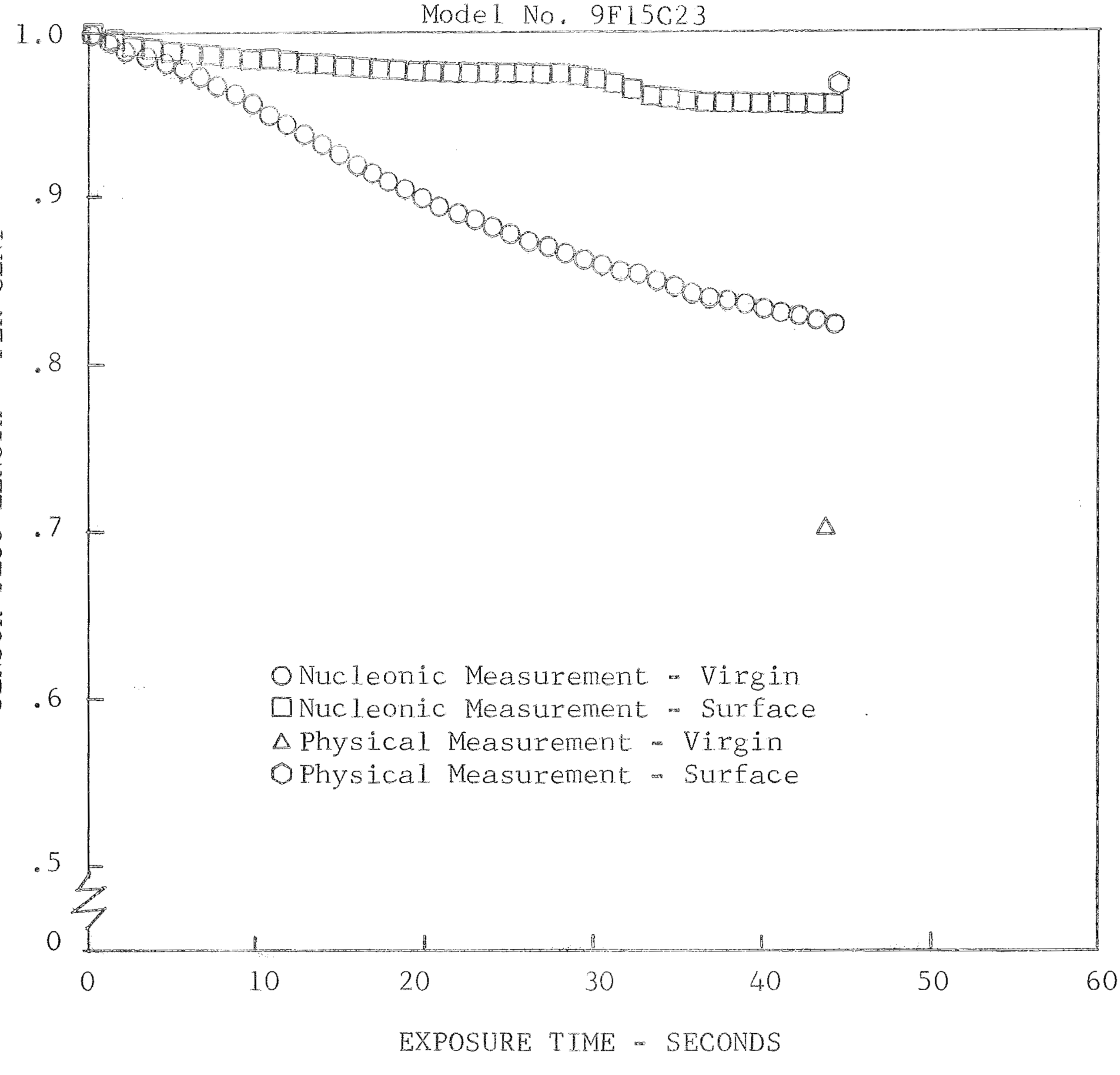

Figure 47

TEST MODEL PERFORMANCE DATA

MATERIAL RECESSION HISTORY

Phase VII

Laboratory and Breadboard Nucleonic System in Parallel

Breadboard Output with $In_2^{114m} = f(In_1^{114m})$

Model No. 9F15C23

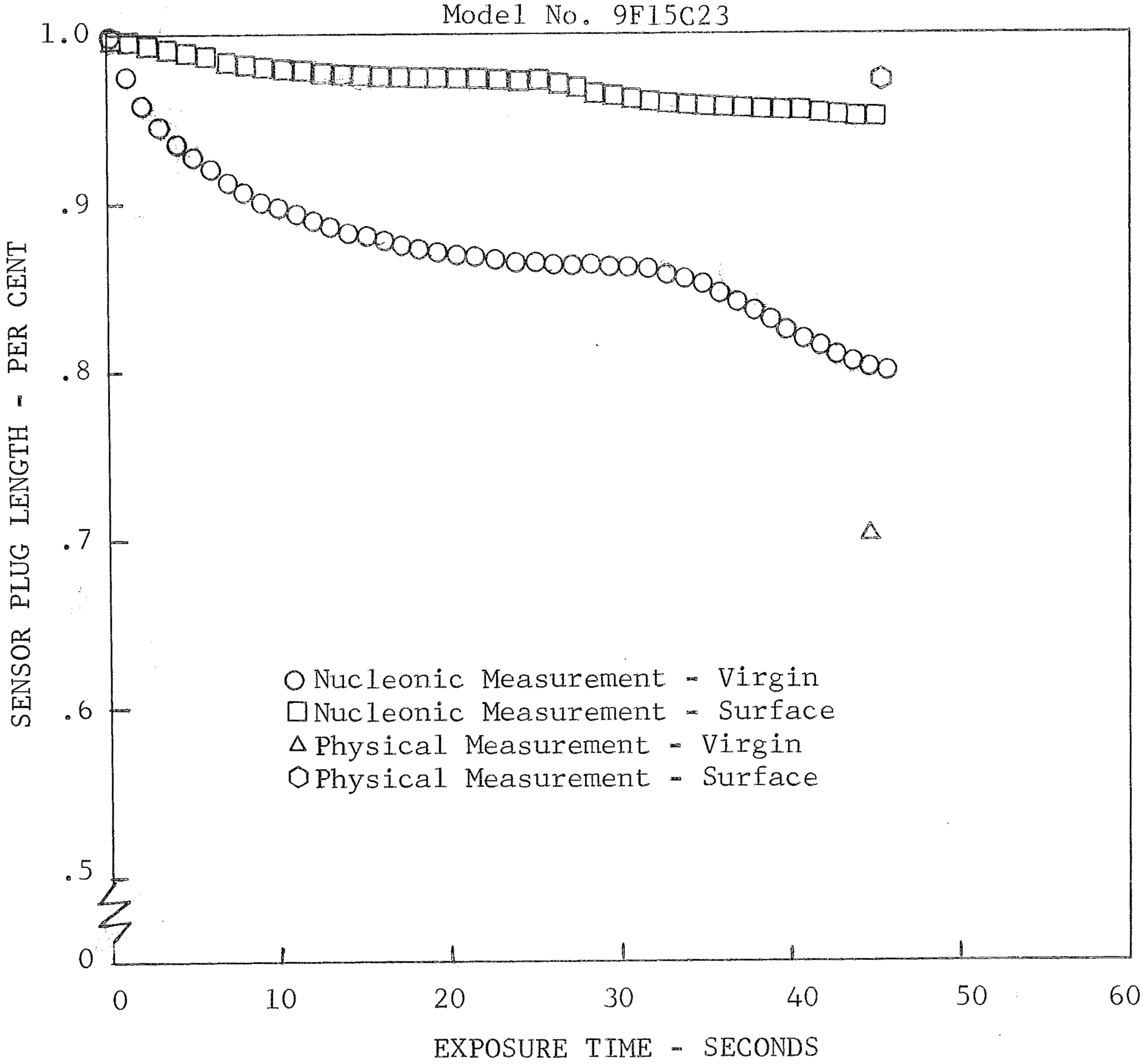

Figure 48

TEST MODEL PERFORMANCE DATA

MATERIAL RECESSION HISTORY

Phase VII

Laboratory and Breadboard Nucleonics System in Parallel

Laboratory Output

Model No. 9F23C24

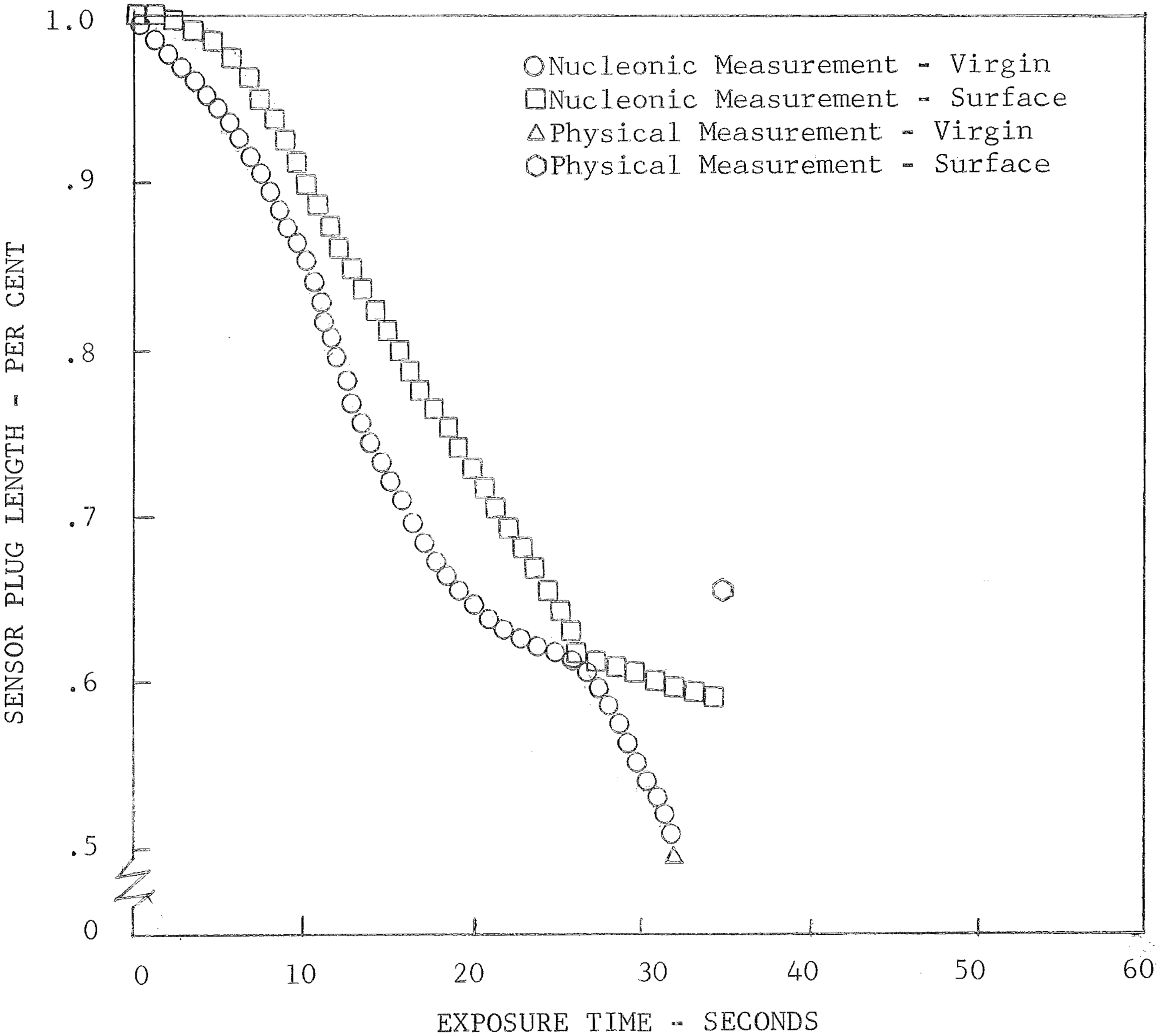

Figure 49

TEST MODEL PERFORMANCE DATA

MATERIAL RECESSION HISTORY

Phase VII

Laboratory and Breadboard Nucleonics System in Parallel

Breadboard Output with $In_2^{114m} = f(In_1^{114m})$

Model No. 9F23C24

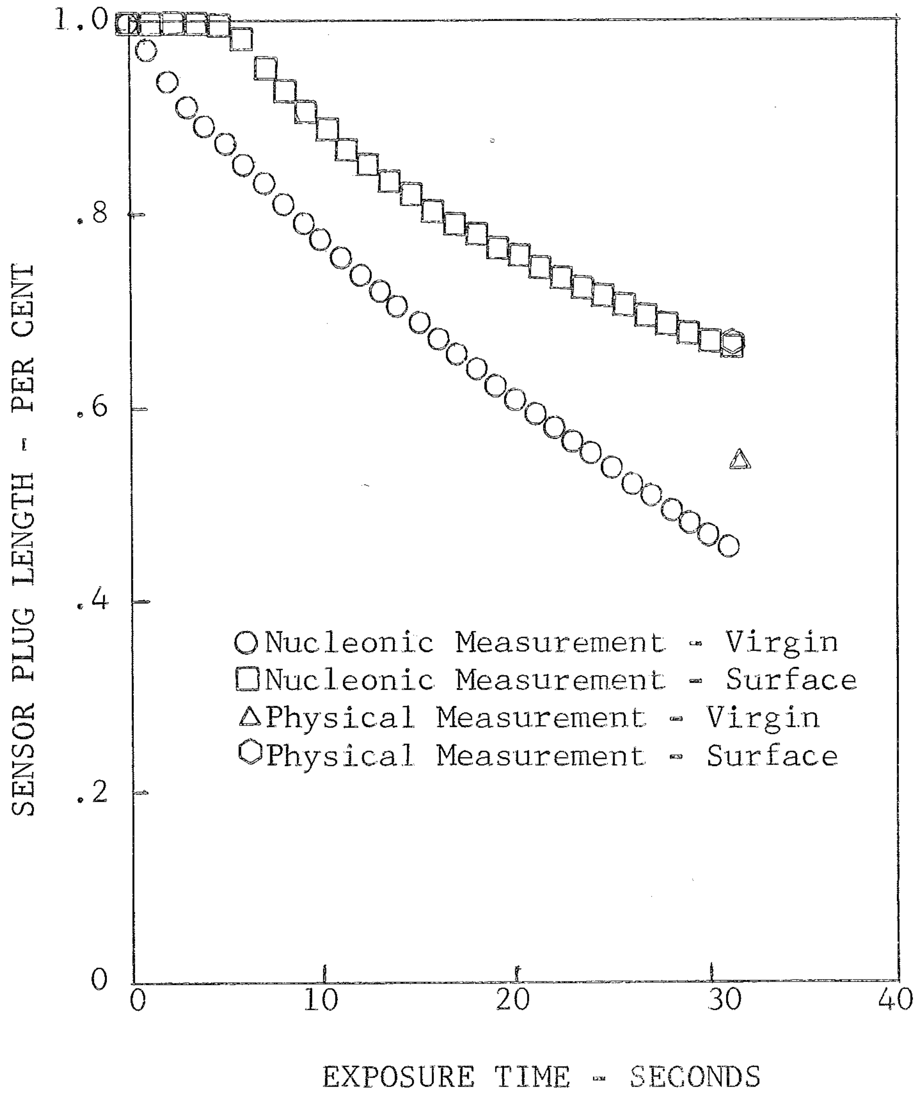

Figure 50

TEST MODEL PERFORMANCE DATA

MATERIAL RECESSION HISTORY

Phase VII

Laboratory and Breadboard Nucleonics System in Parallel

Breadboard Output with $In_2^{114m} = 0$

Model No. 9F23C24

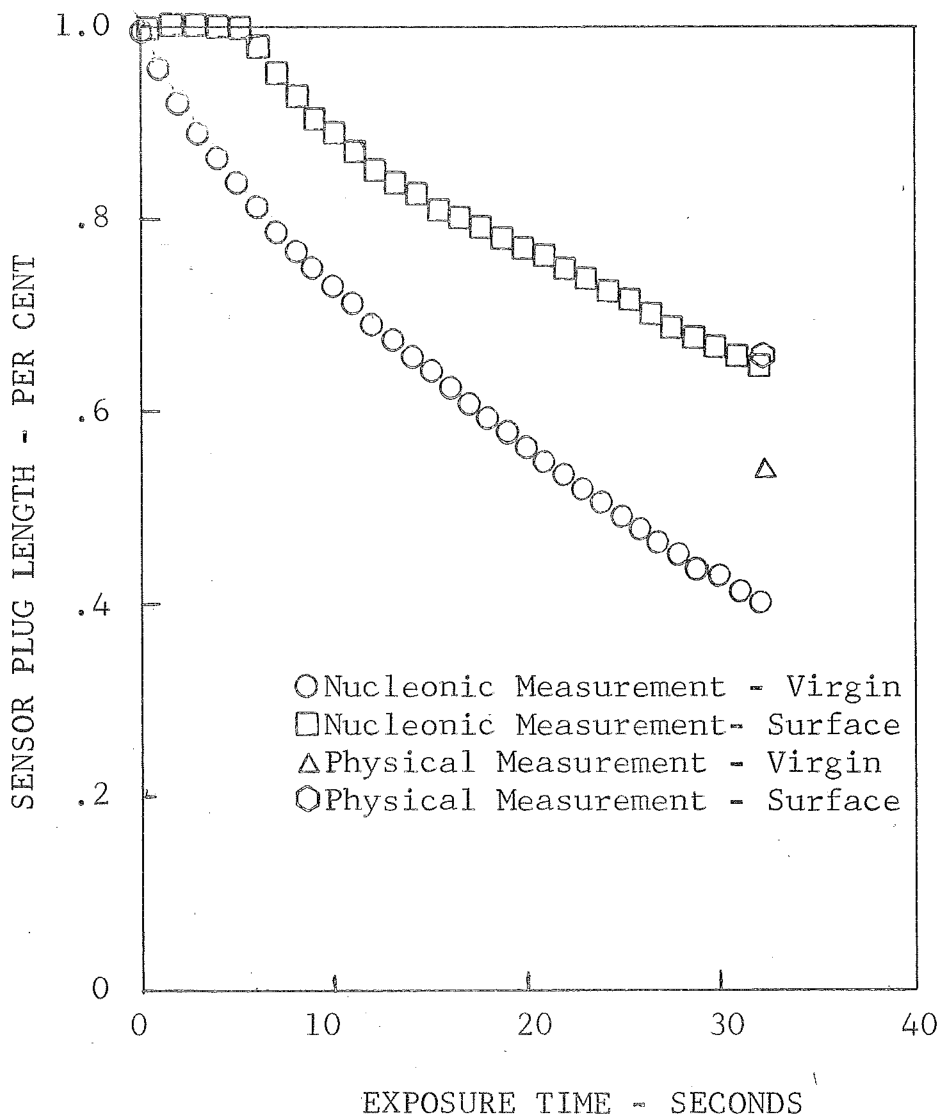

Figure 51

SECTION V

CONCLUSIONS AND RECOMMENDATIONS

1.0 CONCLUSIONS

1) The feasibility of measuring char and char-virgin material interface recession by dual albation measurement techniques has been proven by tests at plasma jet environments approximating vehicle entry conditions.

2) The breadboard dual ablation measurement system is effective in the measurement of material ablation by nucleonic techniques.

3) Using the laboratory standard nucleonics system, accuracy can be maintained at greater than 97 per cent. Minor circuit modifications would result in comparable accuracy for the breadboard dual ablation measurement system.

2.0 RECOMMENDATIONS

It is recommended that a flight prototype dual ablation measurement system be manufactured and tested. Design modifications prerequisite to maximum system accuracy should be incorporated.